Development of a Dry Coupling Material for Ultrasonic Transcutaneous Energy Transfer

by

Jeremy Edward Norman

Submitted in partial fulfilment of the requirements for the degree of Master of Applied Science

at

Dalhousie University
Halifax, Nova Scotia
July 2017

Dedications

The work described in this thesis was carried out under the supervision of Dr. Robert Adamson to whom the Author is indebted for his ideas, encouragement and understanding during the period of research, and for his help and advice during the preparation of this thesis.

The Author would also like to thank his parents for the love and support he has received throughout the highs and lows of his postgraduate work.

Finally, the Author would like to thank the Faculty of Biomedical Engineering at Dalhousie University for the honour and opportunity to work in such a rewarding field of research.

Table of Contents

List of Tables

List of Figures

Abstract

Ultrasonic transcutaneous energy transmission (UTET) is a novel technology with great potential for electrically powering active biomedical implants. To make UTET devices viable, a key piece of technology is required. A "dry" acoustic coupling bridges the ultrasound transducer and the patient's skin without the need for coupling gels. This dry coupling material allows a patient to wear a device daily and for long periods of time. The dry coupling consists of a solid medium through which an external transducer delivers ultrasound to an implanted device. This thesis investigates the use of silicone as a dry coupling medium. This thesis contains two main chapters. A manufacturing chapter in which the process for producing a dry coupling material has been developed. The chapter explores the many problems and solutions encountered in creating dry coupling samples. This included acoustic impedance matching the dry coupling to skin by doping the silicone with ZnO powder, creating a bubble free silicone, development of the sample moulds, adding adhesive properties to the dry coupling, and finally, the procedures for curing thick samples, thin samples and the adhesive layer. An experiments chapter in which the validity and effectiveness of different manufacturing techniques for dry coupling is proven by experimentation and theoretical analysis. These experiments characterized the acoustic properties of the dry coupling material and porcine skin, tested the effectiveness of the adhesive layer as a means of anchoring the device to the patients skin, investigated potential avenues into increasing the dry coupling's acoustic impedance, mapped and modeled the relationship between the ZnO loading fraction and the dry coupling's acoustic reflectance, and finally, a power transfer efficiency (PTE) test showed that the final dry coupling design improved the PTE from $64.6\%_{max,}$ for untreated silicone, to $88.1\%_{max}$.

List of Abbreviations and Symbols Used

Symbols

$\mathbf{k_t}$	electromechanical coupling coefficient
$\boldsymbol{f}$ **[Hz]**	frequency
$\boldsymbol{\eta'}$	area normalized efficiency
$\boldsymbol{Z}$ **[MRayl]**	characteristic acoustic impedance
ρ [kg/m^3]	density
c [m/s]	speed of sound
$\boldsymbol{R}$	reflectivity
$\boldsymbol{l_w, l_T, l_s}$ **[m]**	length of water, inter-transducer distance, length of silicone
$\boldsymbol{t}$ **[s]**	time of flight
$\boldsymbol{c_s, c_w}$ **[m/s]**	speed of sound in silicone, water
$\boldsymbol{E}$ **[N/m^2]**	Young's modulus
$\boldsymbol{m_{total}, m_{base}, m_{cross}, m_{add}}$ **[kg]**	total mass, mass of base, crosslinker, additive
$\boldsymbol{V_{total}, V_{base}, V_{cross} V_{add}}$ **[m^3]**	total volume, volume of base, crosslinker, additive
$\boldsymbol{P_{out}, P_{in}}$ **[W]**	power out, power in
$\boldsymbol{\beta}$	conversion factor between reflectivity and voltage
$\mathbf{R^2}$	coefficient of determination
$\boldsymbol{V_{pp}}$ **[V]**	peak to peak voltage
$\boldsymbol{V_{out}}$ **[V]**	voltage out
$\boldsymbol{P_{out}, P_{in}}$ **[Pa]**	pressure out, pressure in
$\boldsymbol{R_1, R_2, T_1, T_2}$	reflection and transmission coefficients
$\boldsymbol{\alpha}$ **[dB/mm]**	attenuation coefficient
μ	mean
γ [dB/mm]	propagation constant
β [m]	wavenumber
ω [rad/s]	frequency
$\boldsymbol{A^{tr}, A_p, A_n}$	overall transfer matrix, piezoelectric and material transfer matrices

$\boldsymbol{F}$ **[N]**	force
$\boldsymbol{v}$ **[m/s]**	velocity
$\boldsymbol{Z_L}$ **[Ω]**	load impedance
λ [m]	wavelength

Abbreviations

UTET	ultrasonic transcutaneous energy transmission
PZT	lead zirconate titanate
PTE	power transfer efficiency
PMN-PT	lead magnesium niobate lead titanate
NDT	non-destructive testing
EM	electromagnetic
PSA	pressure sensitive adhesive
TEWL	trans epidermal water loss
PIB	polyisobutylenes
UV	ultraviolet
MVTR	moisture vapour transmission rate
ZnO	zinc oxide
SSA	soft skin adhesive
VNA	vector network analyzer
St. Dev	standard deviation
KLM	Krimholtz Leedom Matthaei
B&K	Bruel and Kjaer

Chapter 1: Introduction

Ultrasonic transcutaneous energy transmission (UTET) is a promising new technology for delivering electrical power to active biomedical implants.[1][2] In UTET an external ultrasound transducer coupled to the skin generates ultrasonic vibrations that travel through tissue to an internal ultrasonic transducer that uses the ultrasound energy to generate electrical power. A key piece of technology required to make UTET devices viable is a "dry" acoustic coupling that allows a patient to wear a device daily and for long periods of time. In contrast to the liquid or gel couplings used in diagnostic and therapeutic ultrasound applications, this dry coupling consists of a solid medium through which an external transducer delivers ultrasound to an implanted device. This thesis investigates the use of soft silicones as a dry coupling medium for UTET applications. To our knowledge it is the first study looking at dry acoustic couplings for UTET devices.

In their review paper, Basaeri et al [3] comprehensively covered the UTET field of research. Figure 1.1 summarizes the publication activity in the field of UTET from 2001 to 2015. The figure shows that there is steadily increasing activity in UTET research.

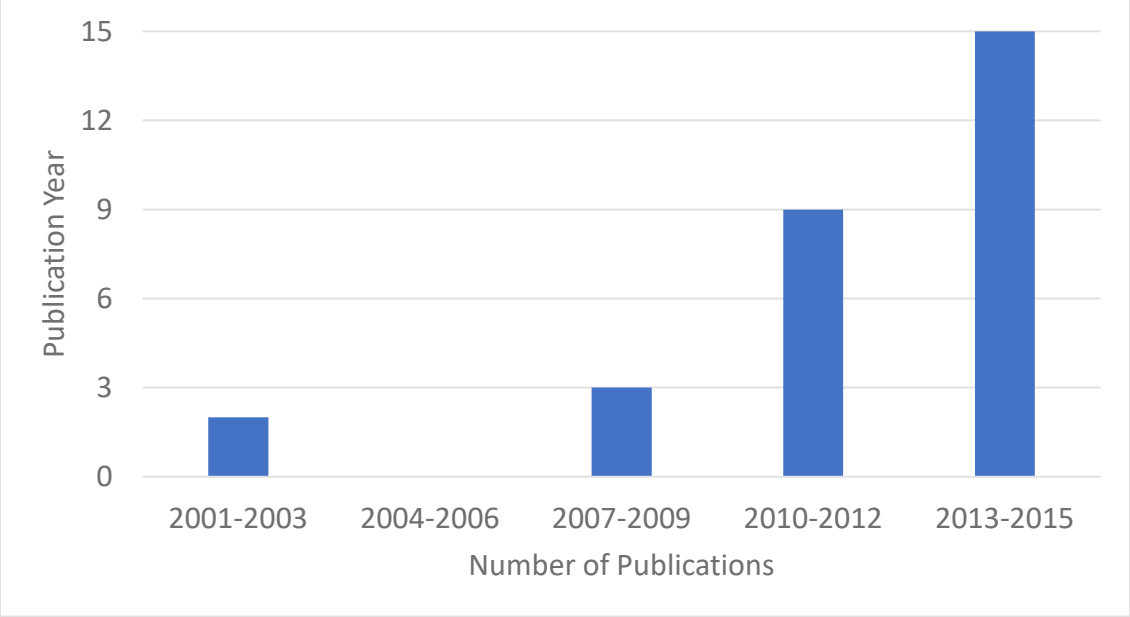

Figure 1.1: UTET Publications from 2001 to 2015

One of the first successful uses of UTET occurred in 2001 when Kawanabe et al [4] used lead zirconate titanate (PZT) transducers to transmit power and data across the tissue of a goat in vitro. Operating at 1 MHz, with a 30mm diameter, their system obtained a power transfer efficiency (PTE), that is the ratio of the electrical power produced by the receiving transducer over the electrical power sent into the transmitting transducer, of 20%.

In 2007 Arra et al [5] used PZT transducers to transfer power and data through water. Their system used two transducers, the transmit having a 30mm diameter, and the receive having a 25mm diameter. PTE values ranged from 21% at 105mm to 35% at 5mm of separation.

In 2009, Ozeri et al [1] used 15 mm diameter PZT transducers, achieving a PTE of 27% through 5mm of pig muscle. Ozeri et al [2] then improved upon their design with a kerfless Gaussian-shaded transmitter reaching a PTE of 39.1% through 5mm of pig muscle tissue. The transducers produced a Gaussian-shaped diffraction field which had smaller pressure variations in the near-field and negligible pressure side-lobes. These features resulted in the observed gain in efficiency.

In 2011, Shigeta et al [6] designed PZT transducers with operational frequencies at 1.2 MHz. The transducers, with diameters of 44mm, attained a PTE of 50.4%.

In 2013, Lee et al [6] used 50 mm diameter PZT transducers with operating frequencies in the 200-300 kHz range, and achieved a maximum PTE of 55% in water and 18% through pig tissue. Also in 2013, Leadbetter, Brown, and Adamson [7] presented their results on using 5mm diameter composite lead magnesium niobate lead titanate (PMN-PT) transducers. This material can be designed with a much higher electromechanical coupling coefficient, k_t compared to PZT. With these transducers, a maximum PTE of 45% was obtained in water.

In 2016, Radziemski et al [3] achieved a PTE of 22% transmitting through 5mm of porcine tissue operating at 1 MHz and an input power of 2 W. These articles are just small sample of the research that has been published on UTET. For a full picture of the research the articles and their findings are listed in Table 1. The data in the table was collected by Basaeri et al [3].

Author	Year	Transduction mechanism	Medium	Efficiency (%)	Input power (mW)	Output power (mW)	Operating frequency (kHz)	TX area (cm2)	RX area (cm2)	TX volume (cm3)	RX volume (cm3)	Depth (mm)	Power density (mW cm−3)	Power Intensity (mW cm−2)	η′ (%)
Kawanabe	2001	PZT-plate	Goat Tissue	20	1700	340	1000	7.07	7.07	3.534	3.534		96.21	48.09	20
Suzuki	2002	PZT-plate	Skin	20	10500	2100	1000	7.07	7.07	1.414	1.414	40	1485.15	297.03	20
Arra	2007	PZT-plate	Water	25	250	62.5	840	7.07	4.91	1.718	1.19	100	52.52	12.73	36
Lee	2007	PZT-diaphragm	Pork tissue	0.01	1.5	1.5E-4	1.5		0.38		0.031	25	0.005	0.0004	
Shigeta	2009	PZT-plate	Water	0.35	229	0.8	4200	2.688	9.62	0.174	0.467	70	1.71	0.0832	0.098
Zhu	2010	Electrostatic	Air			2.14E-5	38.78					5			
Shih	2010	PZT-diaphragm	Pork tissue	0.015	1.23	0.00018	35		0.38		0.031	60	0.0058	0.00047	
Ozeri	2010	PZT-plate	Pork tissue	27	260	70	673	1.77	1.77	0.53	0.53	5	132.1	39.55	27
Ozeri	2010	PZT-plate	Pork tissue	39.1	256	100	650	1.77	1.77	0.53	0.53	5	188.67	56.5	39.1
Mazzilli	2010	PZT-plate	Water	10	30	3	1033	19.63	0.316			50		9.49	621.2
Shigeta	2011	PZT-plate	Water	50.4	20	10.08	1200	15.2	15.2	2.86	2.86	32.3	3.52	0.66	50.4
Larson	2011	PZT-plate	Rat hind limb	0.022	2300	0.51	1000	5.31	0.01		0.001	120	510	51	11.68
Maleki	2011	PZT-plate	Tissue			0.33	2150	52.4	0.05	5.345	0.0051	30	64.7	6.6	
Sanni	2012	PZT-plate	Water	1	800	8	200	0.78	0.78	0.078	0.078	70	102.56	10.26	1
Sanni	2013	PZT-plate	Water	0.2	488	0.976	200	0.78	0.78	0.078	0.078	80	12.51	1.25	0.2
Lee	2013	PZT-plate	Pork tissue	21	15.5	3.25	255	19.63	19.63	15.7	15.7	23	0.21	0.17	21
Charthad	2014	PZT-plate	Chicken breast			0.1	1000		0.01		0.0014	30	71.43	10	
Kim	2014	PZT-plate	Pork tissue	1.4 E-4	11700	0.016	0.35		0.4		0.0152	100	1.05		0.04
He	2014	PZT-diaphragm	Pork tissue	0.096	51	0.049	40.43	23.76	0.1			22		0.49	22.81
Mazzilli	2014	PZT-plate	Water	1.6	1750	28	1000	21.3	0.3			105		93.33	113.6
Ozeri	2014	PZT-plate	Water			20	765	1.77	1.77	0.53	0.53	150	37.73	11.3	

Author	Year	Transduction mechanism	Medium	Efficiency (%)	Input power (mW)	Output power (mW)	Operating frequency (kHz)	TX area (cm2)	RX area (cm2)	TX volume (cm3)	RX volume (cm3)	Depth (mm)	Power density (mW cm−3)	Power Intensity (mW cm−2)	η′ (%)
Shmilovitz	2014	PZT-plate	Water			35	720	1.77	1.77	0.53	0.53	85	66.04	19.77	
Chou	2014	PZT-plate	Oil	1				0.15	0.15	0.046	0.046	25			1
Lee	2014	PZT-plate	Pork tissue	18	15.5	2.6	250	19.63	19.63	15.7	15.7	18	0.165	0.13	18
Song	2015	PZT-plate	Water	0.15	7704	12	1150	10.7	0.08	2.14	0.016	200	750	150	20.06
Seo	2015	PZT-plate	Water				10000					20			
Fang	2015	PZT-plate	Pork tissue			3	3500		1.1		0.066	4		2.73	
Zhou	2015	PZT-plate	Water				672		1.28		0.256	67			
Christensen	2015	PZT-plate	Water	1.95	62.5	1.22	1058	1.29	1.29	0.24	0.24	40	5.08	0.94	1.95
Christensen	2015	PZT-diaphragm	Water	0.016	62.5	0.001	3.5	1.29	0.5	0.24	0.005	40	0.2	0.002	0.041
Vihvelin	2016	PZT-plate	Porcine tissue	25			1300	0.5	0.5	0.06	0.06	5			25
Radziemski	2016	PZT-plate	Porcine tissue	22	2000	440	1000	4.91	4.91			5		89.61	22
Seo	2016	PZT-plate	Rat hind limb		0.12		1850		0.005			8.8			

Table 1: Summary of UTET Research

1.1 Design Options

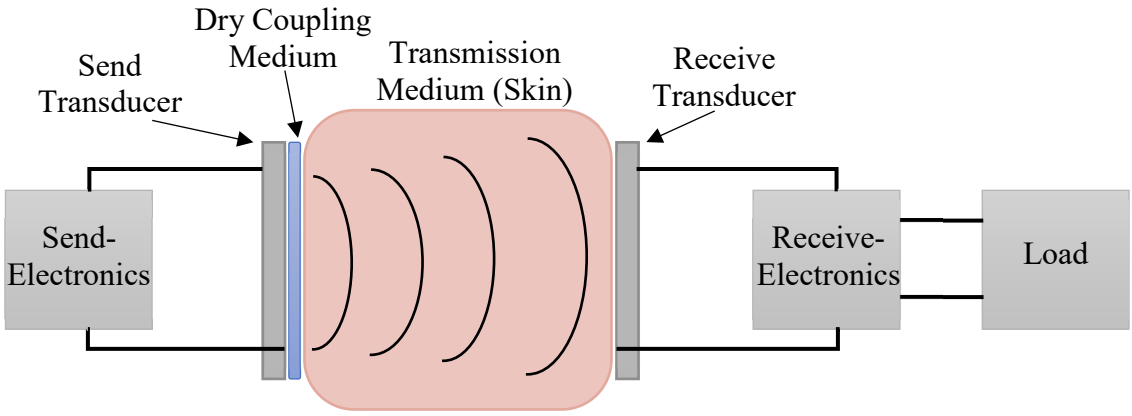

Figure 1.2: Diagram of the UTET device.

In the UTET device, the transmit unit contains electronics that deliver an electric signal to the piezoelectric transducer which converts the electric signal to an acoustic signal. This signal is transferred into the transmission medium (human skin) through the coupling medium. Implanted under the patient's skin is the receive unit. The receive unit contains a piezoelectric transducer which converts the acoustic signal back into an electric signal. The receive-electronics convert this electric signal into a form usable by an implanted device (e.g. charge on a capacitor or battery). This signal pathway is represented in Figure 1.2. The UTET device also typically contains magnets within both the send and the receive units. These magnets align the transducers, maximizing the overlap of the transmitted ultrasound beam with the receive transducer. The magnets also provide a small compressive force which gently holds the transmit unit to the patient's head.

For traditional ultrasound applications such as diagnostic imaging, a coupling gel is typically used to acoustically interface a transducer with the patient. However, in an application like UTET where ultrasound is delivered continuously over many hours, coupling gel is likely to dry out or wash away over time and so a solid-state solution is needed. There exist dry coupling solutions for non-destructive testing (NDT) applications, however these couplings are made to transfer ultrasound into material with much higher acoustic impedances than skin, usually operate at much higher power levels and

frequencies than those used in UTET, and are too stiff to couple well to soft tissue. These discrepancies make the NDT dry coupling materials inappropriate for UTET applications.

Most implantable devices that are powered wirelessly use electromagnetic (EM) induction. A major problem with EM devices is their size limit. As the induction coils get smaller they rapidly become less efficient at transferring power. Thus, the EM devices have reached a barrier to size that cannot be surpassed. These larger devices make it difficult to find suitable implant locations but can also be quite bulky and noticeable on the user's head (Figure 1.3). Examples of devices that use EM to power them are miniaturized electromyogram systems, powering a camera capsule for bowel imaging, and implanted hearing aids [8].

Figure 1.3: EM Induction Coil for Cochlear Implant

The advantage of UTET over EM is that is can bypass the size limit imposed by the poor efficiency of small EM devices. These smaller devices allow for greater range of implantable sites on the body, reduced surgery time, increased magnetic resonance imaging compatibility due to smaller alignment magnets, and better aesthetics for the patient.

For interfacing with human skin, a softer material is required. One class of material that meets these requirements is silicone. Silicones have an acoustic impedance close to that of skin and can be made to have a much lower stiffness compared to NDT dry coupling materials. Additionally, silicone can be formulated as a pressure sensitive adhesive (PSA) which provides a better connection to the skin through wetting (increasing the surface area

in contact with the skin).[9] The alignment magnets' compressive force aids in the adhesive's wetting of the skin. The adhesive also provides a bond to the skin. This bond, plus the force provided by the magnets, allows the UTET device to withstand forces that would detach the device due to the patient's motion.

This thesis describes the development pathway towards a dry coupling system suitable for use in a UTET designed for use in applications powering implanted hearing aids. The final system developed in this work consists of Sylgard 184 which encases the external transducer and an adhesive layer of soft silicone adhesive deposited on the surface of the Sylgard (Figure 1.4). The Sylgard's acoustic impedance is matched to human skin by loading it with zinc oxide powder to allow for maximum power transfer and minimization of reflection losses. This optimization increased the PTE of the system by 23.5%. This is a meaningful increase in efficiency, demonstrated by the fact that large manufacturers will add a new product with smaller differences in capacity. Energizer, for example, makes continuous low drain batteries like their 346 and 317 batteries with a difference of only 17.4% in battery capacity. The design of an adhesive layer on top of a dry acoustically matched coupling layer for transmission of power into human skin has not previously been investigated.

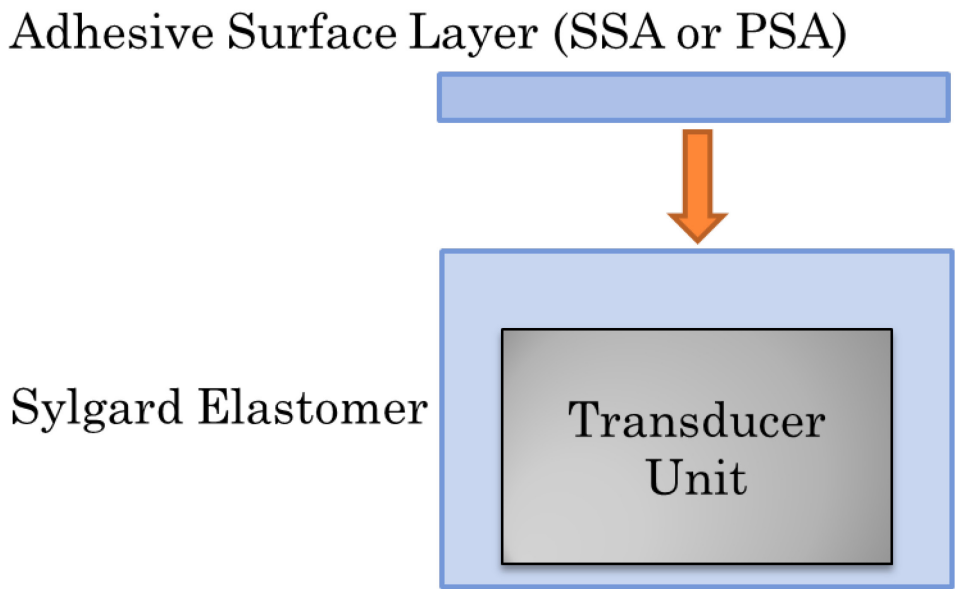

Figure 1.4: Final Design Concept of the Dry Coupling

1.2 Dry Coupling Design Requirements

The design of the dry coupling material conformed to a number of requirements and constraints that defined the application. The most important of these are detailed below:

1. **Minimal Energy Loss**

The dry coupling material must pass ultrasound through it while minimizing energy lost due to reflections and attenuation.

Reflection

Reflection losses occur due to acoustic impedance mismatch between the skin and the dry coupling material. Air bubbles play a major role in reflection losses because the acoustic impedance of air is 4 orders of magnitude lower than that of skin. This difference in acoustic impedance means that any sound that encounters an air bubble will be almost completely scattered.

When a sound wave reaches an interface between different materials it is reflected back due to the change in characteristic acoustic impedance between materials. Characteristic acoustic impedance is an inherent property of every material. It is the product of the density of the material multiplied by the speed of sound through the material and represented by the symbol Z.

Equation 1

$$Z = \rho c$$

Where ρ is the density and c is the speed of sound. The fraction of the amplitude of the pressure wave reflected is the reflectivity and is represented by the symbol R. The reflectivity can be calculated by dividing the difference in acoustic impedance between two materials by their sum.

Equation 2

$$R = \frac{Z1 - Z2}{Z1 + Z2}$$

This equation predicts that the greater the difference in acoustic impedances between the two media, the greater the reflectance. This mechanism of reflection is demonstrated by Figure 1.5.

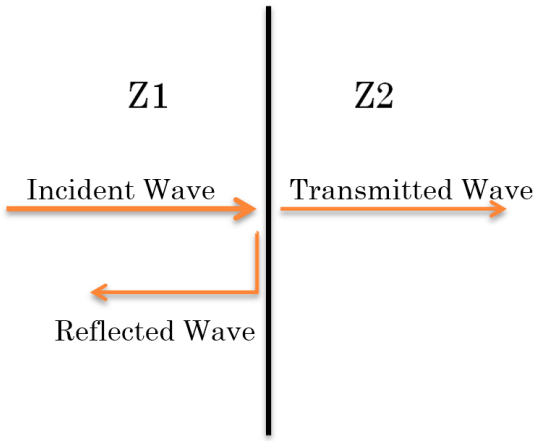

Figure 1.5: Acoustic Reflection

The issue of coupling the external ultrasound transducer to the internal transducer requires coupling and transmission of the ultrasound signal through human tissue. Human skin has a much different acoustic impedance (1.659 – 2.115 MRayl)[10] compared to that of materials typically used to make ultrasound transducers (e.g. 35 MRayl for PZT)[11] and an even greater difference in impedance to that of air (400 Rayl).[11] When a stiff transducer material is pressed against the skin, ridges in the skin form air-gaps that almost completely reflect the ultrasound due to the extremely high impedance mismatch between the transducer and air, inhibiting the transmission of sound from the external unit to the internal unit. This issue can be addressed by using an acoustic coupling material capable of wetting the skin.

It is also vital that air bubbles be prevented from forming in the materials used for the coupling. Figure 1.6 shows how ultrasound is almost completely blocked by air bubbles

encountered while traveling through a material. The top pair of images show an object being imaged (the red ball of clay) on the left and the ultrasound image on the right displaying a cross section of the object's surface geometry. The bottom pair of images shows a material (silicone) that is filled with small air bubbles on top of the clay ball. The ultrasound image shows that air bubbles nearly completely reflect the ultrasound back to the imaging transducer and no ultrasound was able to penetrate through the silicone to image the clay ball.

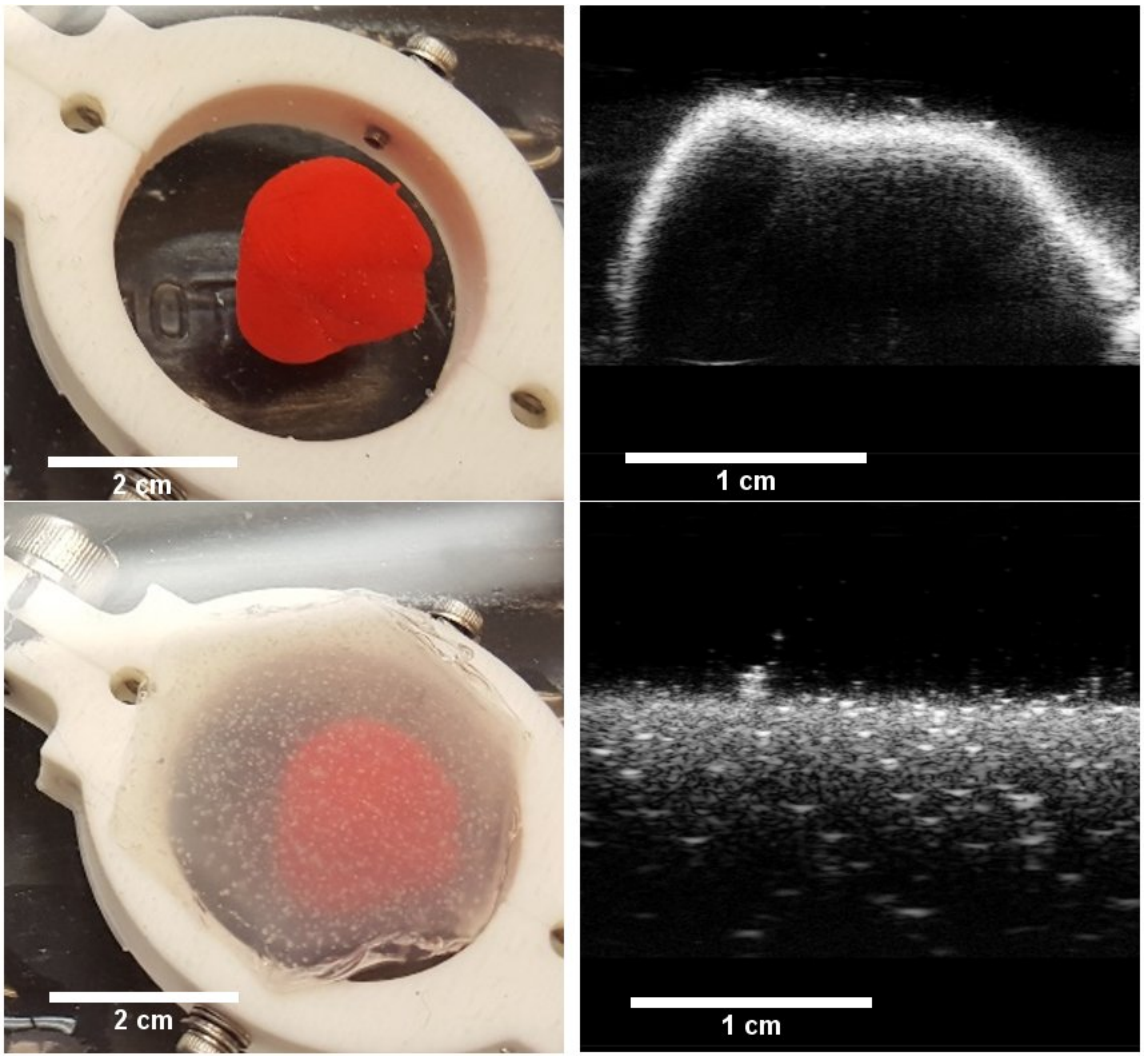

Figure 1.6: Ultrasound Blocked by Bubbles in Silicone

Attenuation

Attenuation losses are a combination of absorption, diffraction and scattering. Absorption losses can be mainly attributed to the conversion of acoustic energy to heat. The more viscous a medium is, the more heat is generated due to friction and the more acoustic energy is lost.

Diffraction losses are not significant because the devices operate in the near field.

Scattering losses occur primarily due to scattering from particles in the medium that are smaller than a wavelength and exhibit an impedance mismatch with their surroundings. The energy lost due to scattering is increased as the size of the particle increases relative to the wavelength and as the difference of acoustic properties between the particle and the medium increases. The loss due to scattering is also linearly dependent on the density of particles within the material.[12]

Overall, attenuation losses increase with particle size, particle density, operating frequency, viscosity of the medium and the thickness of the material that the sound must travel through.[13] Losses due to reflection occur due to acoustic impedance mismatch. Reflection losses can be minimized by eliminating air gaps and matching the acoustic impedance of the dry coupling to the acoustic impedance of skin. Attenuation losses can be minimized by designing the dry coupling to be as thin as possible without compromising the dry coupling's ability to protect the transducer against impact damage and allowing it to have sufficient malleability to conform to the skin.

2. Biocompatible on Human Skin

The dry coupling material must be in contact with human skin for long periods of time, thus it is important for the material to be biocompatible with skin. The material will only be in contact with the epidermis. One important aspect of biocompatibility is the water vapour permeability. The skin gains and loses hydration throughout the day by water absorbing through and evaporating from the surface of the skin. If the moisture stays in contact with the skin for prolonged periods of time, the skin can become macerated.[14] Macerated skin is softer than normal and has a pale or whitish discolouration. When the skin is in this weaker condition, it is more susceptible to bacterial or fungal infection. If the material in contact with the skin has the ability to allow moisture vapour to escape it can

prevent maceration and subsequent infection of the skin. The material must also not be cytotoxic to the cells (mostly keratinocytes) that live near the surface of the skin and must not leach cytotoxic chemicals into the skin. The epidermis is not vascularized and therefore depends on oxygen from the surrounding air to diffuse though to the cells.[15] Another important characteristic for biocompatibility is therefore oxygen permeability. Materials that meet these requirements can be found in use as skin pressure sensitive adhesives (PSAs). In general, these can be broken down into acrylics, polyurethanes, polyisobutylenes and silicones.[16]

3. Adhere to Skin

The material must be able to adhere to human skin for long periods of time. Adhesion will allow the device to stay in place while the patient is moving throughout their day. Adhesion also allows for greater conformability to the surface topography of the skin. Conforming to the surface topography allows for a stronger bond to the skin and enables better transmission of ultrasound by excluding air gaps between the dry coupling and the skin. The adhesion depends on a number of factors including the surface energy of the dry coupling and the skin, and the surface topography of both surfaces. Adhesion is very difficult to design for in vivo due to the large variations in these factors. On a single person factors like the oiliness, sweatiness (i.e. the trans epidermal water loss or TEWL), soil level and topography vary greatly from one location to another; for instance the TEWL is typically 9.7 g/m^2h on the forearm and 101.4 g/m^2h on the palm.[17] Certainly, the low surface energy and multiple other confounding factors make adhering to skin very difficult and the dry coupling material will have to strike a balance between high adhesion, which may cause mechanical trauma to the skin upon removal, and low adhesion that would be inadequate to hold the device in place and form a good acoustic connection.

Fortunately, because of the importance of skin adhesion for a wide range of therapeutic applications, a number of pressure sensitive adhesive materials have been developed that can achieve good adhesion to skin.

Polyurethanes

These polymers are reported to exhibit a high degree of water absorption and water vapor transmission capabilities, and to have a good balance of cohesion and adhesion properties.[16]

Acrylics

Acrylic PSAs are single-component systems that are inherently tacky without requiring additional compounding. Acrylic polymers with a wide range of adhesive properties can be prepared by copolymerizing different monomers.[16]

Silicone

Silicone PSAs are made of silicate resin and silicone polymer. The unique molecular structure of silicone imparts good skin-adhesion properties and favorable diffusion characteristics creating excellent gas and liquid permeability.[16]

Polyisobutylenes

Polyisobutylenes (PIBs) are paraffinic hydrocarbon polymers with low moisture and gas permeability, and are relatively inert, odorless and nontoxic. Polyisobutylene PSAs are generally composed of mixtures of high and low molecular weight PIBs. Their molecular structure leads to chemical inertness and good resistance to weathering, ageing, heat and chemicals, however it also results in low air, moisture and gas permeability.[16]

4. **Comfortable**

The dry coupling must be comfortable to wear for long periods of time. If the coupling material is too hard, too adhering, non-permeable to water or oxygen or too heavy, the device may feel uncomfortable to wear which will discourage the patient from using the device or may cause undue pain. A goal of the dry coupling's design is to cause minimal discomfort.

Additionally, if the compressive pressure produced by the magnets exceeds 33mmHg (4.4 kPa), there is a risk of the patient developing pressure ulcers.[18] According to MED-EL, a company that manufactures hearing aids that use EM induction to wirelessly power their hearing aid implants, the MED-EL Bonebridge applies up to 7.5mmHg of pressure while the Cochlear BAHA Attract applies between 30 and 45mmHg of pressure.[19] As a result

of the higher pressure, the BAHA Attract has a limited period of use before the patient must remove the hearing aid.

5. **Low Cost/Replaceable**

Finally, the dry coupling must be low cost and replaceable. The dry coupling may fail due to a number of reasons. The adhesive layer is particularly vulnerable due to its softness and relatively low tensile strength. The adhesive could wear out either through mechanical failure, or becoming too soiled to adhere well. If mechanical failure is a common occurrence it is important that the dry coupling be inexpensive to manufacture and easily replaced.

1.3 Reason for Choosing Silicone

Silicone was selected because it had been used as acoustic lenses for medical ultrasound probes, had good biocompatibility on the skin and is in widespread use in medical skin adhesive applications such as wound dressings.[9] Benedek and Feldstein describe silicone adhesives as having "such unique benefits as inherently good compatibility with skin, skin adhesion over time, and high moisture vapour and oxygen transmission rates."[9] They describe silicone as having inherently good properties for the purpose of use as a biocompatible pressure sensitive adhesive (PSA). These properties include their flexibility over a wide temperature range, low interactions between molecules, low surface tension, transparency to ultraviolet light, stability at high and low-temperatures, very high electrical insulation properties, resistance to chemical attack, and excellent weathering resistance. The most important properties for the purpose of the dry coupling material are silicone's low surface-energy adhesion, high gas permeability and acoustic impedance close to that of human skin.

All silicone PSAs have surface energy low enough to allow them to adhere to a variety of skin types. The low surface energy also gives the ability to wet onto, and conform to, the skin's topography. Silicone PSAs also have low adhesion to hair follicles making their removal much less traumatic than other typically used medical adhesives such as acrylates and polyurethanes.[20] Resistance to moisture, UV radiation, oxidative effects, and biological attacks are other factors leading to their acceptance in medical applications.[9]

It is desirable for medical PSAs to be permeable to gases and water vapour in order to avoid maceration of the skin. The MVTR (moisture vapour transmission rate) is used to quantify the amount of moisture an adhesive or film will transmit over a given time. Despite silicones being very hydrophobic, medical silicone adhesives have similar MVTR values to other adhesives such as polyurethanes and acrylics, and have been used in many medical applications, including wound management, diagnostic devices, and ostomy appliances.[9]

Finally, silicone's similar acoustic impedance to that of human skin made it a reasonable choice for the dry coupling material. Silicone is commonly used as an acoustic material in ultrasonic applications, particularly in lenses for medical ultrasound probes. Fuji et al. found that silicone had excellent impedance matching with the human body and that adjusting the amount of filler in the silicone could further match the acoustic impedance to that of the human body.[21] These properties make silicone a good candidate for the development of a dry coupling for a UTET device.

1.4 Chapter Summaries

This thesis contains two main chapters. Chapter 2 on manufacturing describes the development of processes suitable for producing dry coupling systems. After investigating a number of designs, a dry coupling system consisting of a mechanically tough but non-adhesive silicone matched to the skin's acoustic impedance and a thin adhesive silicone layer was developed. The manufacturing chapter describes the following processes developed in order to produce these devices:

- A method for doping ZnO powder into Sylgard 184 to increase the material's acoustic impedance to match the acoustic impedance of skin.
- Methods for removing bubbles formed during fabrication of the dry coupling.
- Design of moulds used to create thick and thin cylindrical samples with flat, parallel surfaces
- A process for adding an adhesive layer to a non-adhesive silicone substrate.
- Procedures for curing thick samples, thin samples and the adhesive layer

Chapter 3 on experimental verification and validation examines the effectiveness of different manufacturing techniques through a combination of experimentation and

theoretical analysis and measures the performance of the dry coupling system. The experiments described in this chapter are outlined in the following table:

HDG	Title	Purpose	Result
3.2	Water Bath Test for Baseline Efficiency	Get a baseline measurement of efficiency to compare dry coupling PTE.	Showed that silicone was a promising material for a dry coupling with low loss.
3.3	Applied Pressure Effect on Power Transfer Efficiency	Find the lowest applied pressure at which an acceptably high PTE can be attained.	Acceptable efficiency could be achieved at clinically acceptable contact pressures through an adhesive silicone sample.
3.5	Reflectivity and Speed of Sound at Various ZnO Loading levels	Investigate a strategy to minimize reflections by controlling the acoustic impedance of the silicone through loading with ZnO powder.	ZnO loading silicone was an effective way of increasing the acoustic impedance of the dry coupling.
3.6	Measuring Attenuation of Silicone and Skin Impedance Confirmation	The acoustic attenuation in the loaded silicone must be characterized to obtain a complete picture of the acoustic behaviour of the material.	The attenuation of the matched silicone was high enough to be a concern for thick dry coupling layers.
3.7	Adhesive Layer Thickness	The thickness of the adhesive layer was measured to model its effect on the PTE of the system.	A simple method to measure the thickness of the adhesive layer of the dry coupling was demonstrated.

HDG	Title	Purpose	Result
3.8	Power Transfer Efficiency	Determined if there is an efficiency advantage to using ZnO to load the dry coupling for acoustic impedance matching.	Showed ZnO loading confers an efficiency advantage over unloaded silicone and that a low-loss adhesive layer can be made.
3.9	KLM Model of System Behaviour	Model was used to understand the Power Transfer Efficiency experimental data	The results from the PTE data is reflected in the model. The model could be used in future work for optimization.
3.10	Vibration Test	Determine the effectiveness of the adhesive layer of the dry coupling.	Adhesive could withstand extreme loading on a surface with low adhesion properties for a much longer period than a user would normally wear the device.
3.11	Real World Validation Test	Test the adhesive quality of the samples and to test how comfortable they were to have on a person's skin.	The adhesive is adequate for use in real world conditions not only for its strength but it's comfort, removability and its ability to be washed and regain strength.

Table 2: Summary of Experiments

The procedures developed over the course of this thesis for manufacturing and testing a dry coupling material represent a practical, repeatable means by which other dry coupling materials for UTET applications can be developed. The methods used for determining the appropriate loading fraction to achieve a desired acoustic impedance could be used to tailor UTET dry couplings to work in different areas of the body or even to individual subjects.

From the results from this thesis, a clinically viable UTET device with a dry acoustic coupling to skin could be designed and built.

Chapter 2: Manufacturing

This chapter describes the manufacturing process for the matched silicone and soft skin adhesive layer. Many iterations were spent ironing out different problems during the manufacturing process.

This chapter will discuss the development of silicone as an acoustic impedance matching material; issues and solutions with bubble removal; the development of moulds to create thick and thin cylindrical samples with flat, parallel surfaces; the process of adding adhesive properties to the Sylgard 184 samples; and finally, the procedures for curing thick samples, thin samples, and the adhesive layer.

2.1 Early Work

As a first step towards designing a dry coupling, an appropriate material had to be selected. While there are a number of different biocompatible polymers in widespread use as detailed in Chapter 1, silicones were investigated in this study as potential dry coupling materials due to their biocompatibility and previous use as both acoustic material for ultrasonic probe lenses and a pressure sensitive adhesive for wound dressings. There are thousands of different silicone compositions available, many of which are proprietary and hardly any of which have specified acoustic properties at ultrasonic frequencies. Rather than try to systematically determine the best possible silicone for this application, a few specific materials were selected and tried. Lessons from each silicone informed selection of the next until a satisfactory dry coupling design was achieved.

This section describes some of the key qualitative and quantitative observations that drove decisions about which silicones to use and which silicone properties were important to the design. For the sake of brevity, the author has omitted experimental details and focused on results. For quantitative experiments, full descriptions of experimental methods are given in Chapter 3.

As a starting point for investigation into appropriate materials, Polytek Platsil Gel 10 and Gel 00 were ordered and used. This silicone is part of a class of platinum-catalyzed silicones with excellent biocompatible properties. The Platsil Gel 10 was designed for use in casting special effects prosthetics and were chosen because they were designed to

maintain contact with the skin for extended periods of time since actors wear the masks and other prosthetics made out of the material for prolonged periods. It was thought that for comfort and skin conformity reasons a very soft material would be preferred and the Gel 10 and Gel 00 formulations were both very soft silicones.

Unfortunately, both Platsil Gel 10 and Gel 00 generated bubbles while curing to the point where the material looked cloudy after curing at room temperature and pressure. These samples were 2 cm in thickness and 6 cm in width and length. The silicone, no matter what its thickness, required 24 hours to be fully cured. The cloudiness became apparent gradually over the curing time, with the silicone beginning as a clear liquid after mixing, and gradually taking on the milky-white appearance seen in Figure 2.1 through the 24-hour cure. The optical opacity was an indication that microscopic bubbles were forming during the curing process. The source of the bubbles could have been from hydrogen molecules not completely used up in the cure reaction or from dissolved air entrapped in the mixture.[22]

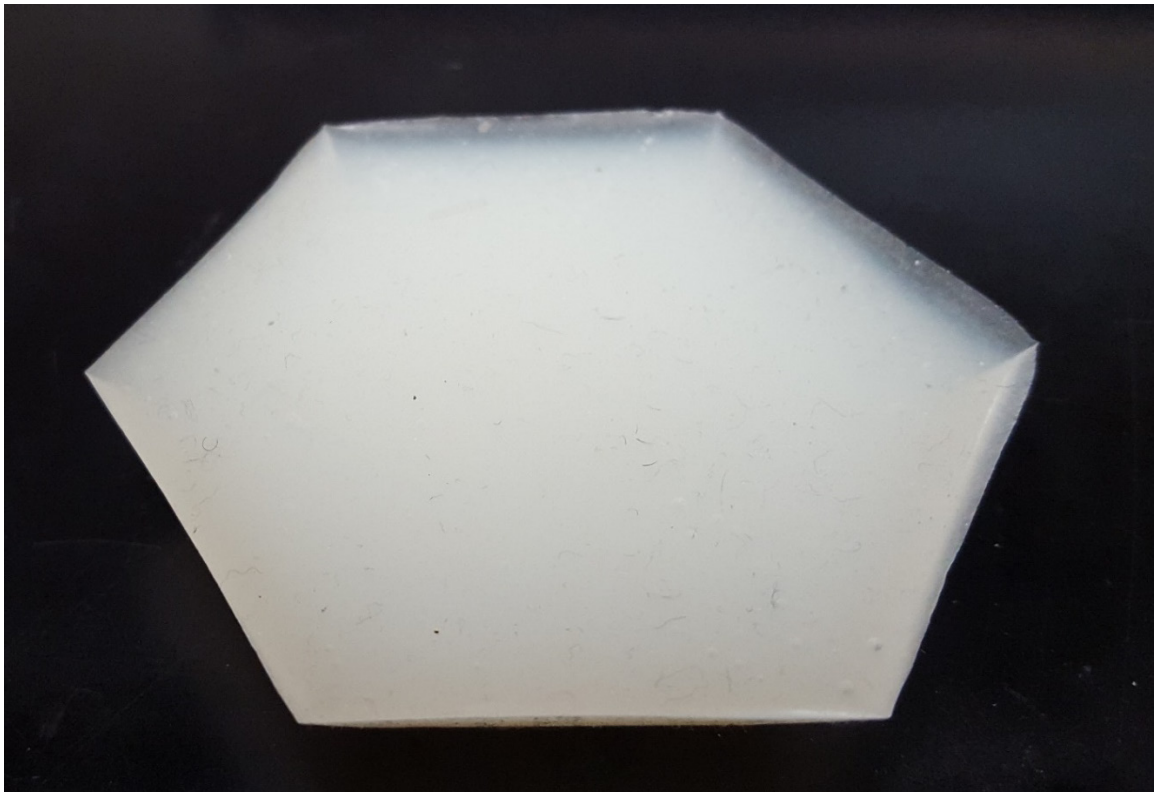

Figure 2.1: Cured sample of Platsil at room temperature and pressure

In order to address this issue, the author tried curing the silicone in a pressure chamber. It was hypothesized that curing the silicone under high pressure would prevent bubbles from nucleating within the silicone thus preventing the formation of bubbles. A pressure chamber was built (Figure 2.2) and the Platsil was cured at 100 psi for the full cure.

Figure 2.2: Pressure chamber for high pressure curing of Platsil

When the silicone was removed from the pressure chamber, it initially appeared to have worked. The silicone was completely clear throughout the bulk of the material. However, given time at atmospheric pressure, bubbles began nucleating at the surface as shown in Figure 2.3. Several attempts were made at curing under even higher pressure and by heating the pressure chamber, achieving a maximum pressure of 150 psi for 24 hours, however this was not able to prevent the bubbles from nucleating after being exposed to atmospheric pressure.

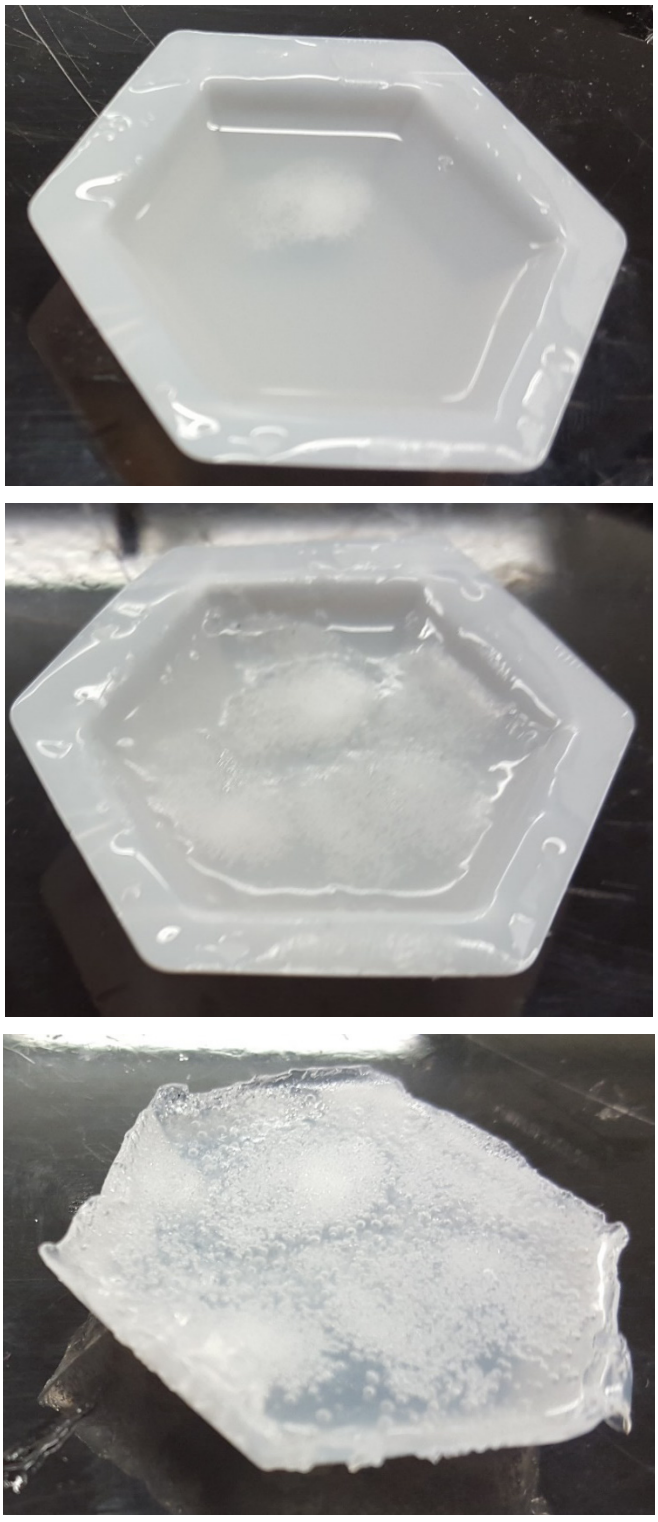

Figure 2.3: Progression of nucleating and expanding bubbles at atmospheric pressure in Platsil after high pressure cure

The failure of high-pressure curing to prevent the formation of bubbles led us to try the opposite approach, namely to cure the silicone under vacuum (Figure 2.4). The theory was that instead of suppressing bubble formation, vacuum curing would draw bubbles out to the surface during the curing process, resulting in a bubble-free material. This method was partially effective. Bubbles were pulled to the surface at the beginning of the cure, but eventually the curing process made the silicone viscous enough that the material would hold the shape of the surface after the bubbles had popped, leaving it pock marked and very uneven. Even after the material became this viscous the curing reaction would generate bubbles within the bulk of the silicone that could not escape the sample (Figure 2.5).

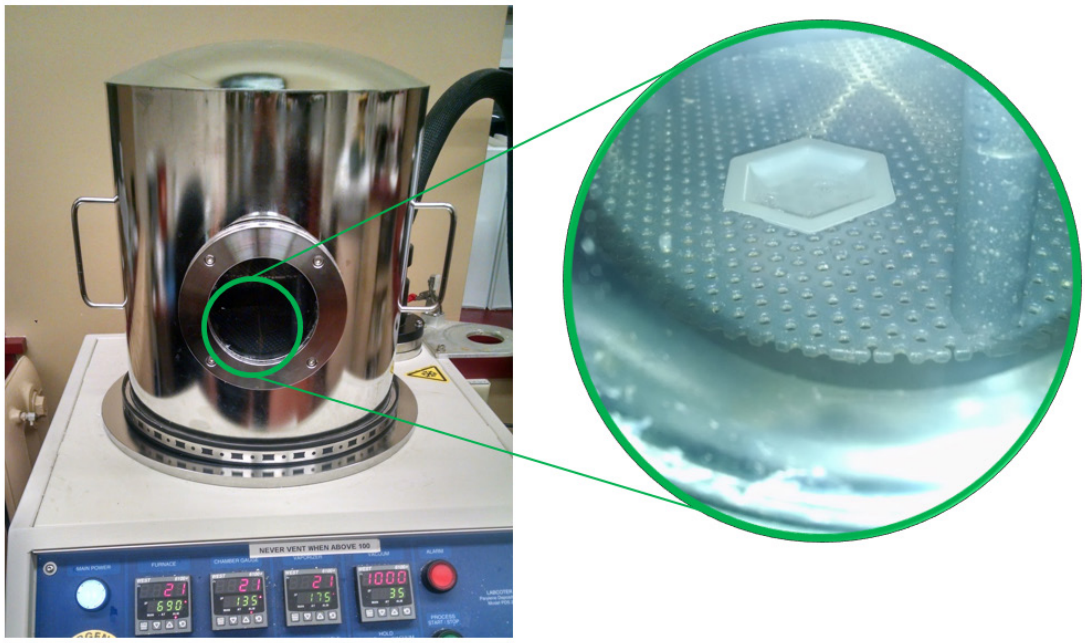

Figure 2.4: Vacuum Degassing of Platsil

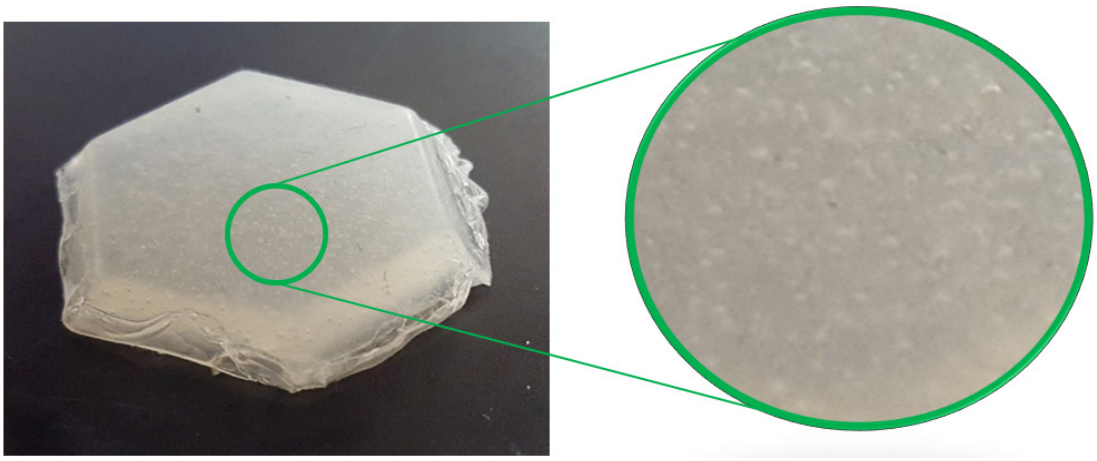

Figure 2.5: Bubbles Still Remain in Platsil After Vacuum Degassing

Because of the difficulty in removing bubbles entrapped within the Platsil silicones it was decided to find a different silicone that was inherently bubble-free after curing. Epoxies ETC makes a silicone called Optically Clear Silicone Potting and Encapsulating Compound 20-1625. Since the author had found that optical opacity was a good indicator of the presence of bubbles it seemed likely that a silicone designed to be optically clear after curing would be bubble free. This silicone was also much softer than even the Platsil Gel 00 and, unlike the PlatSil silicone, it was mildly adhesive and would adhere to skin after curing. The adhesive property would later be found to be advantageous and, as a result, adhesion would be added as a design requirement.

These samples were cured in smaller moulds and were a maximum of 1 cm in height and 3 cm in length and width. The samples were injected into the moulds using a gun and cartridge system (Triggerbond 50 ml) with a nozzle that mixed the two-part solution as it was dispensed. The silicone cured in 4 hours at room temperature into a clear, tacky and very soft, solid gel (see Figure 2.6).

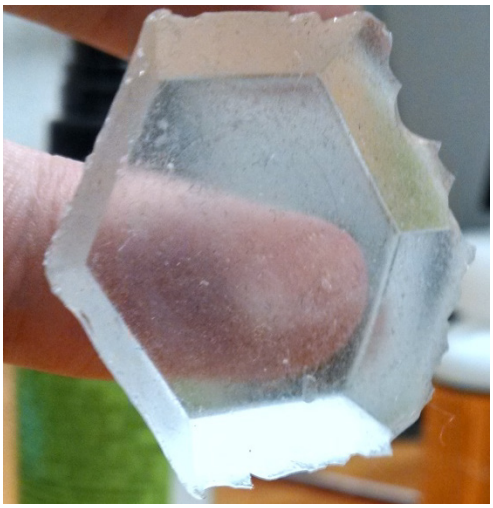

Figure 2.6: Cured Epoxies Etc. Optically Clear Silicone Potting and Encapsulating Compound

The efficiency of ultrasound transmission through an interface between skin and this silicone was measured for different contact pressures (see Section 3.3). The results of the test showed that after adhesion occurred, very high levels of efficiency could be achieved with extremely small compressive forces. This demonstrated that having good surface adhesion was critical to achieving the design goals.

The tackiness and wetting of the adhesive meant that the silicone was able to conform to the geometry of the skin, providing contact with a greater surface area of the skin and pushing out the air entrapped between the skin and the dry coupling thus increasing the power transfer efficiency of the dry coupling (Figure 2.7). As an example of surface wetting, Figure 2.8 shows a Sylgard sample with an adhesive coating as it is applied to a table with a rough, textured surface. As the sample is placed on the table, the adhesive wets and conforms to the surface geometry which is apparent from the darker region under the sample. In addition to removing entrapped air, the adhesive would aid the magnets that were used to align and hold the external device to the head, providing a more secure attachment than a non-adhering dry coupling that relied on magnetic forces alone.

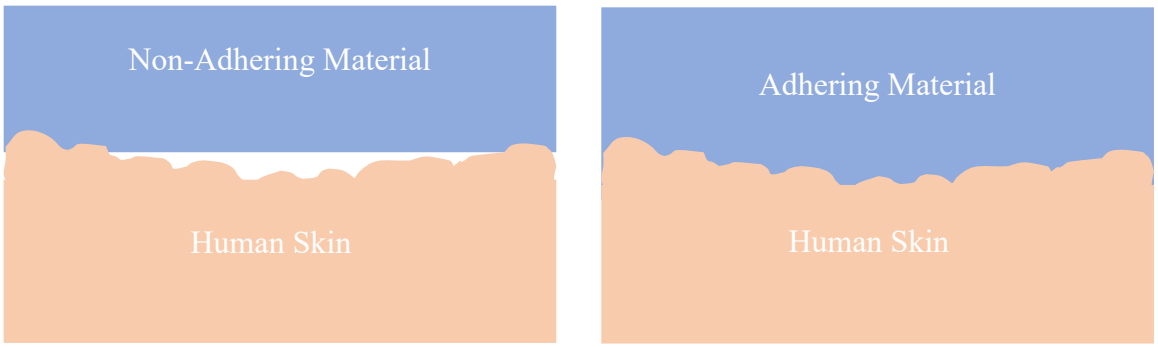

Figure 2.7: Adhering materials conform to the skin's topography. This helps remove air gaps from the interface between the dry coupling and the skin. These air gaps block the transfer of ultrasound and greatly reduce the power transfer efficiency of the UTET device.

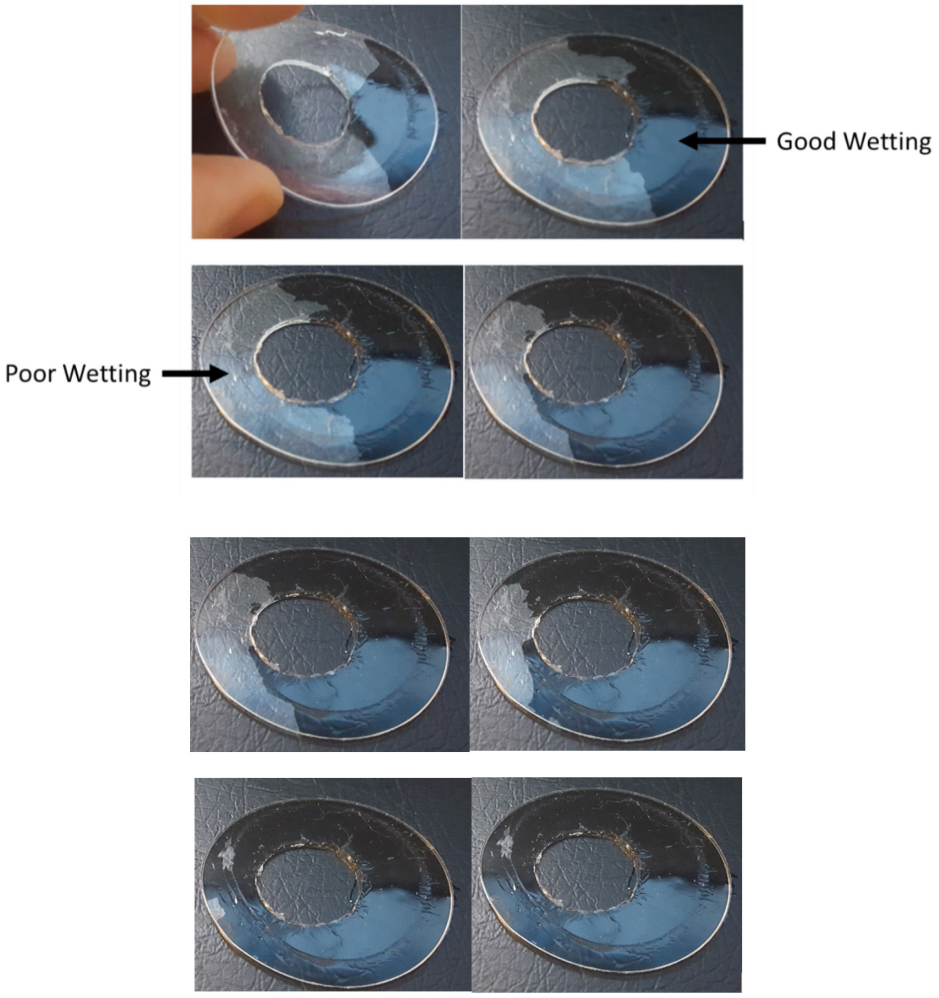

Figure 2.8: Adhesive silicone pushing out air gap as it conforms to the surface's geometry.

To reduce reflection losses, the dry coupling needed to be matched to the acoustic impedance of human skin. Matching to skin is a good approach since, ideally, the surgery will leave only a layer of skin in-between the transmit and receive units. In any case, this method allows the manufacturer to tailor the acoustic impedance to whatever is needed in order to maximize PTE. The acoustic impedance of the silicone was found by measuring the density of the sample and measuring the time of flight for a pulse of ultrasound to travel through the sample, giving the speed of sound in the silicone. The method is represented diagrammatically in Figure 2.9 derived in the following equations.

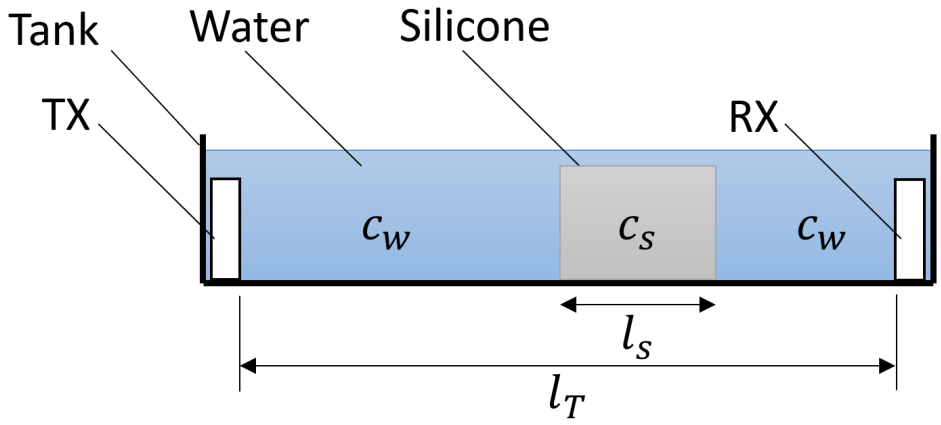

Figure 2.9: Diagram of Speed of Sound Measurement

$$l_w = l_T - l_s$$

$$t = \frac{l_w}{c_w} + \frac{l_s}{c_s}$$

$$c_s = \frac{l_s}{\left(t - \frac{(l_T - l_s)}{c_w}\right)}$$

The speed of sound, c_s, is calculated from the known speed of sound in water, c_w, and the measured l_T, l_s, and t, which are the length between transducers, length of the silicone, and the time of flight, respectively.

The product of the density and the speed of sound gives the acoustic impedance. The acoustic impedance was measured to be 1.0 MRayl +/- 0.015 MRayl. This is fairly low

compared to the acoustic impedance of human skin which can be as high as 2.1 MRayl [23].

After attempting to use silicone thinning and thickening agents mixed into the Epoxies ETC silicone while curing in an attempt to affect a change in the acoustic impedance of the silicone, it was apparent that these agents were not effective. While the Epoxies Etc. silicone exhibited many desirable properties, there were some serious issues with it as well. The silicone only came as one formulation and the thinning and thickening agents being ineffective meant that it would be difficult to match this silicone to human skin's acoustic impedance. Later, when ZnO loading was used as a method to increase acoustic impedance (discussed further in Section 2.2), it was found that when loaded at levels necessary to achieve matching with skin, squeezing the sample caused it to tear apart. Additionally, the unloaded Epoxies Etc. silicone was very soft and easily damaged which made it a poor choice as a protective external casing for the fragile transducer of the UTET device. Finally, the silicone formulation was proprietary and the supplier was unwilling to provide information as to the chemistry or biocompatibility of the material. It was decided to pursue further materials with an aim of finding one that could achieve a controllable acoustic impedance, was robust enough to protect the UTET transducer and withstanding physical damage while still maintaining a high degree of surface wetting and adhesiveness.

In general, there is a trade-off with silicones between toughness and adhesiveness with tough materials tending to be elastomers and adhesive materials being more gel-like and exhibiting higher viscoelasticity and low strength.[24] After investigation into the available options it was decided that the desired dry coupling requirements could be best met by using a composite of two materials – a tough silicone elastomer to encapsulate the transducer and a thin layer of adhesive silicone on the surface. Since adhesive silicones generally adhere well to other silicones, the interface between the two materials would be strong. Dow Corning Sylgard 184 was selected as the elastomer because it was a tough material and cured to a clear (bubble-free) elastomer. Sylgard 184 is a two-part system consisting of a liquid base and a cross-linking agent.

If the adhesive layer was kept thin, then good acoustic transmission could be achieved by only controlling the acoustic impedance of the elastomer material. At first, the hope was

that some control of impedance, by manipulating the ratio of crosslinking agent to base, could be obtained. It was thought that increasing the amount of crosslinking in the Sylgard would make the material stiffer, thus increasing the acoustic impedance. As it turned out, this approach proved ineffective. The alternative approach of increasing acoustic impedance by increasing the Sylgard's density by doping with ZnO powder proved a more fruitful avenue. The exploration of these two methods for altering the acoustic impedance of Sylgard are discussed in Section 2.2 of this chapter.

Since Sylgard, is non-adhesive, desired surface adhesive properties would have to be obtained by either adding another material to the cured Sylgard or mixing the material into uncured Sylgard. These approaches are detail in Section 2.3.

2.2 Acoustic Impedance Matching and Bubble Removal

In order to reduce the losses from reflections, a material with an acoustic impedance matched to human skin's acoustic impedance was needed. It was hypothesized that increasing the concentration of the crosslinking agent would increase the elastic modulus of the Sylgard (Figure 2.10), therefore increasing the speed of sound within the material according to Newton–Laplace equation.[25]

$$c = \sqrt{\frac{E}{\rho}}$$

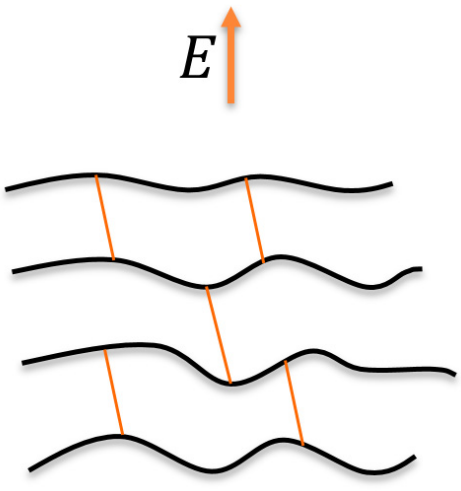

Figure 2.10: Crosslinking Increasing Young's Modulus

After attempting to increase the crosslinker concentration above the ratio recommended by the manufacturer (10:1 base:crosslinker), it was found that cross-linker concentration provided little or no control over the speed of sound even at base:crosslinker ratios as low as 2:1 as shown in Figure 2.11.

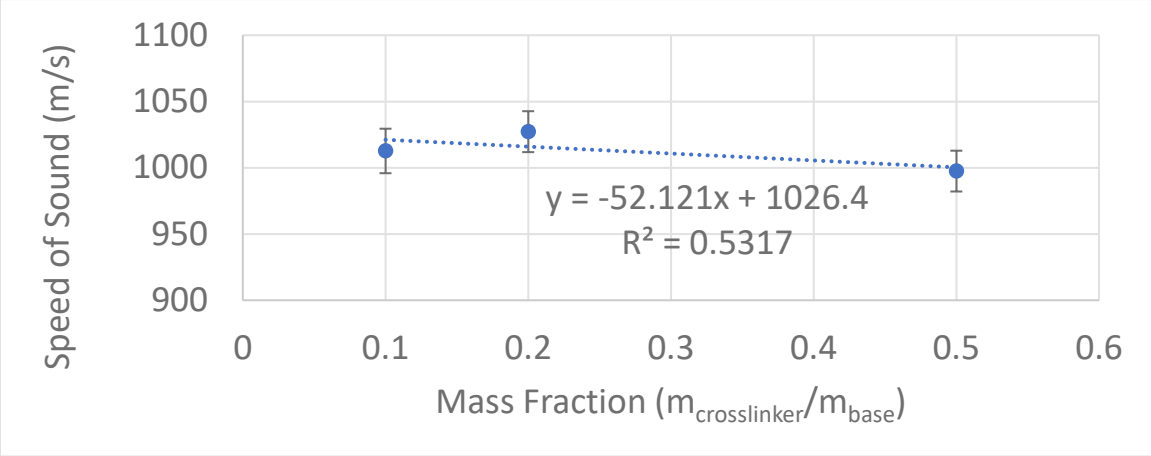

Figure 2.11: Speed of Sound Dependence on Crosslinker Concentration

The ineffectiveness of this approach led us to try a different strategy of increasing the base density (Figure 2.12). The acoustic impedance is the product of the speed of sound of a material and the material's density. Increasing the density generally increases the acoustic impedance if done in a way that doesn't have much effect on the speed of sound.

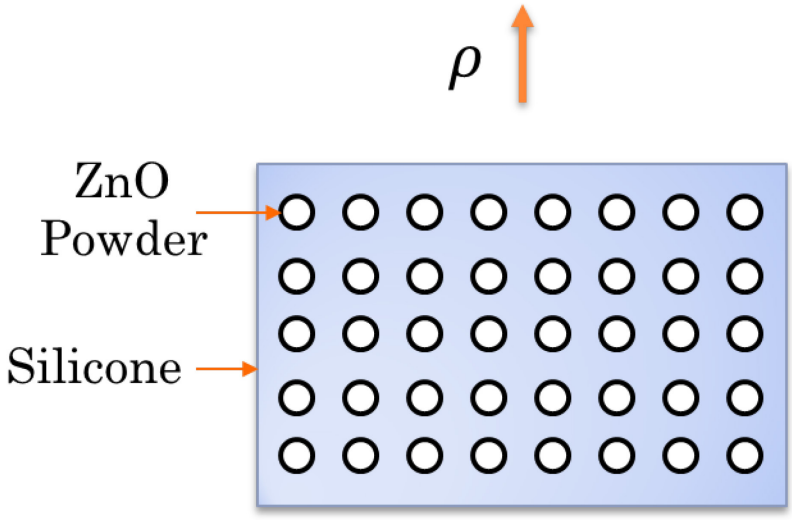

Figure 2.12: ZnO Particles Increasing Density

Yamashita et. al had used a ZnO nanopowder mixed into silicone as it was curing in order to increase the density of the material.[26] The reason of choosing ZnO was due to its very good biocompatible properties. Due to its biocompatible nature, ZnO is used a food additive in order to provide Zn as a nutrient and is also used in sunblock and other cosmetic products. ZnO is also cheap to purchase with Sigma-Aldrich selling 1 kg of their 205532 SKU for $62.50 with bulk pricing also available. More importantly, ZnO has the highest density among widely available biocompatible powders.[26] For these reasons, a ZnO micropowder with < 5µm particle size was procured from Sigma Aldrich (205532-1KG) to be used as a silicone dopant for the purpose of increasing the density of the silicone, shown in Figure 2.13. Smaller particles could potentially increase the PTE by reducing attenuation losses. Sigma Aldrich offers <50 nm size ZnO powder. This represents an avenue for further increasing the PTE of the dry coupling.

Figure 2.13: Sigma Aldrich ZnO powder, <5µm particle size

After initial attempts to combine silicone and the powder it became clear that the challenge would be achieving a mix that resulted in an even suspension of the powder throughout the silicone and did not introduce bubbles.

The first attempt at mixing in the ZnO powder was simply mixing it in with a disposable stick after the base and crosslinker had been mixed. This was then vacuum degassed and

left to cure. This resulted in poor distribution of the powder as can be seen in Figure 2.14. The powder tends to clump together into small spheres separated by a matrix of silicone with low concentrations of powder. This is undesirable because the large clumps of powder represent regions within the silicone with much higher acoustic impedance. This will cause scattering of the ultrasound and greatly attenuate the signal, dropping the power transfer efficiency of the UTET device. Note that the white colour of the sample is now due to optical scattering of the zinc oxide rather than of gas bubbles as previously.

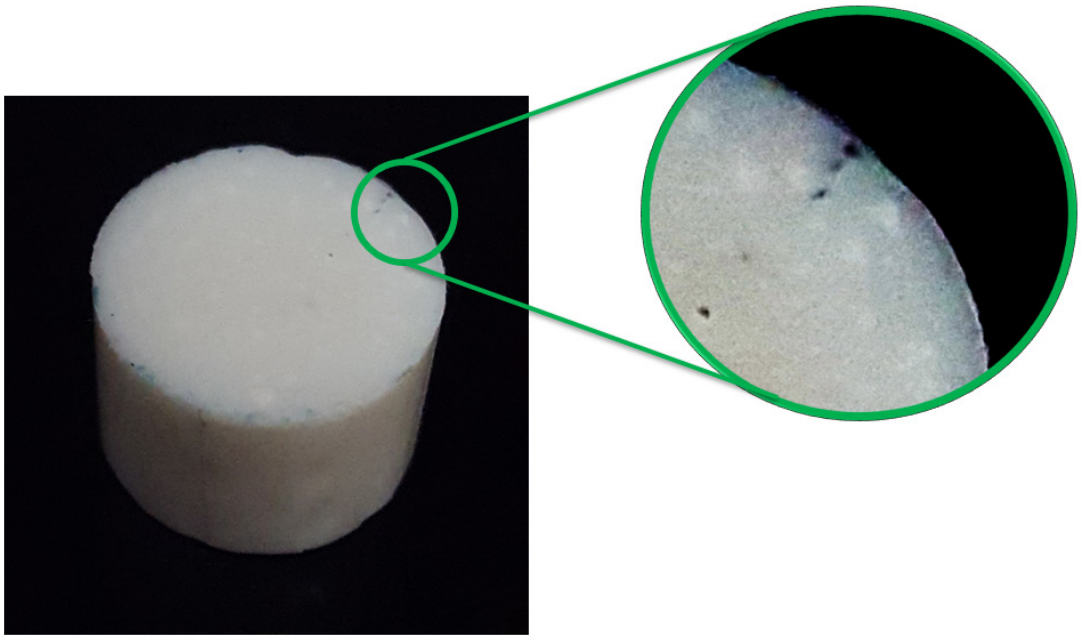

Figure 2.14: Clumping of ZnO powder

A process of mixing ZnO powder into Sylgard 184 to reduce this clumping had to be developed. The solution used in this thesis was to mix the ZnO in a sturdy zipper storage bag. The bag's flexibility allowed the ZnO powder clumps to be crushed using a stick made of Delrin that had filleted edges so as not to rip the bag. The ZnO and Sylgard base were mixed by pushing the Sylgard liquid into the ZnO powder using the Delrin stick until a nearly homogenous solution was obtained as shown in Figure 2.15.

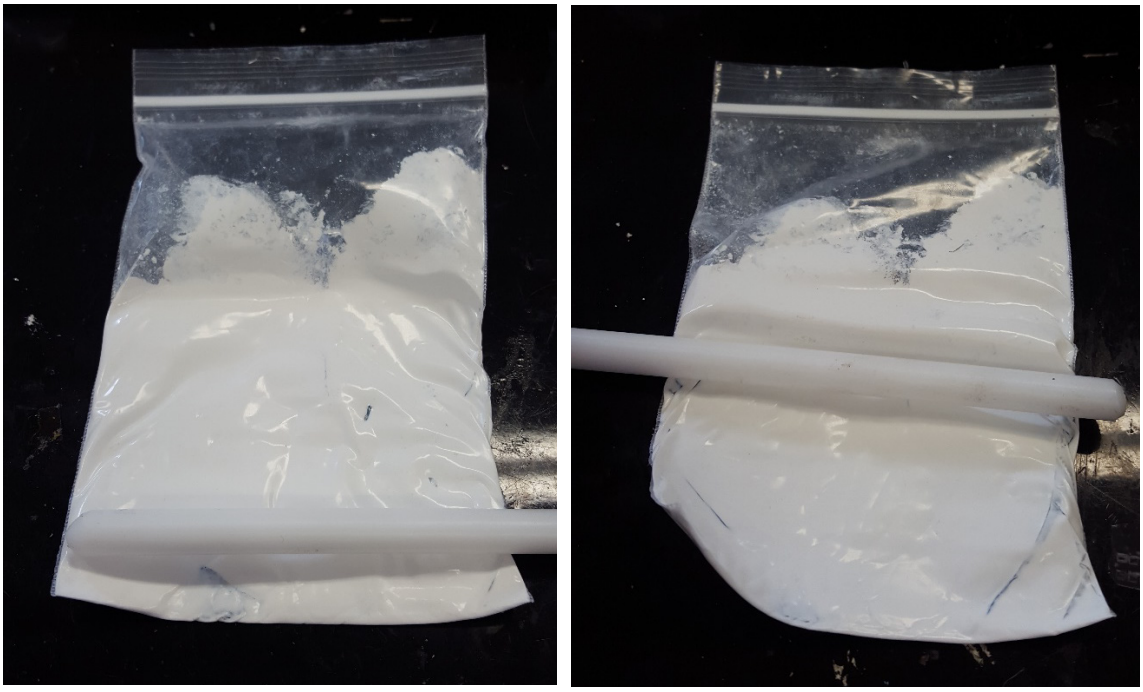

Figure 2.15: Process of mixing ZnO powder into Sylgard 184 base liquid

Then the bag was felt and visually checked for any clumps that remained. The Delrin stick was then used to crush the clumps and the mixing process was repeated until all the clumps were eliminated.

The dry powder naturally contained a lot of air. Some of the air was released into the bag as the powder was mixed into the Sylgard (Figure 2.16) and some of it of was dissolved with the powder into the Sylgard base liquid. The air was released from the bag during mixing to prevent the bag from bursting while under pressure from the mixing process.

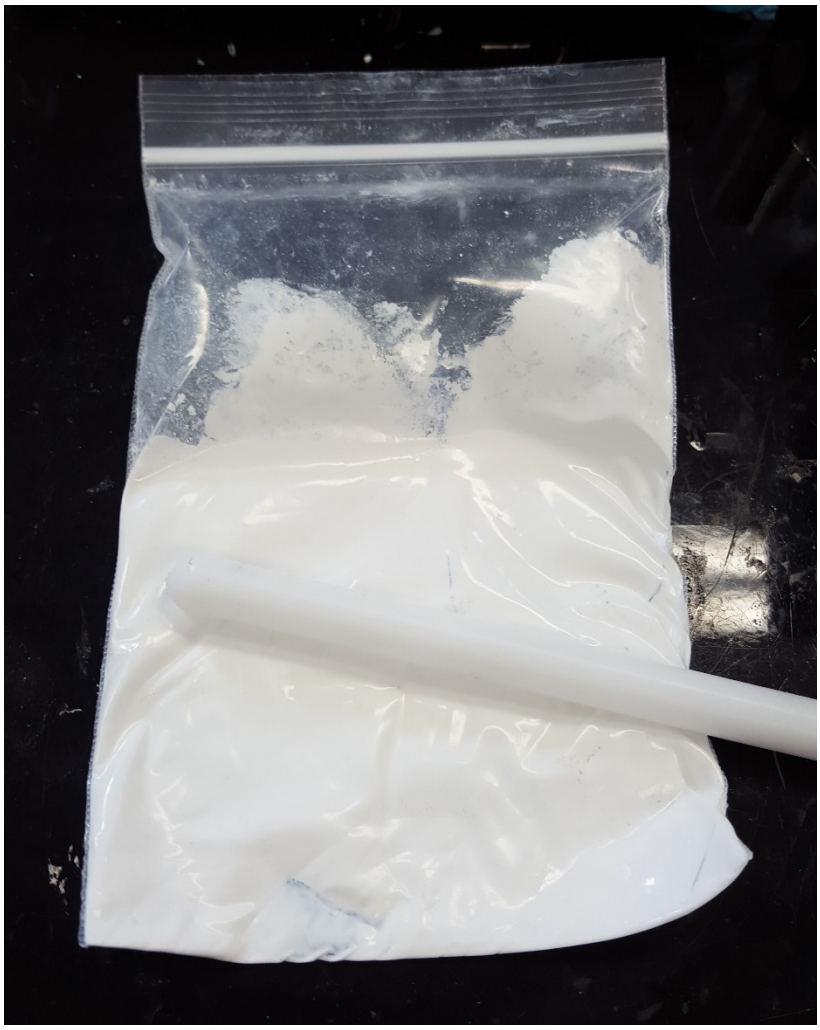

Figure 2.16: Bag inflated due to air released from the ZnO powder as it was mixed into Sylgard 184 base liquid

Additional air dissolved into the Sylgard from the ZnO powder created extra difficulty in removing the air during the vacuum degassing. Simply mixing the crosslinker into the ZnO doped Sylgard base and vacuum degassing this mixture produced a silicone that was filled with bubbles after curing (Figure 2.17). Increasing the amount ZnO powder mixed into the Sylgard increased the viscosity of the liquid. The higher viscosity made it difficult for the bubbles to be removed during vacuum degassing.

Figure 2.17: Bubble-filled, ZnO doped Silicone

A better process for degassing the ZnO doped silicone was needed in order to produce a bubble-free sample. Instead of mixing the crosslinker and ZnO doped base in a small dish then degassing the whole mixture in the mould as the Sylgard cured, the crosslinker was instead injected into the bag using a syringe and mixed into the doped base again using the Delrin stick. The bag was then opened to allow air to escape as it was vacuum degassed. This produced samples that were visibly bubble free, however, when the sample was cut into cross-sections, it was apparent that the sample had several elongated bubbles that ran through vertically which can be seen in Figure 2.18.

A solution was settled upon with an additional degassing step. After degassing in the bag and pouring the degassed mixture into the mould, bubbles would still nucleate along the bottom and sides of the mould. This was likely due to a small amount of air getting entrapped along the surfaces of the mould as the silicone mixture was poured into it. The

additional degassing step after the mixture was poured into the mould was enough to pull this remaining air out of the sample (see Figure 2.18).

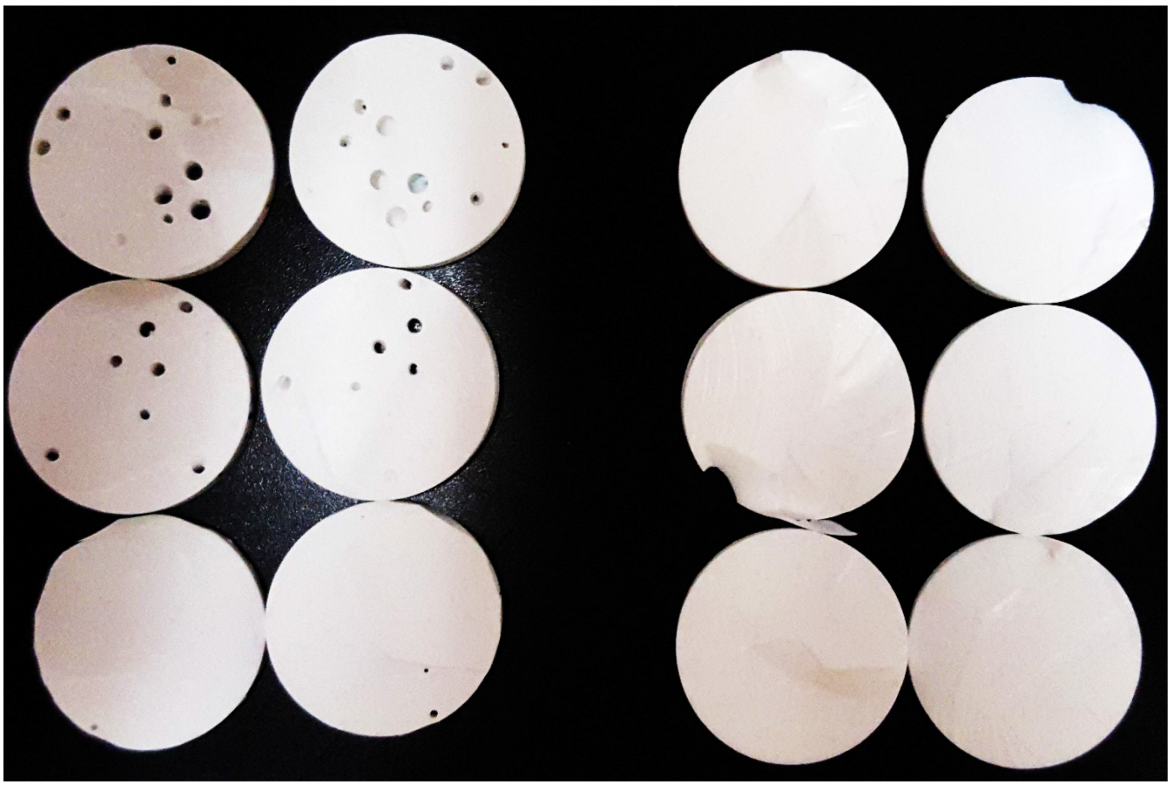

Figure 2.18: Pictured on the left are cross-sections of a sample degassed in the bag only. On the right are cross sections of a sample that was degassed both in the bag and afterwards in the mould.

Finally, there needed to be a method of calculating the amount of ZnO powder to mix with the Sylgard to produce a sample of a desired density

The process of curing the loaded samples started with measuring the amount of Sylgard base by mass. Experiments were done to check if any mass is lost in the curing process. The results showed that the sample's mass before and after cure were 4.54±0.02g and 4.53±0.02g, thus, the mass lost during curing is minimal. To calculate the density of the final loaded sample, the following formula was used

$$\rho_{total} = \frac{m_{total}}{V_{total}} = \frac{m_{base} + m_{cross} + m_{add}}{V_{base} + V_{cross} + V_{add}}$$

Where m_{add} and V_{add} are the mass and the volume of the loading additive (in this case, the ZnO powder) respectively. The mass of the ZnO can be calculated as:

$$m_{add} = \rho_{total}(V_{base} + V_{cross} + V_{add}) - m_{base} - m_{cross}$$

The volumes can be calculated using the known densities of each component:

$$m_{add} = \rho_{total}\left(\frac{m_{base}}{\rho_{base}} + \frac{m_{cross}}{\rho_{cross}} + \frac{m_{add}}{\rho_{add}}\right) - m_{base} - m_{cross}$$

The crosslinker is added to the base in a 10:1 base:crosslinker ratio and has the same density as the base, measured to be 1000kg/m^3.

$$m_{cross} = 0.1\, m_{base}$$

$$\rho_{cross} = \rho_{base}$$

$$m_{add} = \rho_{total}\left(\frac{1.1m_{base}}{\rho_{base}} + \frac{m_{add}}{\rho_{add}}\right) - 1.1m_{base}$$

$$m_{add}\left(1 - \frac{\rho_{total}}{\rho_{add}}\right) = \frac{\rho_{total}1.1m_{base}}{\rho_{base}} - 1.1m_{base}$$

$$m_{add} = \frac{\frac{\rho_{total}1.1m_{base}}{\rho_{base}} - 1.1m_{base}}{\left(1 - \frac{\rho_{total}}{\rho_{add}}\right)} \qquad \textit{Equation 3}$$

Using Equation 3, the mass of the additive can be calculated by measuring the mass of the base, and knowing the density of the base, the additive and the final desired density of the sample. The density of ZnO is 5610 kg/m^3.[27]

Ultimately, the addition of ZnO represents a good enhancement to the design. The reduction in reflective losses, combined with the low cost and low added complexity to the process yields a great improvement to the design.

2.3 Adhesive Layer Application

At this stage, different methods were being tested to find a way to add adhesive capability to the dry coupling. Since the Sylgard 184 is not inherently adhesive it would either have to be modified to be adhesive or have an additional adhesive material added to the face of the Sylgard that interfaces with the skin (Figure 1.4). The adhesive would come in the form

of a silicone pressure sensitive adhesive (PSA). Pressure sensitive adhesives are adhesives that increase their hold with increasing pressure. There were a couple promising products that could potentially fulfill the role of the adhesive layer.

The first was FastelTack Sil, a silicone PSA sheet 0.03mm thick. This extremely thin sheet of PSA is sandwiched between two layers of polyester release films (Figure 2.19).

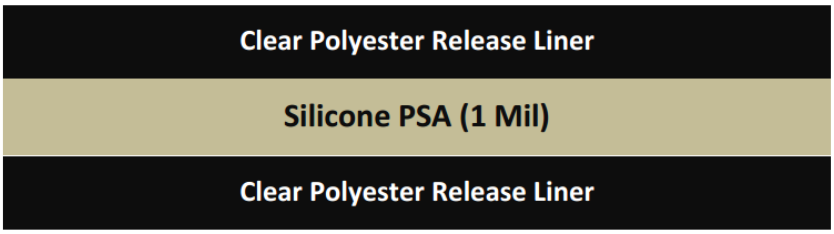

Figure 2.19: FastelTack Silicone PSA Tape [28]

In order to attach the FastelTack PSA to the Sylgard, the release film on one side would be removed, the PSA applied to the surface of the Sylgard and the other release film then removed. In practice, applying the FastelTack Sil proved extremely difficult. Often the PSA would tear and continue to stick to the release liner during removal. After applying the PSA to the Sylgard it was extremely difficult to remove the other release liner as the PSA was more likely to stick to the liner rather than the Sylgard. Finally, attempting to remove the dry coupling, after attaching it to the skin, caused the FastelTack PSA to tear off the Sylgard as the PSA had a much stronger bond with the skin compared to the Sylgard (see Figure 2.20).

Figure 2.20: FastelTack Sil PSA delaminating from surface of Sylgard 184

As a result of the difficulties applying the FastelTack PSA to the dry coupling as well as the poor removal from the skin performance, it was decided to look for a better performing product. The Dow Corning MG 7-9900 Soft Skin Adhesive (SSA) is a silicone PSA intended for wound care, bandages and scar therapy. This kit comes as two liquids that are mixed in equal parts by weight and the curing process can be accelerated using higher temperatures. Since the kit is a liquid that cures into a silicone elastomer it may have been possible to mix this PSA into the Sylgard 184 as it cured and therefore impart adhesive capabilities to the cured Sylgard (Figure 2.21).

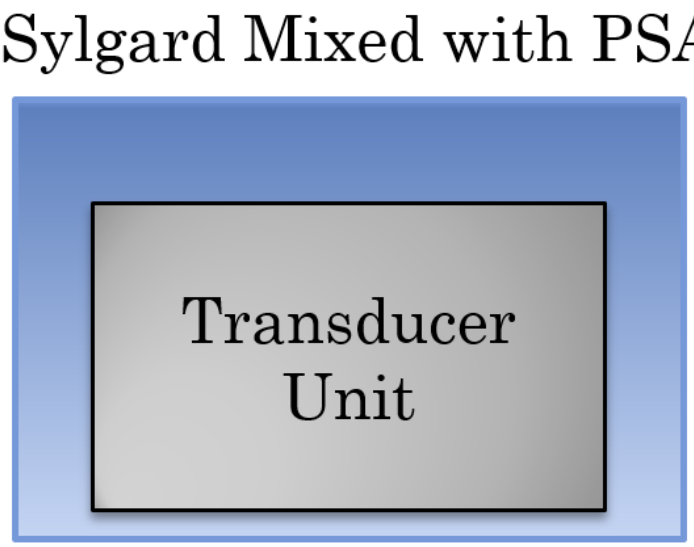

Figure 2.21: Design of UTET Transducer Encased in Sylgard Mixed with Adhesive

After mixing both the Sylgard and SSA independently then mixing them together it was found that the curing agent used with the Sylgard actually crosslinked the SSA to the point where it was no longer adhesive. Mixing the SSA with the Sylgard as they both cured yielded a non-adhering silicone very similar to the Sylgard alone.

The final concept for the adhesive layer involved painting a layer of the still liquid, curing SSA onto the front face of the cured Sylgard (Figure 2.22). After curing, the SSA formed a strong bond to the Sylgard and retained its skin adhering properties (Figure 2.23).

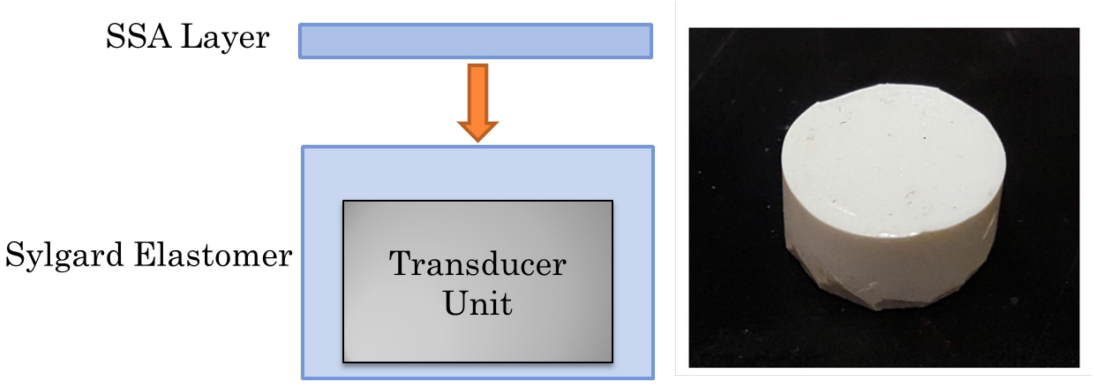

Figure 2.22: Final Design of Dry Coupling: Loaded Sylgard Encases the UTET Transducer with Thin Layer of SSA on Skin-Interfacing Surface

Figure 2.23: Final Dry Coupling Design Attached to Head on Mastoid Tip

With the proper equipment, this layer could be spin-coated onto the Sylgard in order to control the thickness of the adhesive layer. Controlling the thickness layer is important as it affects the overall power transfer efficiency as shown in Chapter 3.9. For this thesis, due to equipment limitations, the mixed SSA was simply poured onto the Sylgard in a thin coat.

2.4 Mould Design

A large challenge in making the samples needed to do the testing in this thesis was creating moulds that produced samples with precise size and shape.

The first mould used was a simple plastic hexagonal boat (Figure 2.24). These were good for testing simple procedures like the curing process for the various silicones and the effectiveness of degassing the silicone.

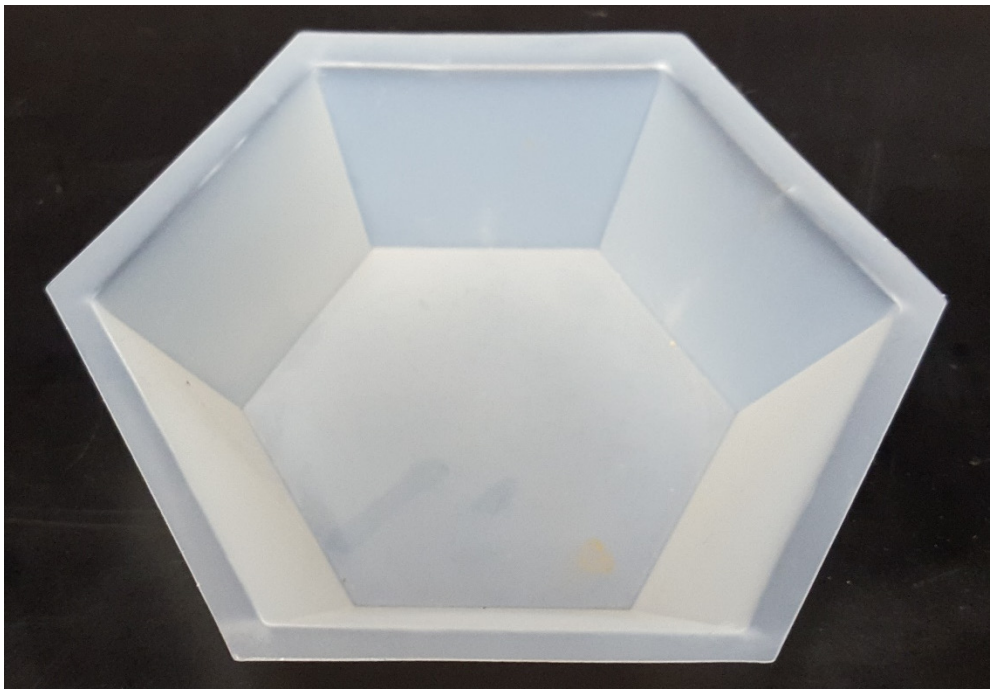

Figure 2.24: Hexagonal boat used to make initial samples to test curing and degassing process

The hexagonal boats were good for these preliminary tests; however, the shape of the cured sample was complex. The final sample was in the shape of a frustum of a hexagonal pyramid with the larger hexagonal surface (the open side of the boat) having a concave curvature.

The first test that samples were required for was the pulse echo measurement for the reflectance of the samples (Figure 2.25). In this test, the sound wave is sent from a transducer into water then to the top surface of the sample. A portion of the wave is reflected back to the transducer due to the acoustic impedance mismatch between the water and the sample. The rest of the wave is transmitted into the sample. The wave then encounters the interface between the back of the sample and the glass reflector and another reflection originating from the back face of the sample is sent back to the transducer.

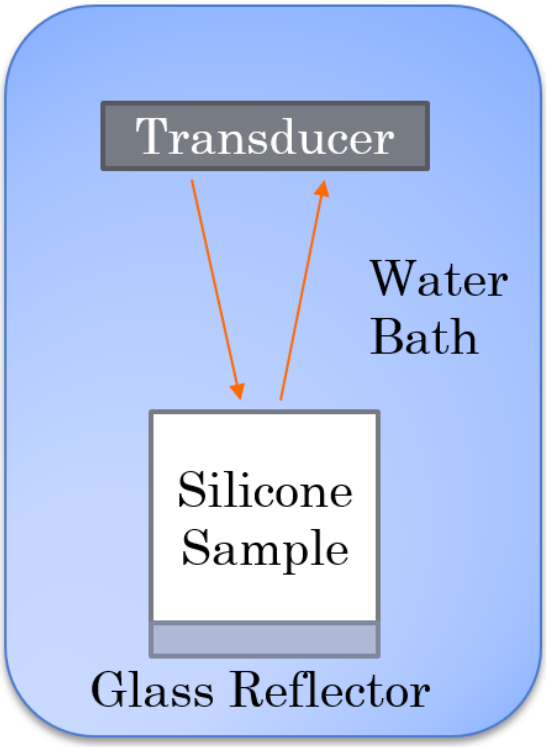

Figure 2.25: Reflectance Test Diagram

For the purposes of the reflectance test, it is only desired to measure the reflection from the front face of the sample. If the sample is of a small enough thickness, the reflection off the back face of the sample will interfere with the reflection from the front face because the pulse hitting the sample induces a vibration that is several wavelengths wide.

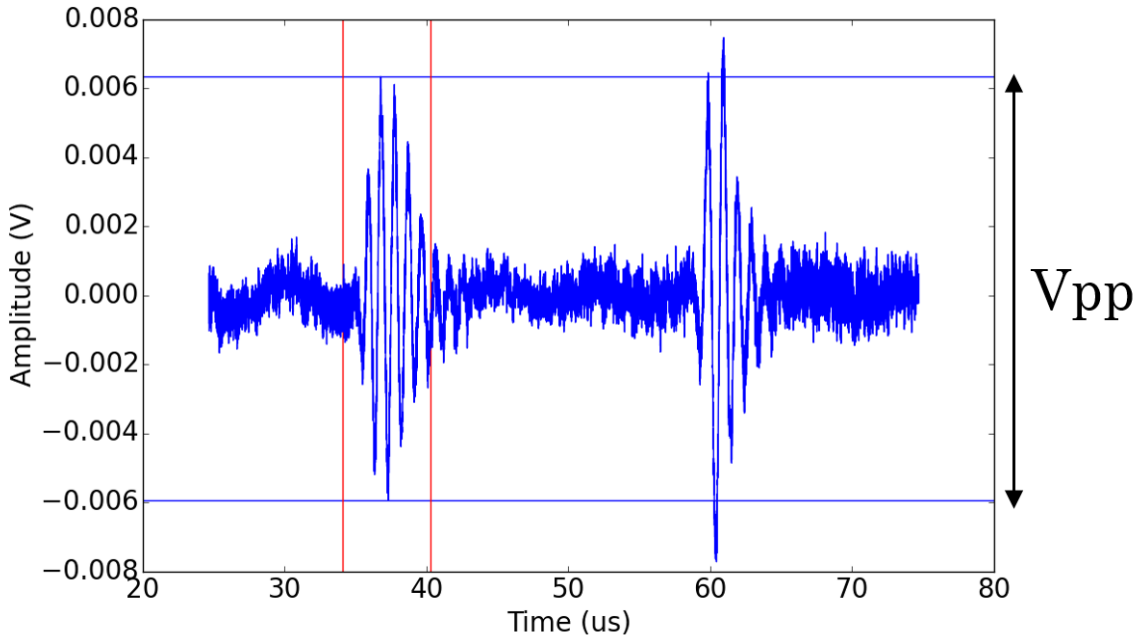

Figure 2.26: Front and Back Face Reflections

Therefore, the sample must be thick enough to completely separate the front and back face reflections (Figure 2.26). Using the hexagonal boat for a mould made it difficult to control for the thickness of the sample because of the complex geometry of the final sample.

In an open face mould like the hexagonal boat, it is hard to control for the tilt of the surface because it is dependant on the flatness of the surface it is cured upon. If the top surface is tilted in relation to the bottom surface, the sound wave will be reflected in a direction away from the transducer resulting in a smaller signal being measured.

Worse, the concave surface of the samples created by the meniscus effect on the open face of the boat induced a lensing effect that gave the reflected wave a focus. Depending on the distance of the transducer to the sample, the focal zone would either increase or decrease the reflected wave's amplitude at the transducer. It was also unknown if adding the ZnO powder to the silicone would change the surface tension of the fluid and therefore change the curvature of each sample depending on the loading fraction of powder in each sample.

Thus, in order to make the reflectance measurements simpler, repeatable and comparable between samples of varying loading of ZnO, a mould that cured each sample with a flat and parallel bottom and top surface, and an easily controlled thickness was required.

The first attempt in improving the mould was a large flat aluminum plate with square Delrin walls and stainless steel standoffs to control the thickness of the samples (Figure 2.27). The top surface would be made flat and parallel by screwing a top plate into the standoffs. The walls of the mould could be detached in order to delaminate the cured silicone from the mould. After taking the walls off the mould the top and bottom plates would have to be pried apart. The mould created a large plate of silicone which could be cut into samples.

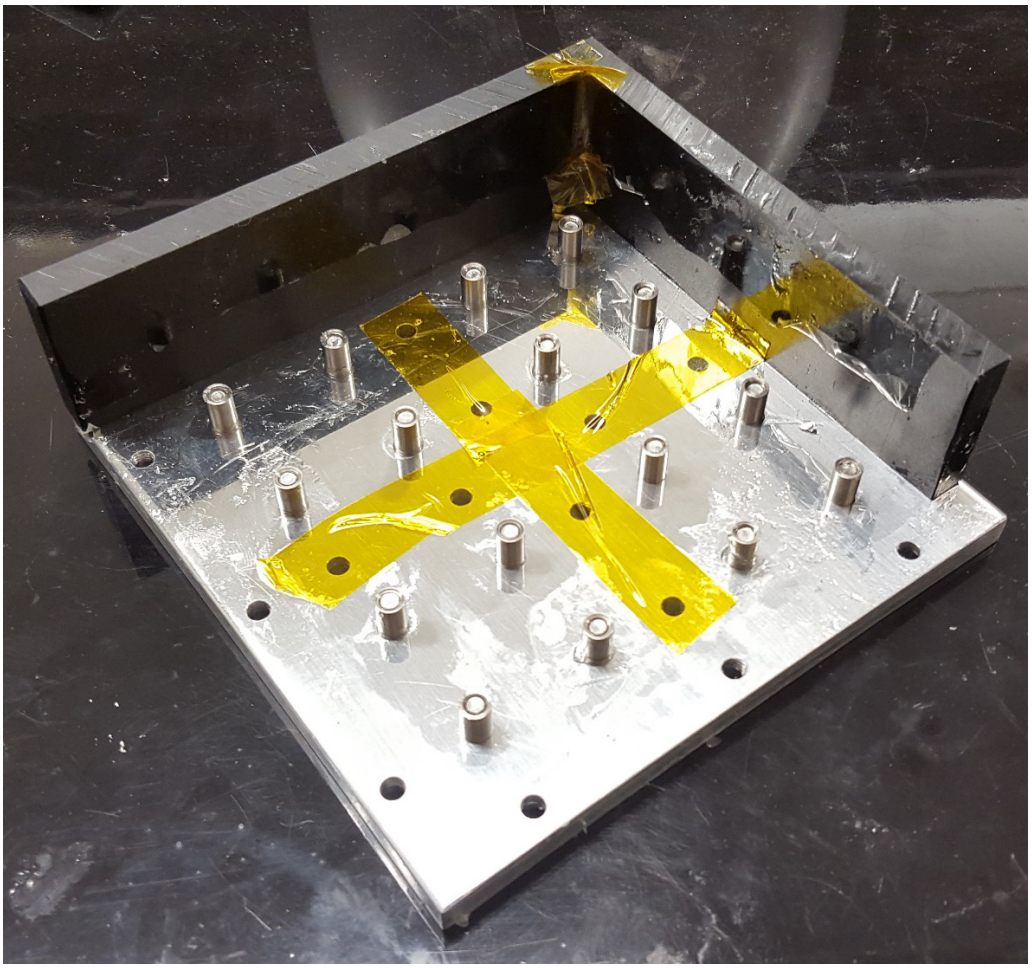

Figure 2.27: Initial Mould for Thick Flat Samples

The mould however was too wasteful and required too much silicone in order to produce samples of varying ZnO loading. A much smaller mould was required in order to save materials and expedite the production of samples.

It was decided that the best size and shape for the samples would be a cylinder with adequately large diameter and thickness. In order to fully reflect the soundwave back to the transducer, the sample's surface area needed to be larger than the cross-sectional area of the sound wave. This meant that, for a cylindrical sample, the surfaces needed a larger diameter than the 8mm diameter of the transducer being used for the test.

The first attempt at making the cylindrical mould consisted of an aluminum tube to create the cylindrical shape. The top and bottom of the sample would be made flat and parallel by curing the sample on the bottom against a flat glass plate, adhered to the aluminum tube using Blu-Tack. The top surface would be created by inserting a brass cylinder, machined on a lathe to have a flat surface, with arms made from cut brass tubing on the sides to control the height of the tube. A cylinder made of Delrin, machined on a lathe to give it flat and parallel surfaces was used as a standoff to control the height of the brass insert. The brass insert would be placed in the aluminum tube on top of the Delrin standoff then the brass arms were super glued onto the brass insert to keep the brass insert at the correct height off the bottom glass plate. Finally, heat resistant tape was placed on the inside of the aluminum tube to provide a smooth surface that the silicone could more easily delaminate from (Figure 2.28).

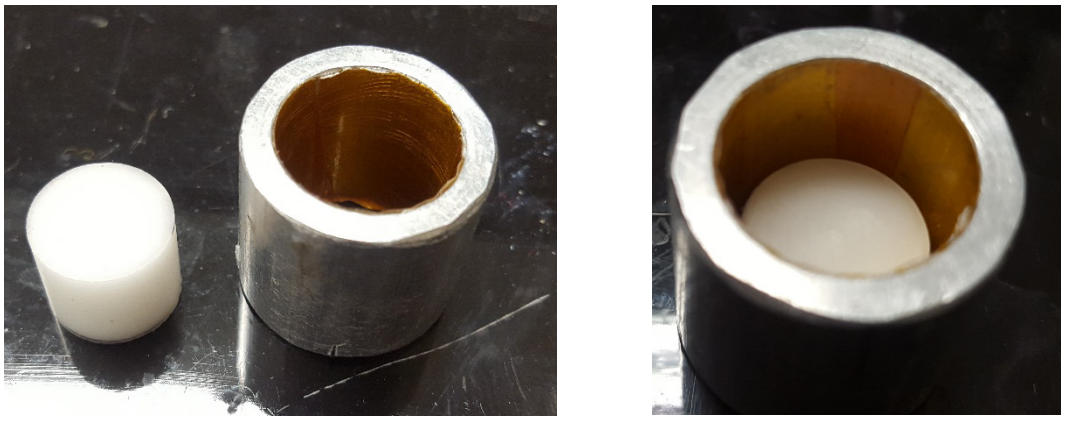

Figure 2.28: Aluminum cylinder mould with heat resistant tape and Delrin insert

The curing process consisted of degassing the silicone then pouring it into the mould with the bottom glass plate affixed to the aluminum. The brass insert was slowly lowered into the silicone in order to allow air to escape, preventing it from being trapped under the brass insert during the curing process. The samples were placed on a hot plate to decrease curing time.

The samples were removed from the mould by removing the glass plate with a razor blade, then pushing the sample through the mould using an arbor press.

There were several flaws with this mould. The heat resistant tape would delaminate from the aluminum along with the sample requiring another layer of tape to be painstakingly applied to the aluminum tube for each sample. The superglue joining the arms to the brass insert was weakened by the heating and cooling of the mould and would often fracture, requiring the arms to be replaced, greatly increasing the time it took to make each sample.

A new mould was developed to address these problems (Figure 2.29). Rather than relying on tape for release, the entire tube would be made out of Teflon, a material with excellent non-stick properties. The Teflon tube would be machined to be thick enough to create a sample with adequate thickness and enough headroom to allow expansion of the silicone as it was degassed and remain inside the mould. The Teflon tube would also be machined to have very flat and parallel surfaces; this would be important in providing a flat, parallel surface for the brass insert to rest against. The brass insert would be machined to have a flange that would rest on the surface of the Teflon. The bottom of the brass insert and its flange would be flat and parallel, thus each surface of the Teflon tube and brass insert being flat and parallel would create a flat and parallel sample. The thickness of the Teflon and the distance between the bottom of the brass insert's flange determined the thickness of the sample.

Figure 2.29: Teflon mould with brass insert

This solved all the problems of the previous mould, but introduced some additional, relatively minor ones. The fact that Teflon is an excellent thermal insulator made it more difficult to high temperature cure the silicone to reduce the curing time. This was solved by covering the mould in an insulating blanket while it was on the hot plate, allowing for more even heat distribution and minimal heat lost to the surroundings.

Another problem was trapping of air underneath the brass insert. This was due to the silicone making initial contact with the most radially distant surface of the brass insert due to the concave surface of the silicone (Figure 2.30). This was solved by applying silicone to the surface of the brass insert before inserting it and allowing the silicone to flow into the silicone in the mould then inserting the brass insert completely.

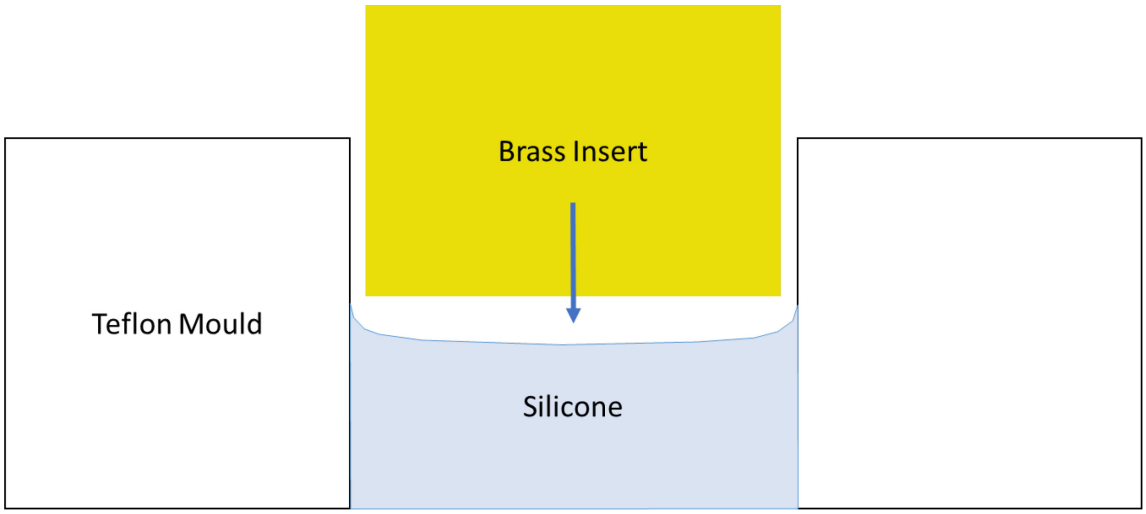

Figure 2.30: Silicone meets the brass insert at the most radial points

The samples were removed from the mould in the same manner as the previous mould. The glass plate was removed using a razor blade, then the sample was pushed through the mould using an arbor press. The brass insert was still attached to the silicone because the silicone flowed up and over it. The excess silicone could be cut off and the brass insert pried off the sample.

Another mould was needed to create thin samples for the purpose of measuring the attenuation and the power transfer efficiency of silicone loaded with ZnO so that its acoustic impedance was matched to human skin. According to the measurement methodology used, the samples needed to be a half wavelength thick and a full wavelength thick (details discussed in Chapter 3). Since the speed of sound in the silicone was measured to be 1000m/s this meant that thicknesses of 0.5 and 1.0 mm were required. Similar to the thicker samples previously discussed, the thin samples would be cylindrically shaped with a diameter larger than the transducer measuring them and have flat and parallel top and bottom surfaces.

The mould was simply a ring-shaped steel shim machined to a thickness of 0.5 mm with a tolerance of -0.05 mm which was the tightest tolerance available from McMaster-Carr. To create the 1 mm thick samples, two shims were superglued together, being careful to keep them centered. The shims were then superglued to a glass plate to create a flat bottom

surface. Another glass plate would be used for the top surface, with pressure applied during curing to press the plate flat against the surface of the shim.

After being degassed, the loaded silicone was slowly poured into the mould to allow for air to escape. The mould was intentionally overfilled so that there were no spaces left (Figure 2.31). A small amount of silicone was poured onto the top plate to prevent air being entrapped by placing the top plate onto the mould. As the top plate was lowered into place, the silicone on the top plate was allowed to flow into the silicone in the mould, the two bodies of silicone formed a cohesive mass with no bubbles entrapped (Figure 2.32). The top plate was then pressed into the mould and placed in a spring-loaded vice to keep the plate flat against the mould (Figure 2.33). The whole rig was then placed on a hot plate to accelerate the curing process.

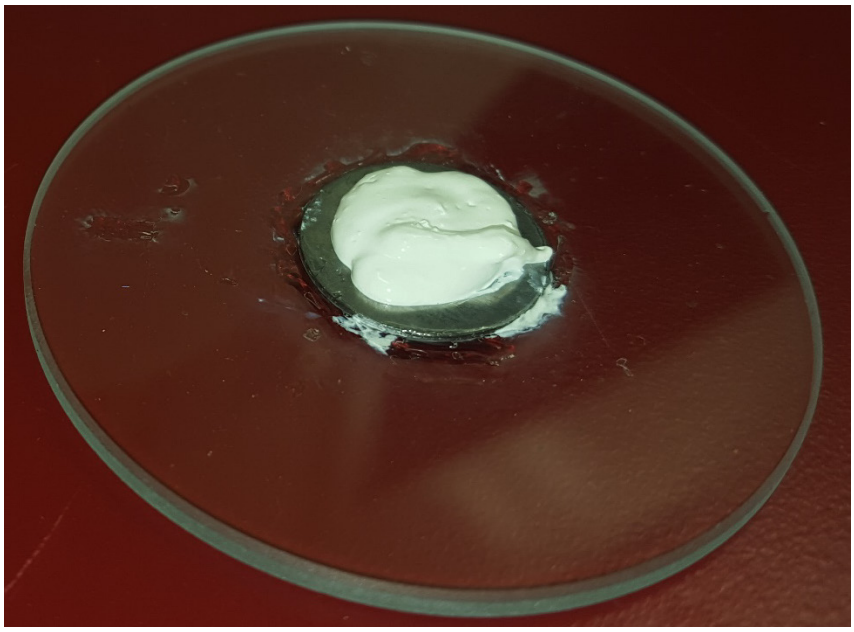

Figure 2.31: Thin sample mould overfilled with silicone

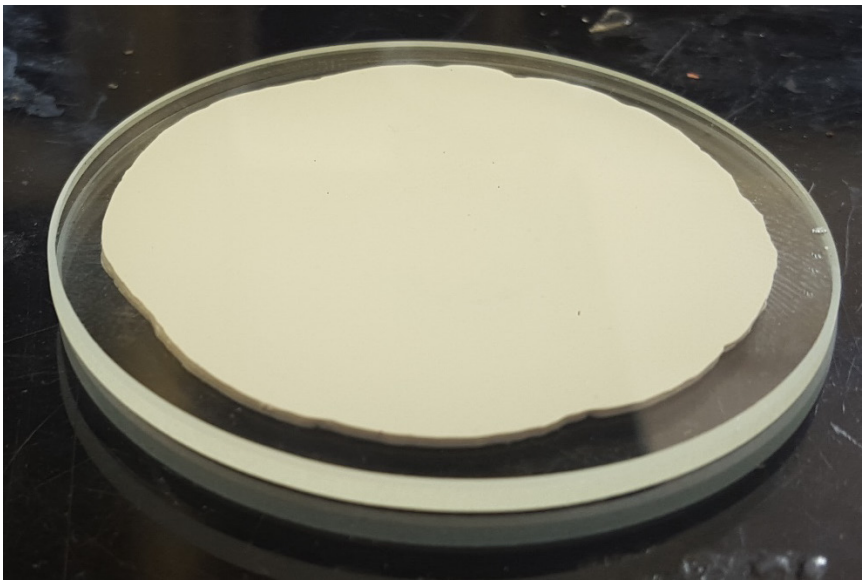

Figure 2.32: Thin Sample top plate in place

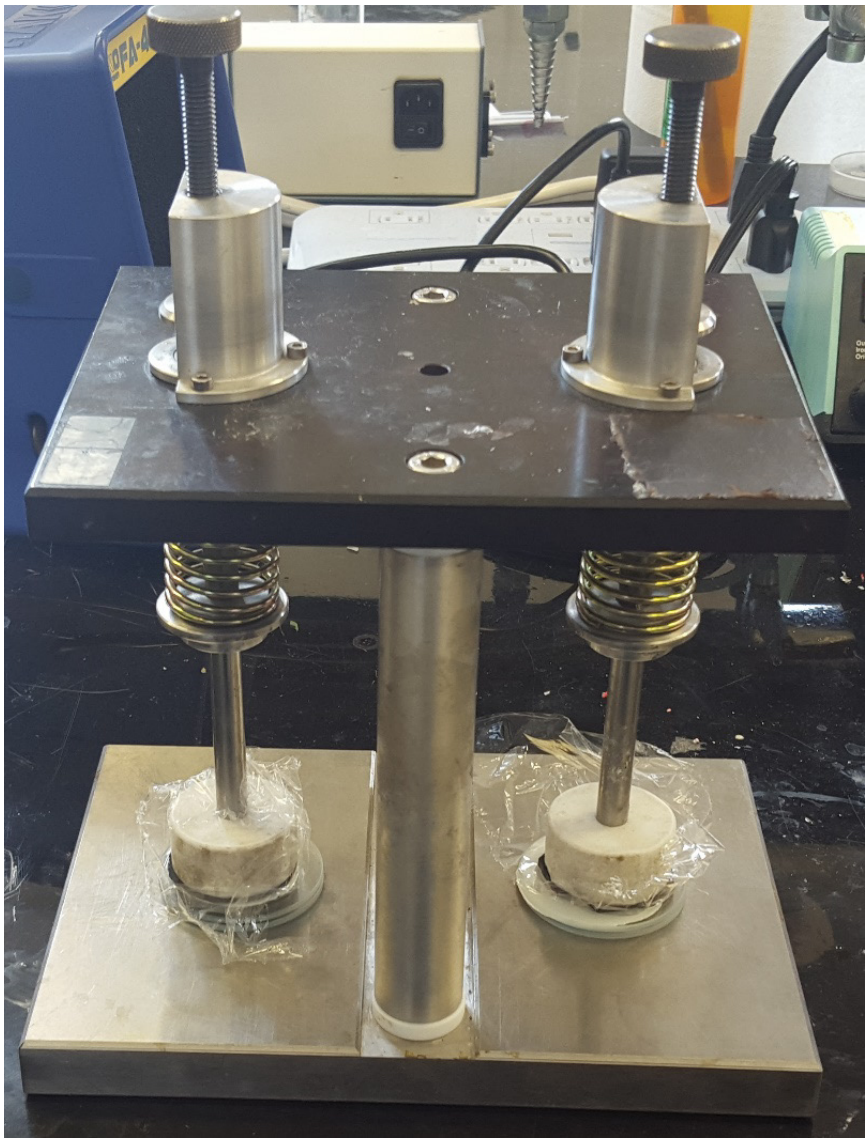

Figure 2.33: Thin sample moulds placed in spring-loaded vice

Since the samples were so thin, the problem of extruding them from the mould became much simpler. The glass plate on the top surface was only adhered to the silicone and was pried off using a pair of thick forceps. The silicone adhering to the walls of the mould could be cut off using a scalpel. The scalpel could then be carefully wedged underneath the sample and used to peel the silicone out of the mould. This left a mould that could be cleaned and reused.

2.5 Curing Processes for Samples

The final process for curing the samples made for reflectance testing consisted of:

Preparing ZnO/Sylgard Base Suspension

1. Set strong zip lock bag on scale and tare.
2. Pour approx. 6 g of Sylgard base into bag, record actual mass of base.
3. Calculate, using mass of silicone base and density ratio, the mass of the ZnO needed to achieve approximate target density of end product.
4. Pour calculated mass ZnO powder into bag,
5. Using rounded Delrin stick, mix ZnO into Sylgard and break down any clumps by crushing them and spreading liquid throughout the bag repeatedly until no clumps remain and fluid looks (colour) and feels (texture/viscosity) homogenous.
6. Open corner of bag and place in vacuum chamber, pump down to 0.1 atm and hold pressure for 5 mins to degas base/powder mixture.
7. Reopen the bag and, using syringe, inject Sylgard 184 crosslinking agent into bag in the amount of $1/10^{th}$ the mass of the Sylgard 184 base.
8. Mix crosslinking agent into loaded base in a similar manner to step 5.
9. Open corner of bag and place in vacuum chamber, degas at 0.1 atm for 5 minutes.
10. Remove bag from vacuum chamber and close seal.

Prepare Mould

1. Clean mould of any previous silicone (glass plate, Teflon bore, brass insert).
2. Apply very thin layer of blu-tack to glass in a circle with diameter larger than Teflon hole and press Teflon and glass plate together.
3. Make sure hole is completely surrounded by blue tack and layer is as thin as possible to ensure flatness. This minimizes silicone spreading on the glass plate, making the removal of the silicone from the glass easier.

Curing

1. Set hot plate to 140°C.
2. Cut corner of bag and squeeze loaded silicone into mould.
3. Place mould in vacuum chamber and degas at 0.1 atm for 20 mins.

4. Remove mould from vacuum chamber.
5. Coat bottom of brass insert with silicone.
6. Slowly lower brass insert into mould, pause to allow silicone under the insert to flow into the silicone in the mould.
7. Press insert into mould so that the insert is flush with the mould's surface to ensure flatness.
8. Place mould on hot plate set to 140°C. Cover mould with silicone mat to insulate heat surrounding mould.
9. Cure at temperature for 30 mins.
10. Release sample using press.
11. Cut excess silicone from brass insert and pry insert off top surface of sample.
12. Measure mass, diameter and height to determine final density of the sample.
13. Record density using permanent marker on sample.

The final process for curing the thin samples consisted of:

Preparing ZnO/Sylgard Base Suspension

1. Set strong zip lock bag on scale and tare.
2. Pour approx. 3 g of Sylgard base into bag, record actual mass of base.
3. Calculate, using mass of silicone base and density ratio, the mass of the ZnO needed to achieve approximate target density of end product.
4. Pour calculated mass ZnO powder into bag,
5. Using rounded Delrin stick, mix ZnO into Sylgard and break down any clumps by crushing them and spreading liquid throughout the bag repeatedly until no clumps remain and fluid looks (colour) and feels (texture/viscosity) homogenous.
6. Open corner of bag and place in vacuum chamber, pump down to 0.1 atm and hold pressure for 5 mins to degas base/powder mixture.
7. Reopen the bag and, using syringe, inject Sylgard 184 crosslinking agent into bag in the amount of $1/10^{th}$ the mass of the Sylgard 184 base.
8. Mix crosslinking agent into loaded base in a similar manner to step 5.
9. Open corner of bag and place in vacuum chamber, degas at 0.1 atm for 5 minutes.
10. Remove bag from vacuum chamber and close seal.

Curing

1. Set hot plate to 140°C.
2. Cut corner of bag and squeeze loaded silicone into mould.
3. Place mould in vacuum chamber and degas at 0.1 atm for 20 mins.
4. Remove mould from vacuum chamber.
5. Coat small area of top glass plate with silicone.
6. Slowly lower top plate onto mould, pause to allow silicone under the top plate to flow into the silicone in the mould.
7. Press top plate into mould so that the plate is flush with the mould's surface to ensure flatness.
8. Place mould in spring loaded rig then place rig on hot plate set to 140°C.
9. Cure at temperature for 30 mins.
10. Release sample by prying off top plate then cutting and peeling out sample from mould.

Curing process for adhesive layer:

1. Mix 1g each of Part A and Part B in a hexagonal boat.
2. Vacuum degas adhesive mixture at 0.1 atm for 10 mins.
3. Remove mixture from vacuum chamber.
4. Clean front face of Sylgard sample, swabbing with methanol.
5. Using cotton swab, brush a thin layer of adhesive onto front face surface of sample.
6. Degas sample with adhesive layer at 0.1 atm for 10 mins.
7. Place sample onto flat surface and cure for 24 hours.

Chapter 3: Experiments

3.1 Chapter Introduction

This chapter details the experimental work done to validate the solutions to the manufacturing problems of the previous chapter. This experimental work also serves to validate the design of the dry coupling as a device optimised for the transmission of acoustic energy into tissue for the purposes of powering an implanted device. Specifically, this chapter comprises the experimental work done to characterise the ability of the silicone dry coupling system to transmit acoustic power and the robustness of the system to expected usage conditions. The chapter proceeds through a set of individual experiments aiming to characterize some aspects of dry coupling performance or to determine appropriate design parameters.

The first experiment was performed to obtain a baseline measurement of the maximum power transfer efficiency (PTE) through a pair of transducers and an unloaded sample of the Epoxies Etc. silicone gel. The relationship between pressure applied to the Epoxies Etc. silicone gel and the PTE was then investigated.

After these experiments, a design decision was made to change the silicone material from the Epoxies Etc. silicone gel to Sylgard 184 for reasons of increased robustness and ability to influence the acoustic impedance of the material. After changing to Sylgard 184, the effect of ZnO doping on the reflectivity, which is directly related to the material's acoustic impedance, was characterised. The attenuation of the material was then characterised. The Sylgard 184 is not adhesive so an adhesive layer consisting of Dow Corning Soft Skin Adhesive MG 7-9900 was applied to the top surface of the Sylgard. Although this adhesive layer is very thin, it still has an influence on the PTE. The adhesive layer's thickness was measured in order to model the layer's effect on the PTE. After optimising the ZnO doping of the Sylgard, the PTE was measured. A KLM model was validated against the measured PTE data, and its prediction of the adhesive layer's effect on the system's PTE was compared to the measured PTE data. A vibration test was used to test the adhesion strength of the dry coupling. Finally, the dry coupling's adhesion was tested against various real-world stress assays.

Many of the experiments in this chapter involved piezoelectric transducers, specifically 1-3 composite PMN-PT air-backed transducers with a loaded epoxy matching layer and a center frequency of 800 kHz previously developed in our lab. The design and performance of these transducers is discussed in detail in reference [29].

The PTE was measured using two methods over the course of this work. For Section 3.2 and 3.3, the PTE was measured by driving the transmit transducer with a function generator and reading the voltage amplitude at the receive transducer connected to a load of known impedance on an oscilloscope. The measurement procedure was automated using a Python script previously developed in our lab which caused the frequency generator to step from 650 to 900 kHz in 2 kHz steps.[30] The voltage out and voltage in were measured on the oscilloscope from which the power and efficiency were calculated.

Part way through the dry coupling work (starting in Section 3.8) this PTE measuring system was replaced by a Copper Mountain S5048 Vector Network Analyzer (VNA) which could directly measure insertion loss -S_{12}. The VNA provides the same information as was previously obtained with the oscilloscope and function generator but in a shorter acquisition time and with an easier set up. For both methods, it is important to obtain efficiency as a function of frequency since changes to layer thickness and transducer separation can move the frequency of maximum efficiency. Methods for finding optimal operation frequency[31] have previously been developed by our lab but were not implemented in the present work.

3.2 Water Bath Test for Baseline Power Transfer Efficiency

Introduction

The water bath test was performed in order to get a baseline number for the maximum PTE achievable through the pair of ultrasound transducers (Figure 3.1). This baseline maximum efficiency was then compared to the efficiency achieved when transmitting through unmatched silicone and skin. If the PTE was equal to or greater than 80% of the maximum found through water, then the silicone represented a good material candidate to move further with. The transducers were acoustically matched to water using ¼ wavelength loaded epoxy matching layers. While the matching layer was designed to match to water,

the transducers are perfectly capable of transmitting into other material as well with acoustic impedance different than water. When transmitting into such materials the transmission efficiency and bandwidth may be reduced due to the imperfect matching. Additionally, water has negligible attenuation (0.0022 dB/cm at 1 Mhz) at the small distances used in this experiment [32]. The low attenuation and minimal reflective losses when transmitting through water means that, for these transducers, the maximum power transfer efficiency achievable at a set distance would be through water.

Methods

The water bath experiments require the use the transducers described in Section 3.1 and for this, a baseline of maximum power transfer efficiency is measured. The PTE is defined as the ratio of electrical power out of the receive transducer to the electrical power input to the transmit transducer (4).

$$PTE = \frac{P_{out}}{P_{in}} \tag{4}$$

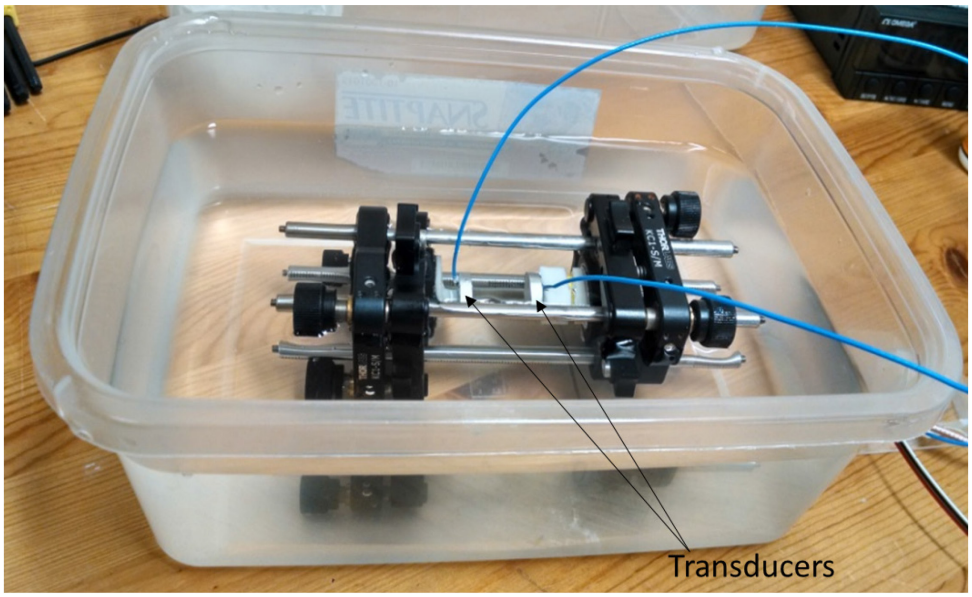

Figure 3.1: Water Bath Experiment Setup

The experiment is set up as shown in Figure 3.1 with a Thorlabs KC1-S cage which was locked in place as the PTE was measured (Section 3.1). The Thorlabs cage is a device that limits the degrees of freedom of the transducers so they can be rotated about the x and y axes (parallel to the transducer face) and translated in the z axis (perpendicular to the transducer face). All three degrees of freedom can be locked with set screws (see Figure 3.2). The transducers are fixed to retaining rings which can be aligned so that the faces of the transducers are kept parallel to each other as they are translated. This setup and the Thorlabs positioning cage is used throughout many of the experiments performed on the powerlink and dry coupling.

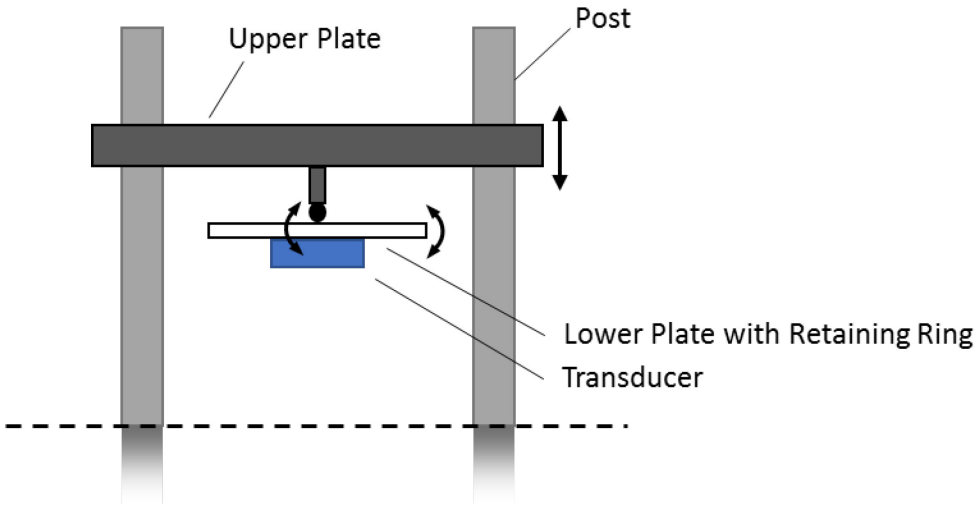

Figure 3.2: Diagram of Thorlabs Cage

Due to the manufacturing approach used, the piezoelectric crystal within the transducer was not centered within the case (see Figure 3.3), therefore the transducers needed to be aligned to maximize the PTE.

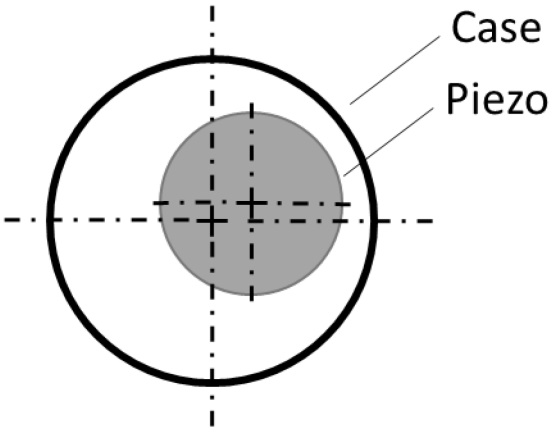

Figure 3.3: Piezoelectric Crystal not Centred in Transducer Case

To align the transducers, an alignment procedure was developed wherein one transducer is fixed in place on a retaining ring using cyanoacrylate. The other transducer is brought into contact with the face of the fixed transducer. The free transducer is shifted incrementally on each principle axis and at each location the PTE is measured (see Figure 3.4). The PTE will increase as the transducers overlap area increases. The optimal position is reached when the subsequent position has a lower efficiency than the previous position (the optimal). After the optimal position is found, the free transducer is fixed in place using cyanoacrylate on the retaining ring. This assumes that the piezo has zero angle relative to the case, which was ensured using standoffs during the manufacture of the transducers.

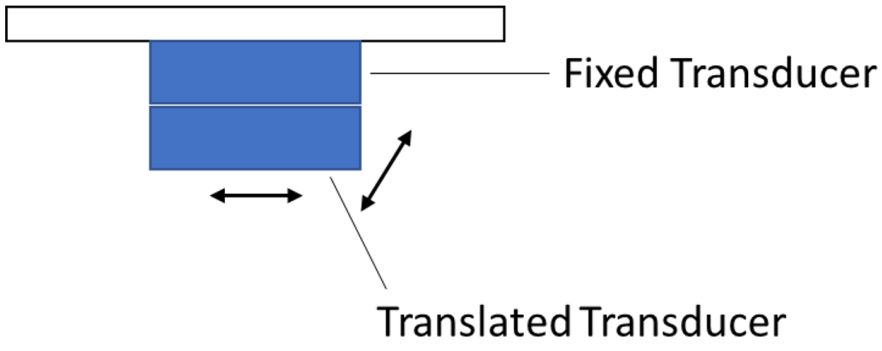

Figure 3.4: Transducer Alignment

After aligning the transducers, the cage is placed in a bath of deionized water. An electrical signal is applied to the transmit transducer using a function generator. The transducer

converts this signal to an acoustic signal through the reverse piezoelectric effect. The sound produced then travels through the water and is generated back into an electrical signal by the receive transducer through the piezoelectric effect (see Figure 3.5).

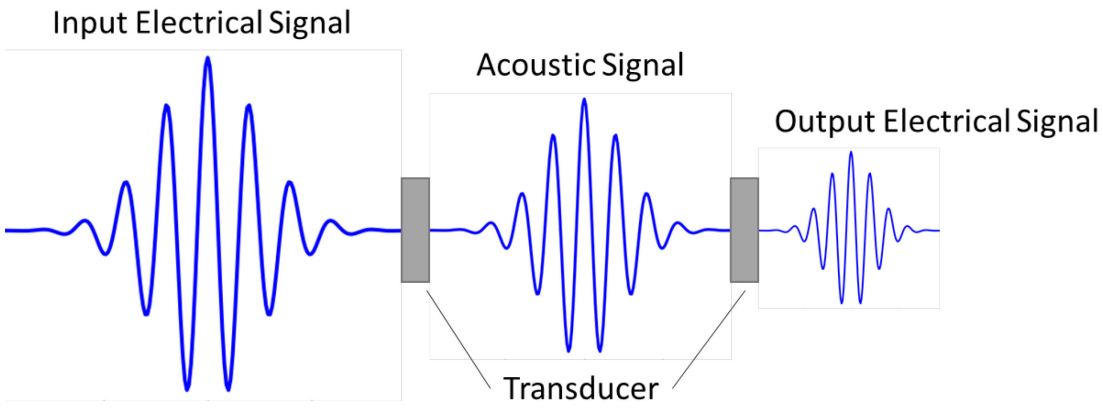

Figure 3.5: Signal Transmission Pathway

To model transmission into human skin, a porcine skin model was used. Raw skin from the back of a pig with hair removed was obtained from a local butcher. The skin was cut into 2cm x 2cm x 0.5cm pieces and frozen. Pieces were removed from the freezer and allowed to warm to room temperature prior to experimental measurements. A skin sample was then inserted behind the silicone sample while in the water bath and the PTE test was performed again.

The transducers used in this testing were designed for another application and were acoustically matched to water. While a fully optimized system would use transducers matched to the impedance of skin, experimental results obtained with the transducers matched to water give valid measurements for the relative efficiency of different acoustic coupling scenarios. Development of a new transducer as part of a fully optimized power link was outside the scope of this thesis. The final device would make use of transducers that were matched to skin as this would minimize losses and maximize the PTE of the system.

Results and Discussion

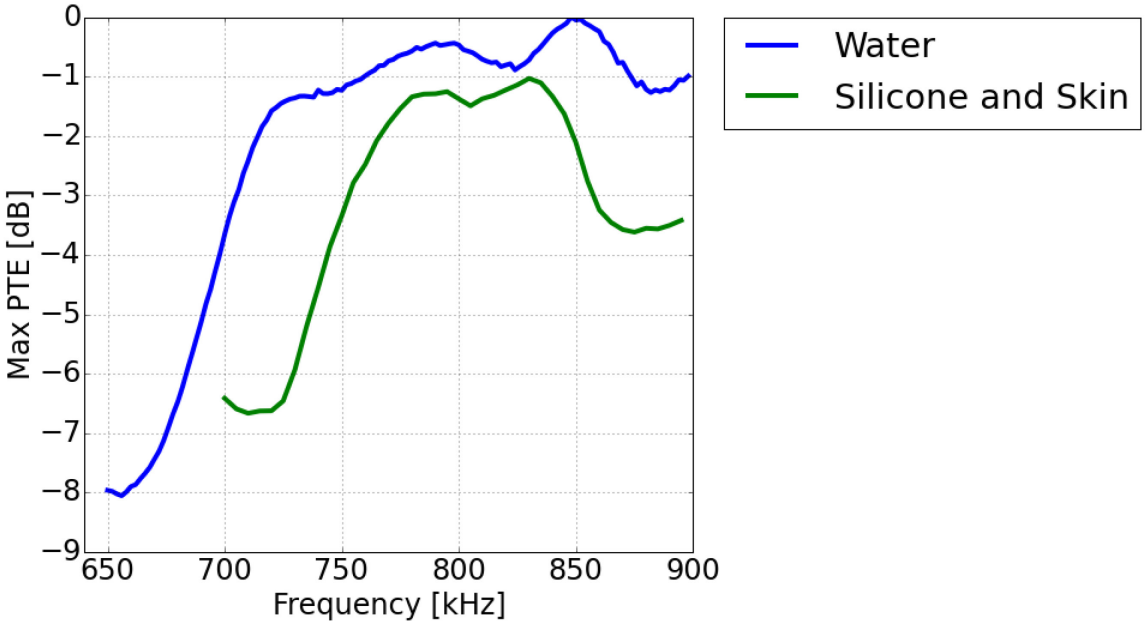

Figure 3.6: Power Transfer Efficiency of Transducers through Water and through Silicone and Porcine Skin Relative to the Maximum PTE through Water

Figure 3.6 shows the initial test of silicone as a coupling material for transducers matched to water. The maximum PTE measurements are plotted relative to the maximum PTE through water. The silicone samples used are described in Section 2.1 and are shown in Figure 2.6. The samples were cured in hexagonal moulds and were a maximum of 1 cm in thickness. The efficiency achieved through unmatched silicone and skin is compared to the efficiency through water. The maximum efficiency of the ultrasound driven through silicone and skin is only 1.03dB lower than the maximum efficiency through only water.

Conclusion

This test shows the promise of silicone as a dry coupling material as there is little efficiency lost (1.03dB) through a 1cm thick sample, compared to transmission through water. This loss is due in part to reflective losses and in part to absorption. The experiment was sufficient to show that silicone was a promising material for a dry coupling from the point of view of acoustic loss. A series of further design improvements would later be made to optimize transmission and more accurately characterize the loss from the coupling material

and interface. With a good candidate material to use as a dry coupling, the effect of pressure applied to the transducer-dry coupling stack on the system's PTE was investigated.

3.3 Applied Pressure Effect on Power Transfer Efficiency

Introduction

A major factor in the comfort level of the user while wearing the device is the amount of compressive force required to achieve maximum contact and power transfer efficiency through the dry coupling material. As contact pressure is increased, the coupling and skin will conform better and air gaps will be squeezed out, resulting in improved acoustic coupling. Both the acute pressure, when the device is first being fixed, and the chronic pressure applied by alignment magnets are relevant to patient comfort.

Experiments were carried out to find the relationship between the pressure applied to the dry coupling and the PTE of the system. The purpose of this experiment is to find the lowest applied pressure at which an acceptably high PTE can be attained.

Methods

The contact pressure was measured by applying a force to one transducer mounted in the Thorlabs cage and measuring the force between the opposite transducer and a fixed mount. The measured force is the same as the force delivered to the dry coupling. The force is measured by a Honeywell FSG010WNPB force sensor. A free body diagram of the setup showing the applied force is shown in Figure 3.7 (porcine skin will be discussed later).

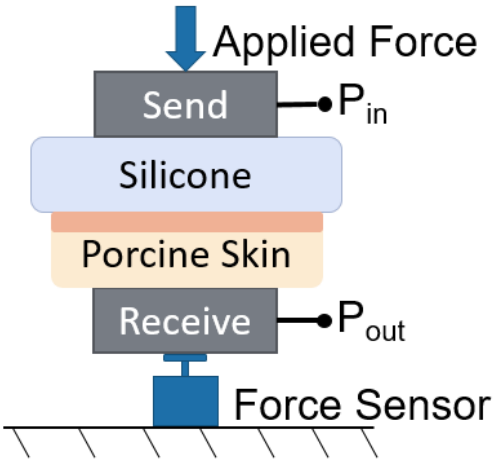

Figure 3.7: Free Body Diagram of Applied Force

The pressure was applied to the transmit transducer which was mounted in a the Thorlabs cage from Section 3.2, and was free to translate along the cage axis (but not free to move in other directions and become misaligned). The pressure was transferred to the dry coupling silicone, the porcine skin and the receiving transducer which was loosely seated on a force sensor where the compressive force was measured. The power in and power out were measured from the transmit and receive transducers respectively and the pressure was calculated by dividing the applied force by the cross-sectional area of the transducer face.

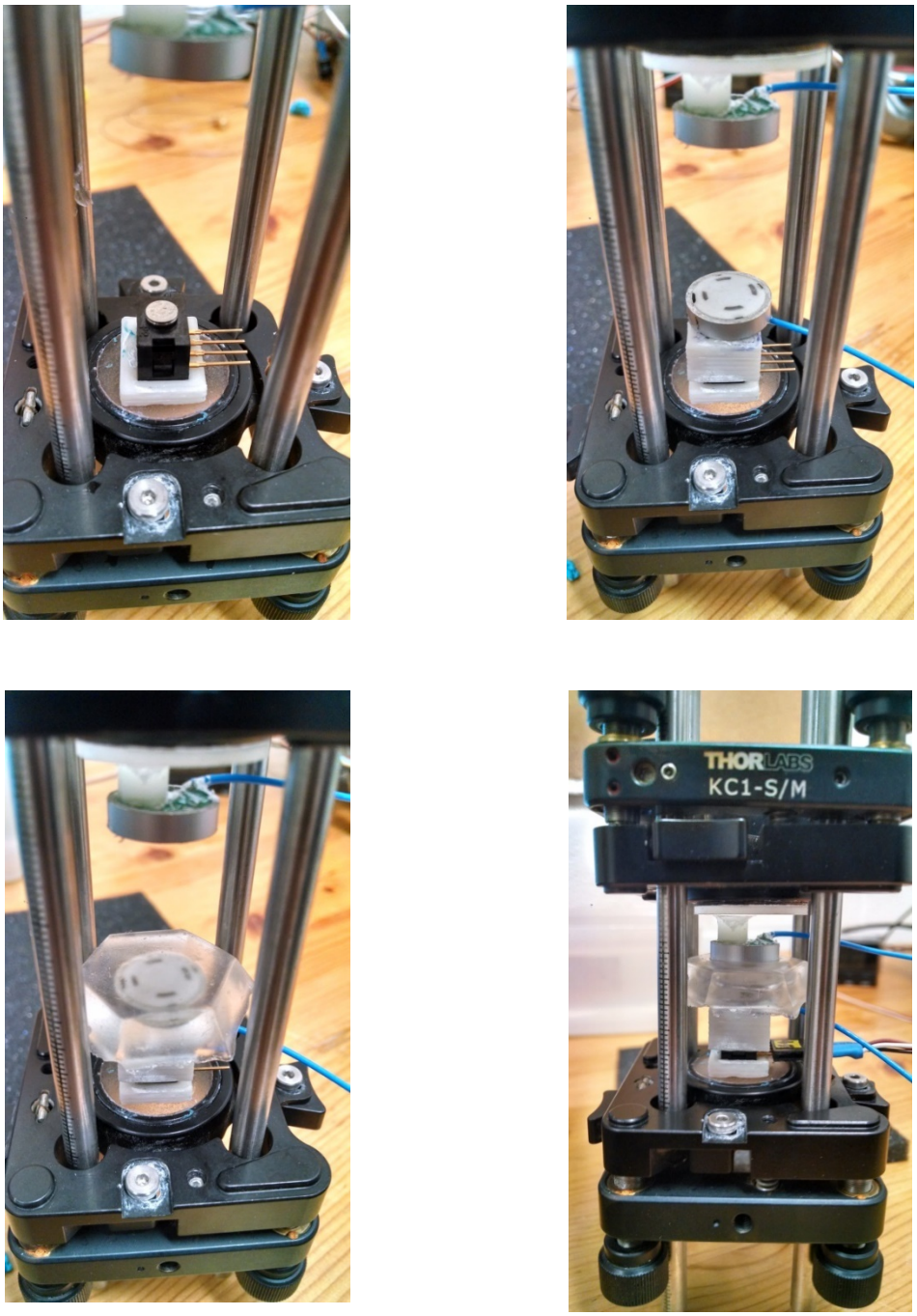

Figure 3.8: Top Left: Force sensor shown on retaining ring in Thorlabs cage. Top Right: Transducer fixed to alignment jig placed on top of force sensor. Bottom Left: Epoxies Etc. silicone placed on top of transducer. Bottom Right: Top transducer lowered onto stack of dry coupling, transducer and force sensor.

Three experiments were carried out as follows:

- Force increasing low to high without porcine skin
- Force decreasing high to low without porcine skin
- Silicone on porcine skin with force increasing

The experiment is set up as shown in Figure 3.8 with a force sensor and a Thorlabs cage locked in place as the PTE was measured. The transducers are aligned as in Section 3.2. This experiment was performed early in this thesis work and used the Epoxies Etc. silicone. The author believes that the results from this experiment are also applicable to the final design because both the Epoxies Etc. silicone, and the final design's adhesive SSA layer are pressure sensitive adhesives and both should respond to changes in applied pressure in the same manner if not to the same degree.

The test materials (skin, silicone) are then placed in between the transducers as shown in Figure 3.7 for the tests that included silicone and porcine skin and Figure 3.9 for the tests that only included silicone. The measurements were taken in the same manner as the water bath tests in the previous section. The force was recorded as the cage was pressed together then locked in place using screws. The efficiency over a range of frequencies was then measured at this force and the maximum efficiency was recorded. The force on the test material was increased incrementally by compressing the Thorlabs cage manually. The experiment differed from the water bath tests in that the bottom transducer was not fixed in place because it had to freely sit on top of the force sensor, thus, in applying the force, some misalignment may have occurred. Any such misalignment could lower the PTE. The possible misalignment would lead to an underestimate for the real PTE achievable through the dry coupling and to increased measurement variability. Some amount of misalignment was acceptable in this experiment given its primary objective of measuring the effect of compressive forces applied to the dry coupling on the PTE of the system rather than finding the absolute maximum efficiency achievable through the dry coupling.

The maximum efficiency over the same frequency range used in the water bath tests (Section 3.2) at each force level was found then plotted.

Results and Discussion

The following data was measured through a single sample of Epoxies Etc silicone only (Figure 3.9).

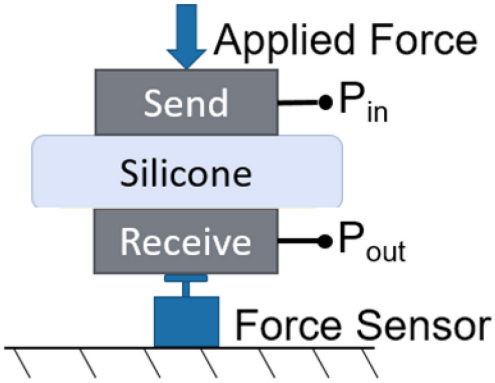

Figure 3.9: PTE Hysteresis through Silicone FBD

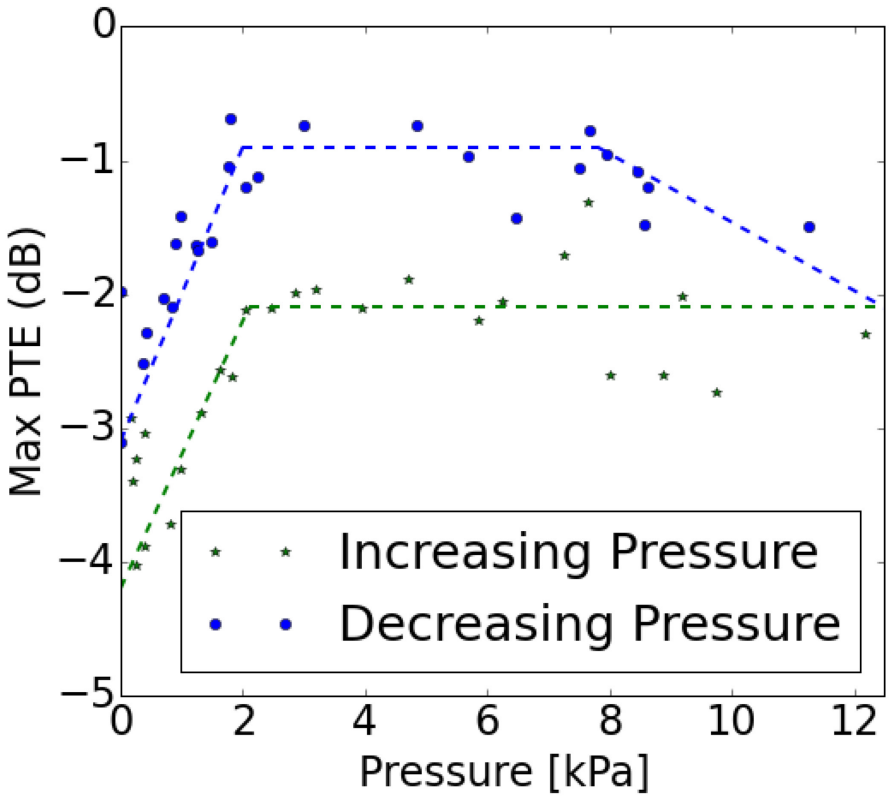

Figure 3.10: Hysteresis of PTE through a Single Adhesive Silicone Sample

Figure 3.10 shows how the adhesive properties of the silicone are advantageous for the power transfer efficiency of the system. The data shows that after applying a pressure of 12kPa, the PTE gradually increased until a maximum PTE was reached at 8kPa. Due to the loose-fitting jig on top of the force sensor, the transducer was likely slightly tilted which caused a decrease in measure PTE when the pressure was increasing. When the pressure was gradually lowered, the transducer realigned and the PTE gradually increased until it reached the best alignment at 8kPa where the PTE leveled off. After levelling off, the higher efficiency is maintained down all the way to zero pressure. This effect is due to the adhesive maintaining the large contact area after the dry coupling was forced into the small gaps on the transducer's surface. The adhesive bond held the dry coupling within the gaps on the surface, providing greater contact area than was obtained when the pressure was increased.

This experiment was limited by the alignment of the transducers. In order to get the force measurements, the receive transducer had to sit on top of the force sensor without being fixed in place. The freedom the receive transducer had likely allowed small changes in the alignment to occur as the pressure was applied and released resulting in quite variable data. The author attempted to minimize this by using a jig to hold the receive transducer. The jig allowed the transducer to slide axially along the force sensor, but prevented the transducer from tilting. This limited the tilt of the transducer to a maximum of 2 degrees which would have resulted in a decrease of the measured power out by 4% as the ultrasound beam moved away from the centre of the transducer. Note that this would have decreased the maximum PTE measured of -0.68dB Max PTE to -0.89dB Max PTE. This is in agreement with the observed random measurement error and is small enough that the trend and hysteresis in the efficiency can be clearly discerned.

Conclusion

This experiment showed that acceptable efficiency could be achieved at clinically acceptable contact pressures through an adhesive silicone sample. Based on this result it was decided that an adhesive contact layer was a key requirement for the dry coupling.

3.4 Change in Silicone Material

Experience with the Epoxies Etc. silicone over the course of the previous experiments showed that its viscoelasticity and low cohesive strength were a major liability. The material degraded substantially after multiple applications of pressure, thus, it was decided that a more durable option was needed. Subsequent experiments used the composite Sylgard 184 and Soft Silicone Adhesive for the reasons outlined in Section 2.1.

The results of Section 3.3 are applicable to the final design. The Soft Skin Adhesive (SSA) layer is composed of silicone that is softer and forms a much stronger bond (from qualitative testing) as compared to the Epoxies Etc. silicone. The stronger bond of the SSA allows the wetting achieved at higher pressures to be held better when the pressure is released. The softer nature of the SSA means that it deforms with less force, thus it should fully wet the surface of the skin by filling in gaps caused by the surface roughness with less pressure; as long as the adhesive layer is much thicker than the ridges on the skin. It seems plausible, then, that increased adhesive strength and decreased stiffness of the SSA is likely to result, if anything, in a high PTE being maintained at even lower pressures than the Epoxies Etc. silicone. Unfortunately, lack of time prevented these measurements from being repeated with the final design.

With the new material chosen, the next step was to create samples with increased acoustic impedance to match that of skin.

3.5 Reflectivity and Speed of Sound at Various ZnO Loading levels

Introduction

A significant fraction of the losses observed in the silicone dry couplings occur due to reflections at the coupling-skin interface. In this section, a strategy to minimize these reflections by controlling the acoustic impedance of the silicone by loading it with ZnO powder is investigated. ZnO loading increases acoustic impedance by making the silicone denser without significantly affecting its stiffness. The ZnO micropowder was added into the silicone solution during the curing phase of the silicone manufacture.

The experiments described in this section measured the reflectivity of loaded Sylgard 184 samples with various ZnO loading fractions. Reflectivity is the fraction of an incident wave

amplitude that is reflected from the surface of a material due to the change in acoustic impedance (see Figure 3.11).[13] By knowing the acoustic impedance of one material and measuring the reflectivity at its interface with a second material, the acoustic impedance of the second material can be calculated.

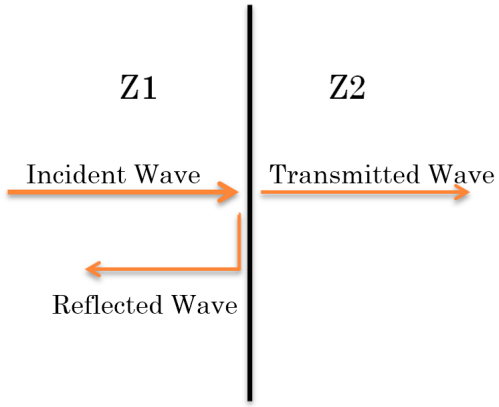

Figure 3.11: Acoustic Reflection and Transmission

Methods

The density of each sample was calculated using the known dimensions of the cylindrical samples to find the volume. The sample mass was measured using a lab scale. For each sample, the peak-to-peak amplitude of the reflection off the front face of the sample was measured. The experimental setup for measuring the reflectivity is shown in Figure 3.12.

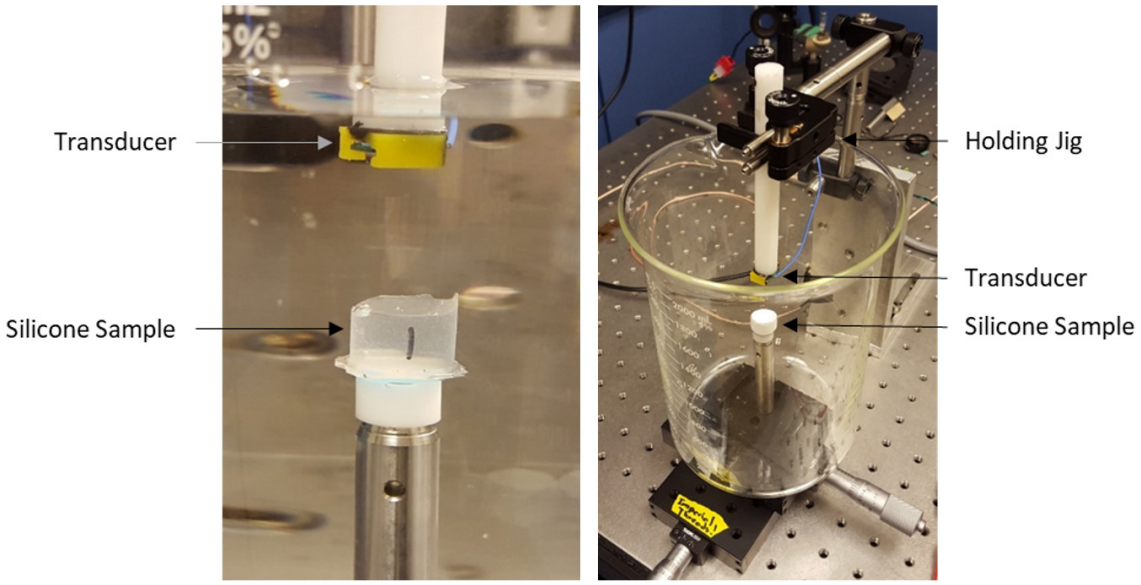

Figure 3.12: Reflectivity Experimental Setup

The samples in these tests were made thick so that the reflection off the back face, when present (i.e. for unloaded samples) did not interfere with the reflection off the front face. Figure 3.13 shows the oscilloscope measurement of the reflected sound signal. A large separation between the first and the second reflection is observed, confirming that the samples were thick enough for the two reflections to be clearly distinguishable.

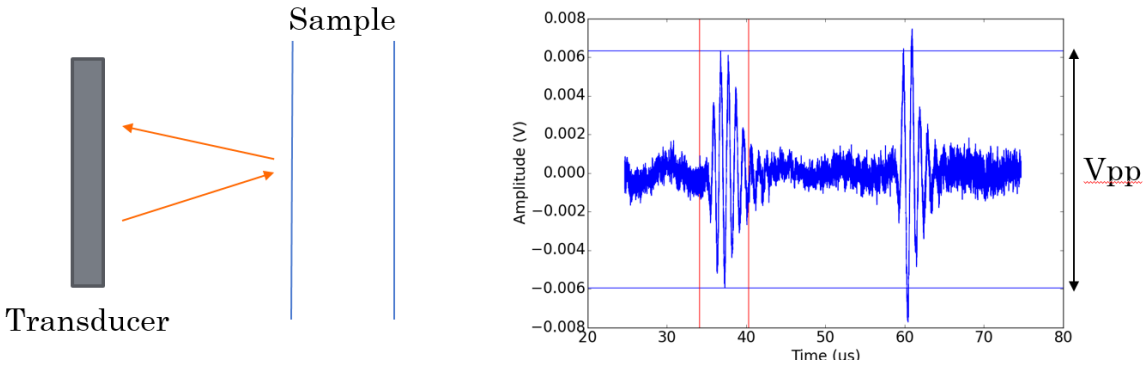

Figure 3.13: Diagram and Oscilloscope Measurement of Reflected Sound Signal

Samples of varying density, and therefore acoustic impedance, were made for these tests. Samples from no loading and a density of 980 ± 53 kg/m^3 up to approximately 1938 ± 53 kg/m^3 were made and tested. A diagram of the measurement is shown in Figure 3.14. The amplitude of the input signal and the standoff distance from the transducer to the front face of the sample were kept constant: the first by keeping the power supply at a constant voltage and power level, and the distance by measuring the time of flight of the first reflection for each sample.

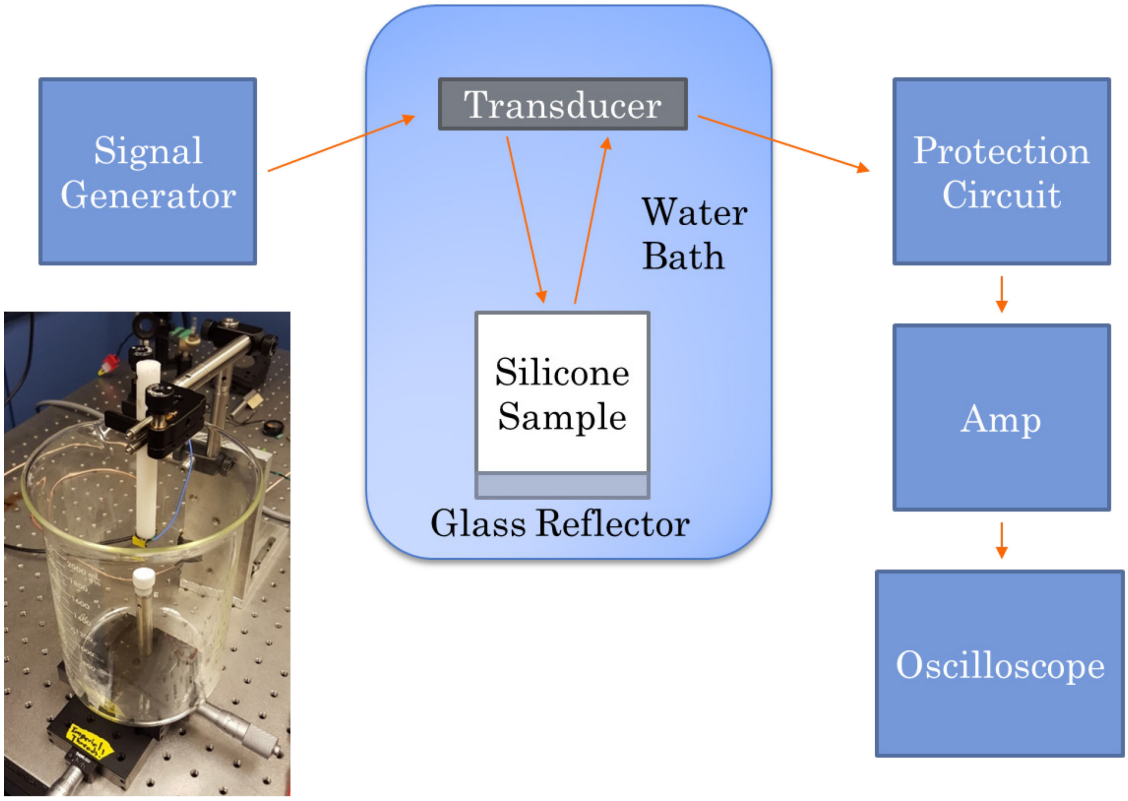

Figure 3.14: Diagram of Experimental Setup for Measuring Reflectivity

The transducer was driven using a 1.0 MHz center frequency, 10-cycle square wave pulse using an Agilent 33220A Function Generator. The transducer converted the electrical pulse into an acoustic pulse which travelled through deionized water to the front face of the sample. A fraction of the incident acoustic wave was reflected back to the transducer from the silicone sample according to the reflectivity equation (Equation 2 in Section 1.2). The transducer converted the received echo back to an electrical signal and sent it to a protection circuit and a 20dB fixed gain amplifier (see Figure 3.15).

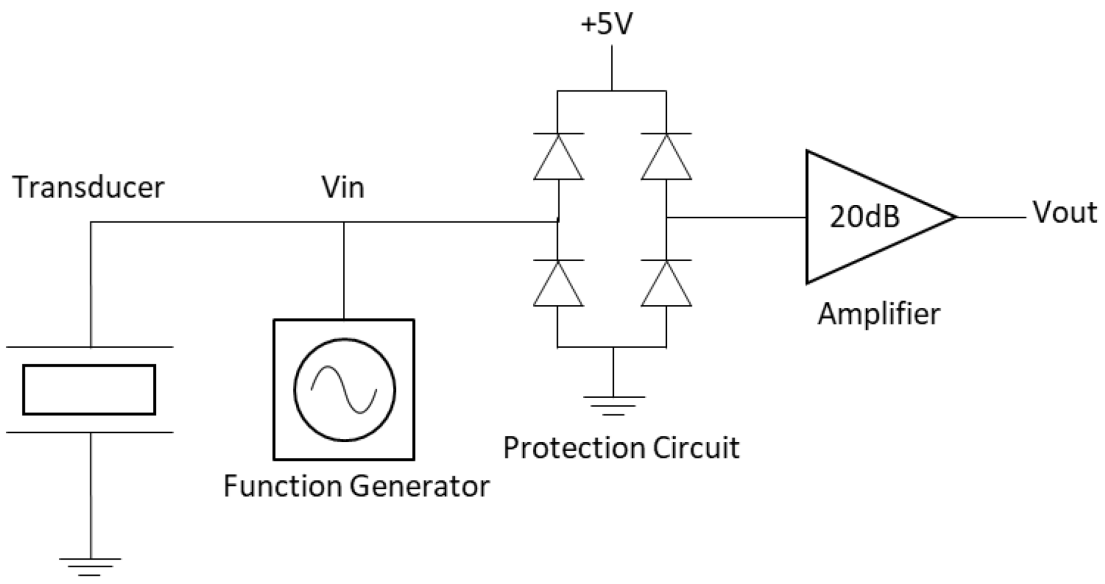

Figure 3.15: Reflectivity Measurement Circuit

The waveform out of the amplifier was captured with a digital oscilloscope. The first echo waveform is isolated and the maximum peak-peak amplitude was measured. This was repeated for each sample of each loading. Comparison of the amplitude obtained with different samples allowed their relative reflectivity to be determined.

In order to determine the variance due to the measuring method (as opposed to process variance), samples of no loading, and therefore with consistent formulation, were made from the same batch of silicone. These unloaded samples were all tested using the method described, thus giving a measure of the variance in the measurement independent of any variance in process or composition. In addition, the process variance was measured by attempting to make samples of the same impedance from different batches of loaded silicone. Results of an F-test between the loaded and unloaded samples are presented in the Results and Discussion. These measurements were plotted and a model for the relationship between density and reflectivity voltage was fitted to the data which showed good agreement.

Results and Discussion

The addition of the ZnO powder increased the acoustic impedance of the dry coupling material by increasing the density of the composite material.

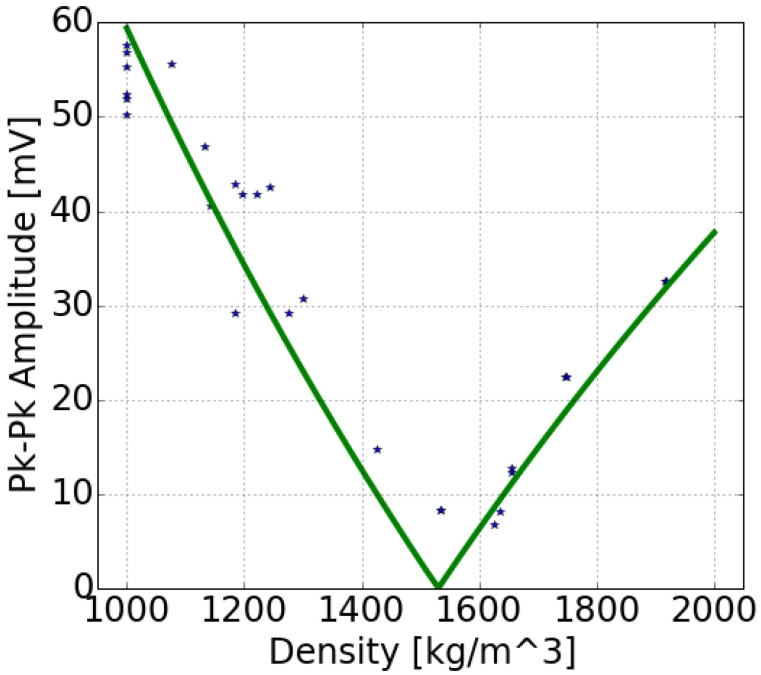

Figure 3.16: Measured and Modelled Density vs Reflectivity Curve

Figure 3.16 shows the reflectivity vs density of the samples made with varying amounts of ZnO loading. The samples were produced using the process described in Section 2.5 of this thesis. As the sample impedance gets closer to the acoustic impedance of water (1.5 MRayls) the reflectivity drops to zero and then, passing that point, increases again. The V shape of the fit is due to the fact that the magnitude of the reflected amplitude is measured. The reflected wave amplitude changes sign from when $Z_1 > Z_2$ to when $Z_1 < Z_2$, but the measurement takes the peak-to-peak voltage and is therefore always positive. The data obtained from the measurements were fitted to a mathematical model of the reflectivity:

$$R = \left|\frac{Z_1 - Z_2}{Z_1 + Z_2}\right|$$

Assuming:

$$Z_{sil} = c\rho$$

$$V_{PP} = \beta \left|\frac{c\rho - Z_{water}}{c\rho + Z_{water}}\right|$$

Where c is the speed of sound in the dry coupling material, ρ is the density of the dry coupling material, V_{PP} is the measured peak-to-peak voltage, β is the conversion factor between the reflectivity and V_{PP}, and Z_{water} is the acoustic impedance of water.

The measurement error was found by calculating the standard deviation of the residual error between the data and the model. This standard deviation was calculated to be 5.65mV.

A least-squares fit was performed to this model using the density, measured V_{PP} data and the known acoustic impedance of water to fit the c and β parameters. The fitted data shows a good agreement with the theory and also is consistent with c, the speed of sound in silicone, being a constant at 980.25 m/s from unloaded to highly loaded samples. The following plot shows a linear regression analysis of the speed of sound calculated from the fitted model parameters vs density. Figure 3.17 shows that the line of best fit is nearly flat with $R^2 = 0.0007$ consistent with no correlation between the ZnO loading and the speed of sound in the material. Previous studies have shown that loading can increase or decrease the speed of sound in silicone, depending on the additive used [26]. Thus, seeing no change in the speed of sound is not unexpected. The variability is likely due to non-homogeneity of the loaded (blue) samples in addition to the measurement error as shown by the spread in the measurements for the unloaded (orange) samples.

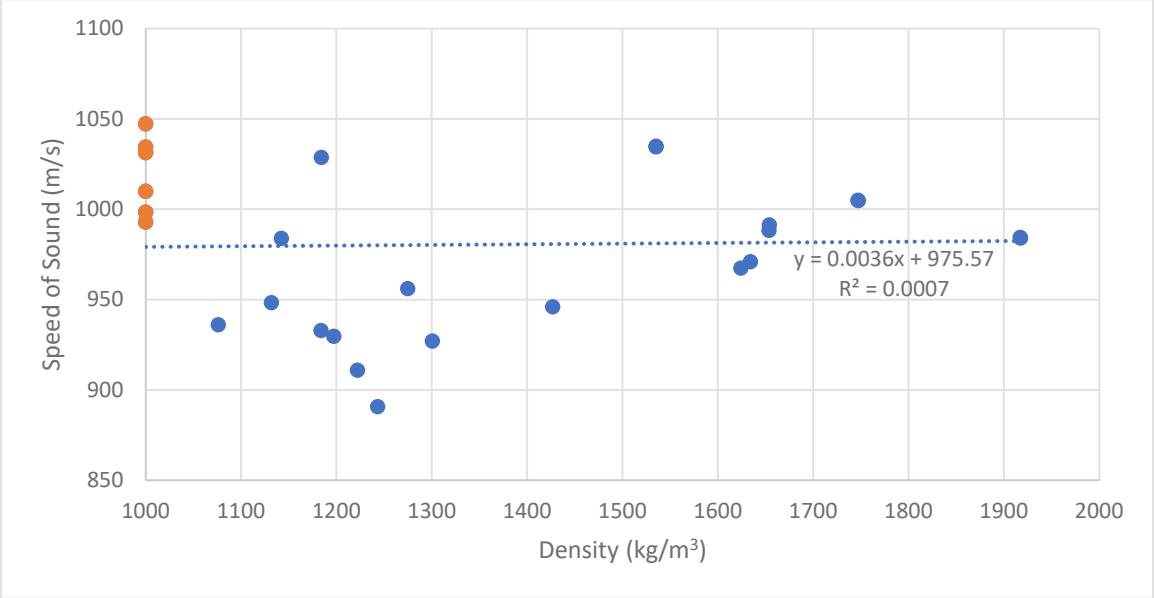

Figure 3.17: Speed of Sound Calculated from Model Parameters vs Density

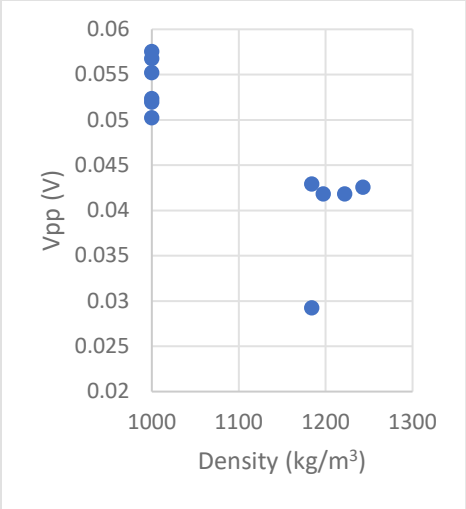

Figure 3.18: Loaded vs Unloaded Variance

The plot in Figure 3.18 shows the measured reflected amplitude V_{pp} for the loaded and unloaded samples. The data on the left at 1000 kg/m^3 in density were the samples made without loading. The data on the right centred around 1200 kg/m^3 were samples manufactured to have a target density of 1200 kg/m^3. An F-test was used to determine if there is any significant difference in the reflectivity variance of the loaded group compared to the unloaded group as would be expected if process error dominated over measurement error. The test produced p=0.08 indicating that the measured variances are not significantly different. This implies that the loading process does not add a significant amount of variation to the measurements.

Since the system is linear, the measured ratio of reflected amplitudes for any two samples is independent of the properties of the transducer used to generate and receive the ultrasound. This is fortunate since one of the transducers used for the initial set of measurements malfunctioned part way through the measurement. It was replaced with another transducer with a different response. In order to ensure that the amplitude ratios measured with the two transducers were indeed consistent, some of the previously measured samples were re-measured with the second transducer and the results, as seen in the table below are consistent with there being no difference from using the second transducer:

Density (kg/m3)	Reflected amplitude with new transducer (mV)	Reflected amplitude with old transducer (mV)	Ratio	Ratio Mean	St. Dev
1197	29.12	34.65	1.19	1.24	0.06
1300	17.32	23.07	1.33		
1917	26.15	31.82	1.22		

Table 3: Comparing sample measurements from old transducer to new transducer

The ratios were varied to a limited degree with a standard deviation much smaller than the mean. Most of the variation is due to the errors in the measuring process, and the variance is well within the variance of the measurements of the amplitude in Figure 3.16.

In order to determine the optimal loading fraction for silicone in order to match its impedance to a particular skin sample, the reflected amplitude from the skin sample is measured and the loading fraction that gives the same reflected amplitude is determined from Figure 3.16. There are two loading fractions that will give the same reflected amplitude from Figure 3.16, but because skin is expected to have an impedance around 2.0 MRayl, it can be assumed that the value on the right (high impedance) side of the minimum is the desired one.

A sample of porcine skin was found to have a peak to peak reflected amplitude of 39.3 mV ± 1 mV which from Figure 3.16 corresponded to a silicone sample made with a density of 2022 ± 14 kg/m^3 and an acoustic impedance of 2.022 ± 0.014 MRayl. This density was used to produce the thin samples used in subsequent Attenuation and PTE measurements (Sections 3.6 and 3.8).

The methods developed in this section can be used to characterize not only silicone but any material as a potential dry coupling for UTET. Additionally, if the material can be cured from a liquid state, the methods using ZnO to increase acoustic impedance in order to match

to skin can be applied. This opens the door for many other polymers to be researched as potential dry coupling materials.

Another potential problem introduced from the ZnO loading could be lowering of the gas permeability of the dry coupling. As discussed in Section 1.3 gas permeability is an important factor for the dry coupling's biocompatibility on skin, allowing moisture to escape the surface of the skin and preventing maceration as well as allowing oxygen to flow into the avascular epidermis.[24] . It was observed qualitatively that ZnO loading also increased the stiffness of the material. It is unknown how the ZnO may have affected the water solubility, chemical stability, or the surface energy of the composite material. The effect of ZnO loading on these properties was not fully investigated in this thesis due to time constraints, however, it would be a good topic for future research If these properties turn out to be adversely affected by the addition of ZnO, then the design could be modified to use a lower loading fraction than the one that maximizes PTE.

Conclusion

This experiment showed that loading the Sylgard 184 was an effective way of increasing the acoustic impedance of the dry coupling. The method was able to create samples with acoustic impedances beyond the range needed to match to skin without compromising the material's durability and without changing the speed of sound. Once a set of reflectivities at various loading fractions were obtained (as in Figure 3.16), the loading fraction needed to match to a particular skin sample could be obtained by simply finding the loading fraction on the high impedance side of the minimum that gave the same reflected amplitude as the skin sample.

3.6 Measuring Attenuation of Silicone and Skin Impedance Confirmation

Introduction

In addition to increasing the acoustic impedance, loading silicone with ZnO powder also increases the acoustic attenuation of the sample. If the increase in acoustic attenuation were large enough, the increased losses due to attenuation might be larger than the decreased reflection losses due to acoustic matching. It was therefore important that the acoustic attenuation in the loaded silicone be characterized to obtain a complete picture of

the acoustic behaviour of the material and its applicability to power transmission applications.

In the following experiments, acoustic attenuation is calculated by measuring the reflectivity of a thin silicone sample of two different thicknesses with the same (known) impedance and (unknown) attenuation overlaid on a material of known acoustic impedance (aluminum). The impedance and attenuation can be obtained from the ratios of the measured echo amplitudes at the water-silicone and silicone aluminum interfaces.

Knowing the attenuation and impedance of the sample, the acoustic impedance of the pork skin can be obtained by using the method in Section 3.5 by matching the measured reflection amplitude at the silicone-pork interface to the mapped reflected voltage-density curve.

Methods

A model was created to separate the effects of attenuation from other losses in the system. For convenience, the author fabricated samples that were a half wavelength and full wavelength in thickness because, as will be shown later, at these thicknesses the phase of each reflected wave is equal.

This experiment uses reflection and transmission coefficients that are calculated using the following formulas:

$$R = \frac{Z_1 - Z_2}{Z_1 + Z_2}, \quad T = \frac{2Z_2}{Z_1 + Z_2}$$

Where R is the reflection coefficient, T is the transmission coefficient, Z_1 is the acoustic impedance of the material the acoustic wave is leaving, and Z_2 is the acoustic impedance of the material that the acoustic wave is entering (see Figure 3.19).

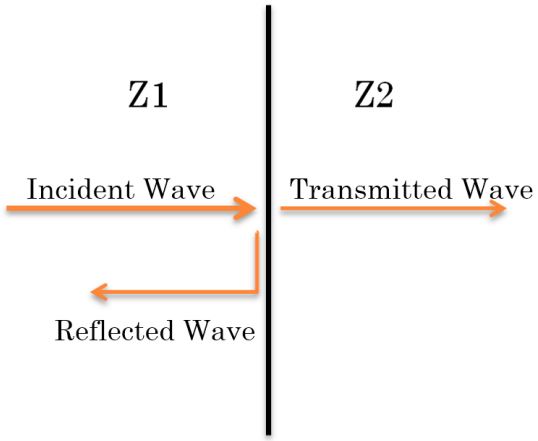

Figure 3.19: Acoustic Reflection and Transmission

The sample was measured on a plate of pure aluminum as the acoustic impedance aluminum is known and consistent.

Figure 3.20 and Figure 3.21 represent the system in this experiment:

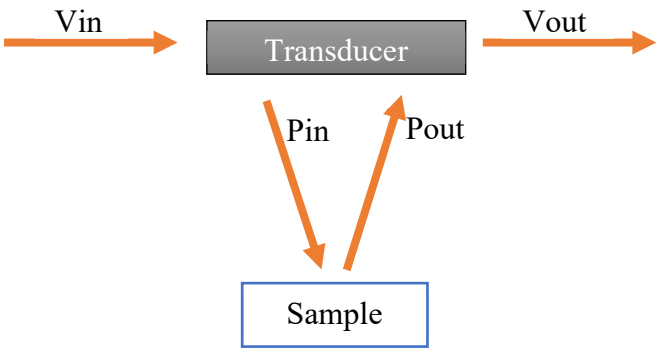

Figure 3.20: Diagram of Signal Pathway

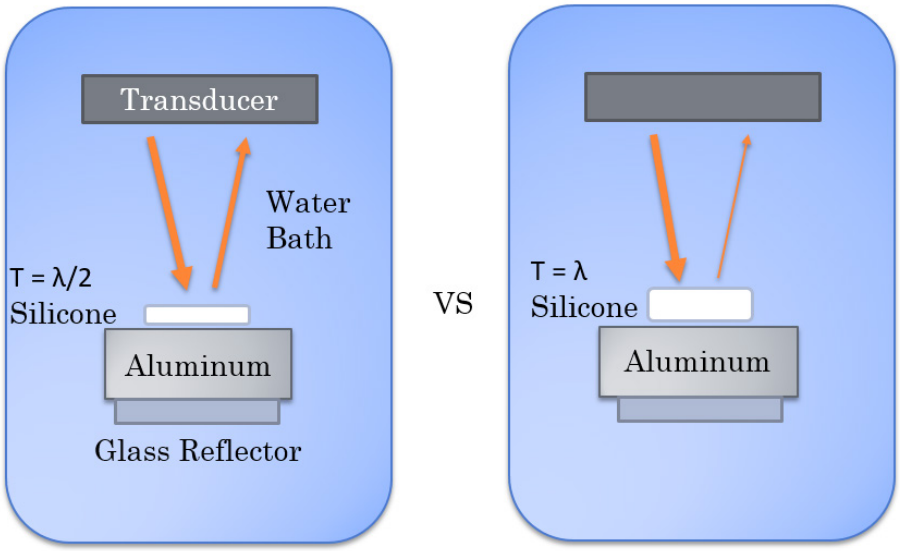

Figure 3.21: Diagram of Attenuation Measurement Setup

System Transfer Function

The voltage out, V_{out}, is measured in this experiment. There is an unknown transfer function between the voltage and pressure associated with the properties of the electronics and piezoelectric transducer. This transfer function is assumed to be linear and is the same for all the measured samples (since it only depends on transducer and amplifier properties). The transfer function is represented by the following equation:

$$\frac{V_{out}}{V_{in}} = \left\{\frac{P_{in}}{V_{in}}\right\}\left\{\frac{V_{out}}{P_{out}}\right\}\left\{\frac{P_{out}}{P_{in}}\right\}$$

Of the terms in this transfer function, V_{out} is measured, $\left\{\frac{P_{in}}{V_{in}}\right\}\left\{\frac{V_{out}}{P_{out}}\right\}$ are unknown and $\left\{\frac{P_{out}}{P_{in}}\right\}$ can be modelled. $\left\{\frac{P_{in}}{V_{in}}\right\}, \left\{\frac{V_{out}}{P_{out}}\right\}$ are properties of the electronics and transducer and so do not depend on the sample composition. V_{in} is the electrical drive amplitude which is held constant through the experiment. These constant terms cancel when taking ratios of measurements for two different materials.

Derivation of Pressure Transfer Function Model

The transfer function $\left\{\frac{P_{out}}{P_{in}}\right\}$ can be modelled from boundary reflectivities; the derivation of this function for a loaded sample is shown:

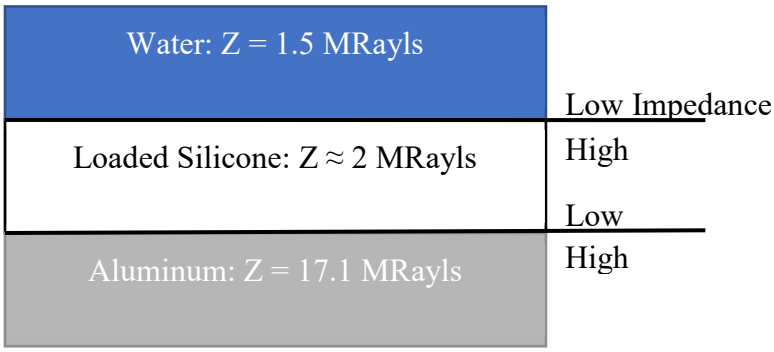

Figure 3.22: Impedances Water, Silicone and Aluminum

Figure 3.22 shows a diagram of the material stack used in this experiment. When sound meets a boundary where the materials change from a high impedance to a low impedance, the phase shift on reflection is 180 degrees [12]. For a loaded silicone sample, every time the sound reflects off the boundary between the water and the top face of the sample from within the sample, the impedance changes from high to low and the phase shifts by 180^o. This makes every other reflection starting with the 3rd reflection negative as shown in Figure 3.23.

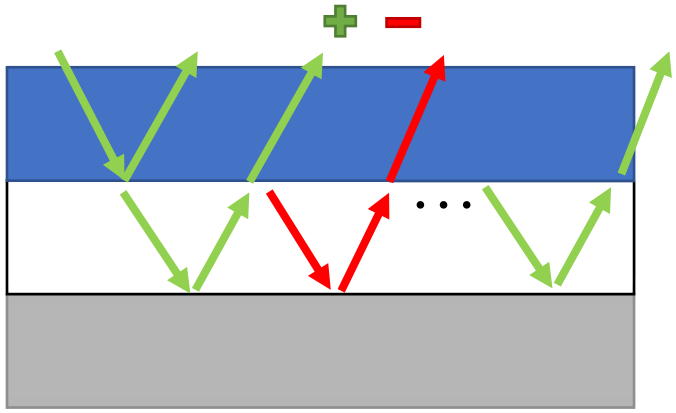

$$R_T = R_1 + T_1R_2T_2e^{2i\beta L}e^{-2\alpha L} + T_1R_2(-1)R_1R_2T_2e^{4i\beta L}e^{-4\alpha L} + T_1R_2(-1)R_1R_2(-1)R_1R_2T_1e^{6i\beta L}e^{-6\alpha L} + \cdots$$

Figure 3.23: Nth Reflection

This is an infinite geometric series and can be represented mathematically as:

$$R_T = R_1 + T_1 R_2 T_2 e^{2i\beta L} e^{-2\alpha L} \sum_{n=0}^{\infty} \left(-e^{2i\beta L} e^{-2\alpha L} R_1 R_2\right)^n$$

which can be summed to give:

$$\frac{P_{out}}{P_{in}} = R_1 + \frac{T_1 R_2 T_2 e^{2i\beta L} e^{-2\alpha L}}{1 + e^{2i\mathrm{B}L} e^{-2\alpha L} R_1 R_2}$$

Where R_T is the magnitude of the total reflection which is equivalent to the transfer function $\frac{P_{out}}{P_{in}}$. The R and T terms are the reflection and transmission coefficients which are calculated using the acoustic impedances of the materials in the system. The term α is the attenuation coefficient. The term $e^{2i\beta L}$ accounts for phase accumulation during round-trip propagation through a material with thickness L and wave number $\beta = \frac{2\pi}{\lambda}$.

The samples were selected to have $L = \frac{\lambda}{2}$ or $L = \lambda$ so that $2\beta L = 2\pi$ or $2\beta L = 4\pi$ and $e^{2\beta L i} = 1$. If the thickness of the sample is a multiple of a half wavelength, the phase term is equal to 1 and does not affect the measurement.

If the ratio of samples with thickness $\lambda/2$ and λ is taken, the following equation is obtained:

$$\frac{\{V_{out}\}_{L=\lambda/2}}{\{V_{out}\}_{L=\lambda}} = \frac{\left\{\frac{V_{out}}{V_{in}}\right\}_{L=\lambda/2}}{\left\{\frac{V_{out}}{V_{in}}\right\}_{L=\lambda}} = \frac{\left\{\frac{P_{in}}{V_{in}}\right\}\left\{\frac{V_{out}}{P_{out}}\right\}\left\{\frac{P_{out}}{P_{in}}\right\}_{L=\lambda/2}}{\left\{\frac{P_{in}}{V_{in}}\right\}\left\{\frac{V_{out}}{P_{out}}\right\}\left\{\frac{P_{out}}{P_{in}}\right\}_{L=\lambda}} = \frac{\left\{\frac{P_{out}}{P_{in}}\right\}_{L=\lambda/2}}{\left\{\frac{P_{out}}{P_{in}}\right\}_{L=\lambda}}$$

The $\left\{\frac{P_{in}}{V_{in}}\right\}$ and $\left\{\frac{V_{out}}{P_{out}}\right\}$ transfer functions and V_{in} are the same for both measurements and cancel out in the ratio. What is left is the ratio of the P_{out}/P_{in} transfer function for each sample, which can be expressed using the model derived above.

The reflection and transmission coefficients can be calculated using the known acoustic impedances of the system. Thus, the only unknown is the attenuation coefficient, which

can be calculated by equating the measured voltage ratio to the modelled pressure transfer function ratio:

$$\frac{\{V_{out}\}_{L=\lambda/2}}{\{V_{out}\}_{L=\lambda}} = \frac{R_1 + \frac{T_1 R_2 T_2 e^{-\alpha\lambda}}{1 + e^{-\alpha\lambda} R_1 R_2}}{R_1 + \frac{T_1 R_2 T_2 e^{-2\alpha\lambda}}{1 + e^{-2\alpha\lambda} R_1 R_2}}$$

From this derivation, it is learned that:

V_{out}	Voltage Out	The voltage seen at the oscilloscope.	Measured.
$\frac{P_{out}}{P_{in}}$	Pressure Transfer Function	Ratio of the pressure reflected back to the transducer over the pressure incident to the sample.	Modeled as: $R_1 + \frac{T_1 R_2 T_2 e^{-2\alpha L}}{1 + e^{-2\alpha L} R_1 R_2}$
$\frac{\{V_{out}\}_{L=\lambda/2}}{\{V_{out}\}_{L=\lambda}}$	Measured Ratio	This ratio is used to cancel out the unknowns, making it equal to the Modelled Pressure Transfer Function Ratio.	Calculated from measured V_{out} for samples with a half wavelength thickness and a full wavelength thickness.
$\frac{\left\{\frac{P_{out}}{P_{in}}\right\}_{L=\lambda/2}}{\left\{\frac{P_{out}}{P_{in}}\right\}_{L=\lambda}}$	Modelled Pressure Transfer Function Ratio	By equating this ratio to the Measured Ratio, enough unknowns are eliminated to separate out the attenuation coefficient	Calculated from modelled $\frac{P_{out}}{P_{in}}$ for each sample thickness.

R_1, R_2, T_1, T_2	Reflection and Transmission Coefficients	Fraction of the acoustic wave that is reflected and transmitted at the boundary between materials	Calculated from known acoustic impedance of water, aluminum, and silicone sample.
α	Attenuation Coefficient	Sound energy lost due to absorption and scattering within the material.	Solved for.

Table 4: Table of Attenuation Model Parameters

Therefore, by taking the ratio of the peak-peak amplitude of the received voltage for the half wavelength sample over that of the full wavelength samples, the attenuation coefficient of the material can be solved. To account for measurement error, two times the standard deviation, found in Section 3.5, is added to and subtracted from the amplitude measurements. Inputting this into the model gives the 95% confidence interval of the attenuation coefficient.

The acoustic impedance of the silicone sample was found by calculating the density of the sample and knowing speed of sound from the measurements described in Section 3.5. The density was calculated by measuring the sample's dimensions, calculating the volume, and measuring the mass.

If pork skin is substituted for aluminum in the system, this method can also calculate the acoustic impedance the pork skin. This offers a validation of the process by which the ZnO loading fraction is selected and demonstrates that it actually achieves an impedance equal to the impedance of pork skin.

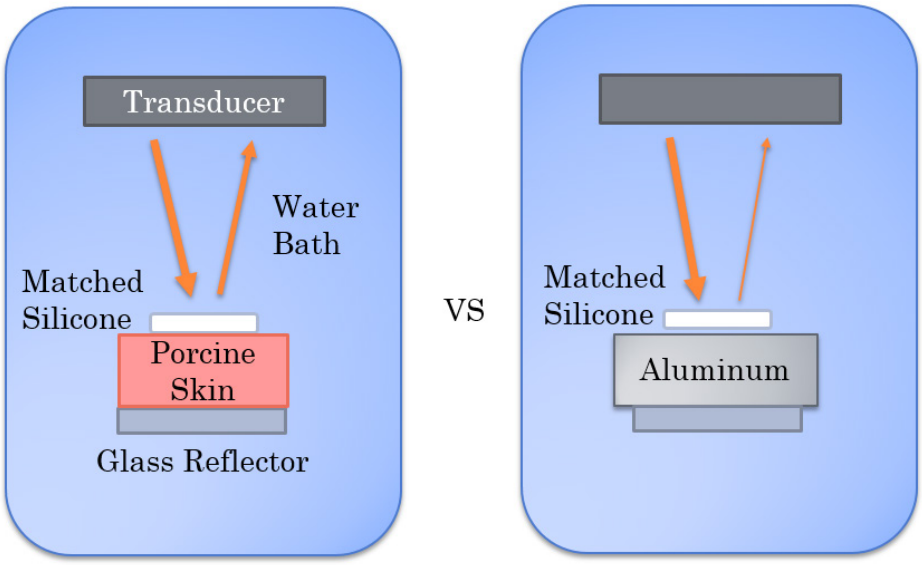

Figure 3.24: Diagram of Measurement Setup for Checking Porcine Skin Attenuation

The ratio $\frac{\{V_{out}\}_{Al}}{\{V_{out}\}_{Skin}}$ was determined by measuring the reflection in the two experimental scenarios shown in Figure 3.24. Using the measured acoustic impedance and attenuation of the loaded silicone, an expression could be derived for the impedance of the porcine skin:

$$\frac{\left\{\frac{V_{out}}{V_{in}}\right\}_{Al}}{\left\{\frac{V_{out}}{V_{in}}\right\}_{Skin}} = \frac{\left\{\frac{P_{in}}{V_{in}}\right\}\left\{\frac{V_{out}}{P_{out}}\right\}\left\{\frac{P_{out}}{P_{in}}\right\}_{Al}}{\left\{\frac{P_{in}}{V_{in}}\right\}\left\{\frac{V_{out}}{P_{out}}\right\}\left\{\frac{P_{out}}{P_{in}}\right\}_{Skin}} = \frac{\left\{\frac{P_{out}}{P_{in}}\right\}_{Al}}{\left\{\frac{P_{out}}{P_{in}}\right\}_{Skin}}$$

$$\frac{\{V_{out}\}_{Al}}{\{V_{out}\}_{Skin}} = \frac{\left\{R_1 + \frac{T_1 R_2 T_2 e^{-\alpha\lambda}}{1 + e^{-\alpha\lambda} R_1 R_2}\right\}_{Al}}{\left\{R_1 + \frac{T_1 R_2 T_2 e^{-\alpha\lambda}}{1 + e^{-\alpha\lambda} R_1 R_2}\right\}_{Skin}}$$

In this case, the attenuation constant, α, remains the same because the same silicone sample is used for both measurements. The reflectivities and transmissivities change depending on whether aluminum or pork skin is used. The properties $\{R_2, T_2\}_{Skin}$ are solved for and are used to calculate the acoustic impedance of the porcine skin sample.

From this derivation, it is learned that:

$\frac{\{V_{out}\}_{Al}}{\{V_{out}\}_{Skin}}$	Measured Ratio	This ratio is similar to the previous measured ratio with the exception that the second measurement's silicone sample is backed by skin. Thus, the difference is seen in the reflection and transmission coefficients of the denominator.	Calculated from measured V_{out} for samples backed by aluminum and porcine skin
α	Attenuation Coefficient	This is the same attenuation coefficient that was calculated previously because the same silicone sample is used.	Known from previous calculation
$\{R_2, T_2\}_{Al}$	Reflection and Transmission Coefficients of Aluminum	Fraction of the acoustic wave that is reflected and transmitted at the boundary between silicone and aluminum	Calculated from known acoustic impedance of aluminum and silicone
$\{R_2, T_2\}_{Skin}$	Reflection and Transmission Coefficients of Porcine Skin	Fraction of the acoustic wave that is reflected and transmitted at the boundary between silicone and porcine skin. Solving for these coefficients allows the acoustic impedance of porcine skin to be calculated.	Solved for

Table 5: Table of Model Parameters for Solving Porcine Skin Acoustic Impedance

Results and Discussion

The measured attenuation coefficient for the loaded silicone with a design density of 2008 kg/m^3 was -2.66 ± 0.15 dB/mm. This is fairly high, meaning that every millimeter the sound power is reduced by 46 ± 1.8%. This issue can be mitigated by keeping the dry coupling

layer thin. There is a minimum thickness needed for the dry coupling in order to have it act as a protective layer to the transducer and so would need to be strong enough not to tear under stresses from predictable loads e.g. dropping the unit or removal from the skin. A very thin silicone sample would have less attenuation but would also be weaker and more prone to tearing from usage. The thin samples made with 0.5mm thickness still have considerable strength and can withstand stretching, compression and scratching by hand. They should certainly be strong enough to remain intact after being dropped. It is likely that a thinner layer, which can withstand the most likely damaging scenarios with a factor of safety, can be designed.

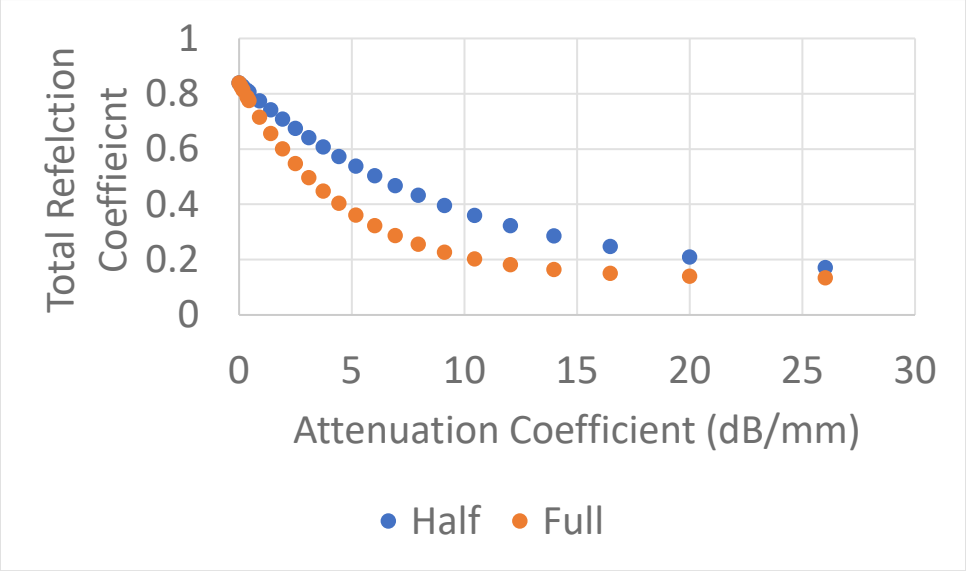

Figure 3.25: Modelled Reflection Coefficient for Half and Full Wavelength Thick Samples as Attenuation Increases

Figure 3.25 shows how the measured amplitude will vary comparing a full wavelength to a half wavelength thickness sample for varying levels of attenuation. At very high and very low attenuation the two curves converge, making it difficult to see a measurable difference in the total reflectivity. This makes sense as there would be little signal reduction in a low attenuation sample and only the top surface reflection in a sample with high attenuation. There is good separation in signal strength for points away from extreme values. This separation makes it possible to measure a difference in signal strength between samples of a half and full wavelength thickness.

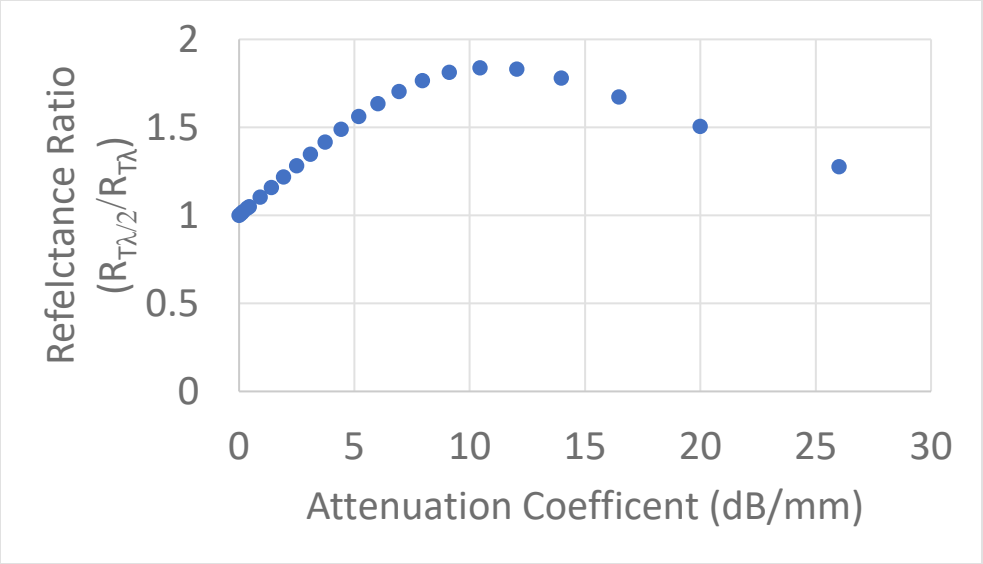

Figure 3.26: Reflectivity Ratio, Total Reflectivity from Samples of Half Wavelength Over Full Wavelength Thickness, as Attenuation Increases

Similarly, Figure 3.26 shows the ratio of the overall reflection of a half wavelength sample over a full wavelength one. It is more clear from this plot that the same half/full ratio is predicted for samples with a very large amount of attenuation as samples with very low attenuation over a range of large to negligible attenuation shown by the hump in this graph.

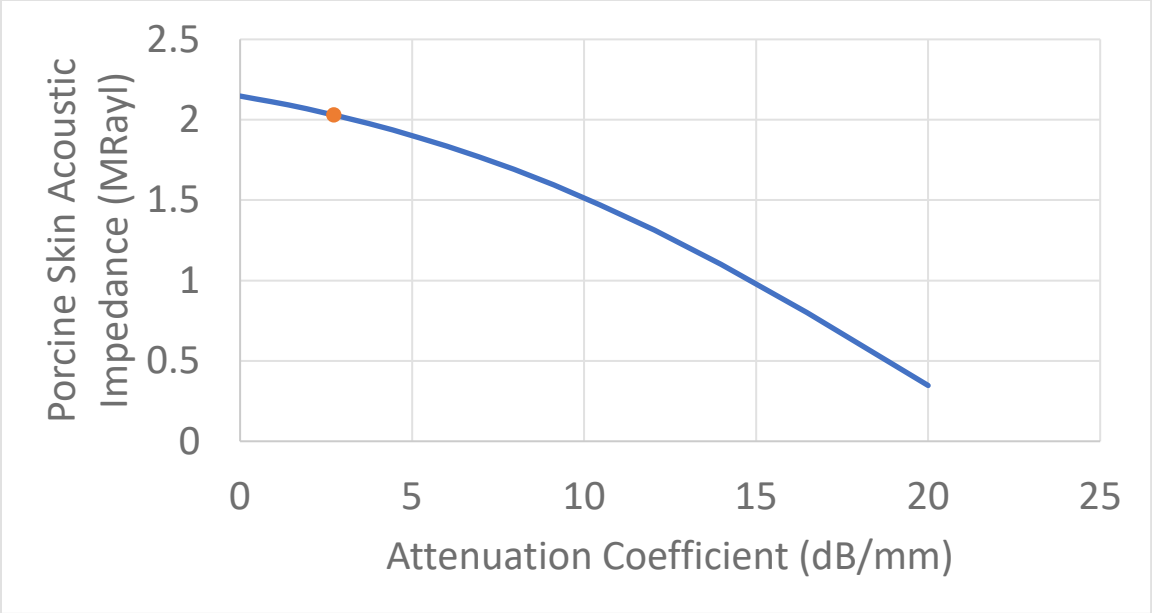

Figure 3.27: Sensitivity of Porcine Skin Impedance to Changes in Sample Attenuation Coefficient

Figure 3.27 shows the sensitivity of the porcine skin acoustic impedance to values found for the attenuation coefficient. Using the attenuation value calculated in this section, the acoustic impedance of porcine skin is calculated to be 2.03 MRayl which is within the range calculated in Section 3.5 of 2.022 ± 0.014 MRayl.

Human skin has highly variable acoustic impedance (1.659 – 2.115 MRayl)[10]. If matching is poorly done, say a patient has skin with an acoustic impedance of 1.659 MRayl and is fitted with a dry coupling with an acoustic impedance of 2.115 MRayl, the system will incur an 12.1% reflection loss in addition to more attenuation losses than is necessary. Therefore, acoustic matching to the patient's skin may prove to be needed.

A series of silicones that range from the lowest to the highest acoustic impedances seen for human skin could be prepared and the best matched one selected for a patient. Skin at the implant site is likely to be different than pig skin or human skin elsewhere on the body and so will require some characterization. A transducer set up to measure the reflectivity off skin and characterized using the method in Section 3.5 could be used in the clinic to measure the implant site skin's acoustic impedance.

Conclusion

This experiment found that the attenuation of the matched silicone was high enough to be a concern for thick dry coupling layers (2.7 dB/mm). Therefore, in order to gain the benefit of reduced reflections obtained from matching, it is important to use the minimal thickness of loaded silicone consistent with requirements for mechanical strength and durability.

The test also provided confirmation that the measurement of the porcine skin's acoustic impedance from Section 3.5 was accurate by independently finding nearly the same acoustic impedance (2.02 vs 2.03 MRayl).

The Sylgard 184 bulk of the dry coupling was now satisfactorily characterised for acoustic impedance and attenuation. Attention now turned to examining the effect of the adhesive layer on the PTE of the system. The first step of which involved measuring the thickness of the adhesive layer.

3.7 Adhesive Layer Thickness

Introduction

An adhesive layer was added to the dry coupling samples. The thickness of the adhesive layer applied to the samples was measured to model its effect on the PTE of the system (see Section 3.9).

Controlling for the thickness of the adhesive layer during application required lab equipment that was not available. The purpose of measuring the thickness of the adhesive layer was to compare the power transfer efficiency of a sample with the adhesive layer to a sample without and, based on the thickness of the adhesive layer, determine the accuracy of the KLM model.

Methods

The thin adhesive layer thickness was measured using digital photography. The sample with the adhesive was placed between two glass slides and then photographed using a Samsung Galaxy S5 camera focused on the front face of the glass slides.

The distance between the top slide and bottom slide edges in contact with the sample was calculated in ImageJ.[33] The distance per pixel was determined by counting the number of pixels between two lines on a ruler in the same plane as the sample edge. The adhesive layer was removed from the silicone sample and the thickness was remeasured. The difference in height between the two measurements gave the thickness of the adhesive layer.

Results and Discussion

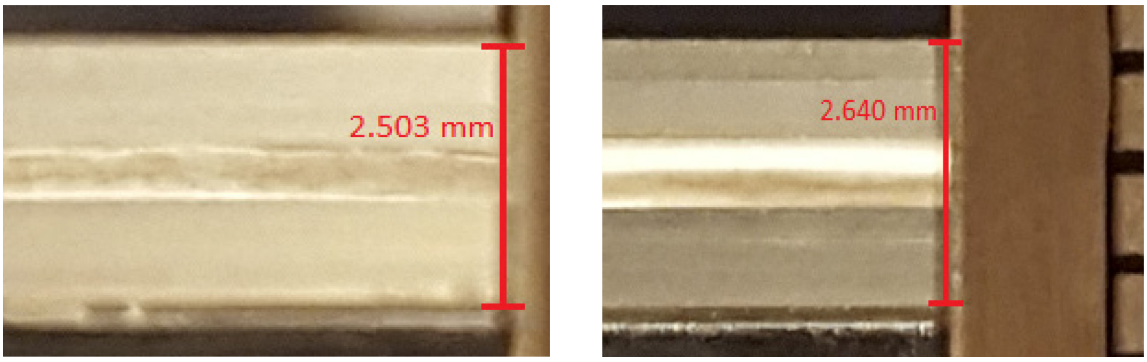

Figure 3.28: Left: Stack Height without Adhesive Layer, Right: Stack Height with Adhesive Layer

Figure 3.28 shows the photographs taken and the measured stack heights. The resolution of the technique was limited to about one pixel giving an estimated thickness uncertainty of 0.02mm. The measured thickness of the adhesive layer was 0.137±0.03mm.

Conclusion

This experiment was a simple method to measure the thickness of the adhesive layer of the dry coupling. Finding the thickness of the layer allowed the effect of the layer's thickness on the PTE of the system to be calculated using the KLM model (Section 3.9). The KLM's prediction could then be compared to the empirically measured PTE (Section 3.8).

3.8 Power Transfer Efficiency

Introduction

The PTE test was the definitive test of the dry coupling design performance. This experiment determined if there is an efficiency advantage to using ZnO to load the dry coupling for acoustic impedance matching. This experiment also determined if the adhesive layer had an effect on the system's PTE.

Methods

A set of experiments was conducted to compare the efficiency of a dry coupling loaded with ZnO to unloaded silicone dry coupling to show the optimization's efficiency advantage. The PTE was also measured to find the effect of the thin layer of adhesive applied to the samples. Finally, the PTE through just porcine skin was used as a measure of maximum efficiency.

Test samples were made at half a wavelength in thickness, one loaded to match the acoustic impedance of porcine skin and one unloaded. The PTE was measured with the Vector Network Analyser as outlined in Section 3.1. Five sets of experiments were carried out as follows:

- Max PTE of porcine skin only
- Matched (loaded) sample, coupled to porcine skin using coupling gel
- Matched (loaded) sample, coupled to porcine skin using adhesive layer
- Unmatched (unloaded) sample, coupled to porcine skin using coupling gel

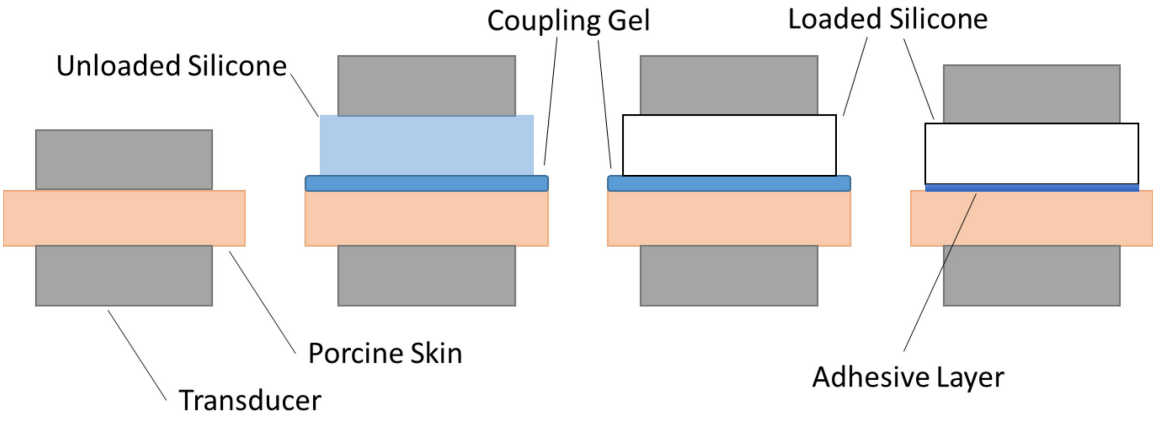

Figure 3.29: Four Material Stacks used for the PTE Experiments

Transducers were fixed to a Thorlabs cage and aligned as described in Section 3.2. Then using coupling gel and the vector network analyzer, the maximum PTE was found by moving the free transducer across the face of the fixed transducer to find maximum PTE in each principal direction. After the best position was found, the free transducer was held in place while the other side of the cage was brought into contact with the transducer which was then superglued in place

The coupling gel had no effect on the PTE as it has the same acoustic impedance as the matching layer of the transducers and is also extremely thin (<10μm).

The cage kept the transducers in the correct alignment and position as the transducers were brought together with the sample stack placed in-between, centered on the transducers. The measurements were taken when good contact and a strong signal that maximized the PTE was achieved. This process was repeated 12 times for each sample stack in order to estimate the variability of the measurement.

Results and Discussion

The power transfer efficiency experiments showed that, despite the added attenuation loss due to the ZnO particles scattering the ultrasound, the reduction in losses achieved by acoustic impedance matching resulted in a net gain in power transfer efficiency.

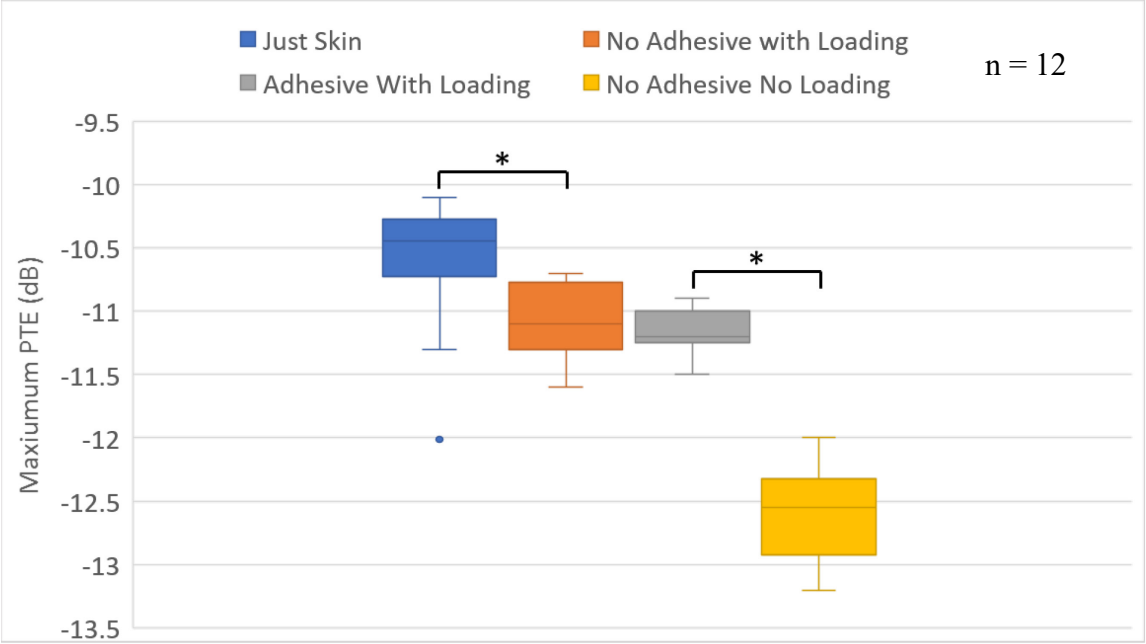

Figure 3.30: PTE of Each Material Stack

Figure 3.30 shows the PTE measured with different stacks of materials between transducers. The error bars are created from the quartiles of the data. The bottom error bar goes from the minimum (exclusive of outliers) to the first quartile (the middle number between the minimum and the median). Similarly, the top error bar goes from the third quartile to the maximum. The "just skin" condition is when the transducers are coupled directly to skin with acoustic gel and represents a ceiling for the efficiency that could be achieved with a dry coupling. Unsurprisingly, efficiency for just skin is higher than with any dry coupling material studied. Comparing just skin to the next highest scenario, the stack with no adhesive with loading, a t-test gave a one-tailed p-value of 0.014.

The fact that there is no statistically significant difference between PTE with adhesive and with no adhesive (one-tailed p-value of 0.185) shows that reduction in PTE due to the addition of the adhesive layer is small, with a 95% confidence interval of the difference between means of $-0.326\text{dB} \leq \mu_{Adh} - \mu_{NoAdh} \leq 0.126\text{dB}$. Compared to the loaded silicone samples with adhesive, the unloaded samples show a significantly lower PTE, with a one-tailed p-value of 7.18E-08 and a 95% confidence interval of the difference between means of $-1.81 \leq \mu_{Load} - \mu_{NoLoad} \leq -1.09$. This indicates that the ZnO loading contributes significantly to improving the PTE of the dry coupling.

The PTE for the just skin group has a mean value of -10.63dB. The mean PTE of the loaded with adhesive samples is -11.18dB which is 88.1% relative to the maximum achievable efficiency. The mean PTE of the unloaded sample is -12.53dB or 64.6% relative to the maximum efficiency. Thus, acoustic impedance matching through ZnO loading increased the overall PTE by 23.5% relative to the maximum efficiency achievable.

Conclusion

This experiment showed ZnO loading confers an efficiency advantage over unloaded silicone and that a low-loss adhesive layer can be made. Despite the increased attenuation due to scattering from the ZnO particles, the combined effect of increased attenuation and reduced reflective losses improved the efficiency of a loaded sample relative to the maximum achievable PTE by 23.5%. The adhesive layer had no statistically significant effect on the PTE. Therefore, a thin dry coupling with loaded Sylgard and an adhesive layer is a viable design with improvements to the PTE compared to a simple unloaded silicone.

Knowing the PTE of each stack allowed the system to be modelled. This also allowed the effect of the adhesive layer on the PTE to be investigated.

3.9 KLM Model of System Behaviour

Introduction

The KLM model allows for the effects of changes to the acoustic properties and thickness of the various layers (loaded silicone, adhesive layer, porcine skin) on the PTE of the system to be estimated. The purpose of this section is to explore the validity of the KLM model by comparing modelled and measured frequency-sweep PTE data, and to compare the model's estimation of the effect of the adhesive layer on the PTE to the measurements taken in Section 3.8.

Methods

The KLM is a transmission line model that allows you to add acoustic or electrical elements by multiplying 2x2 matrices that describe the input-output relationship for that element.

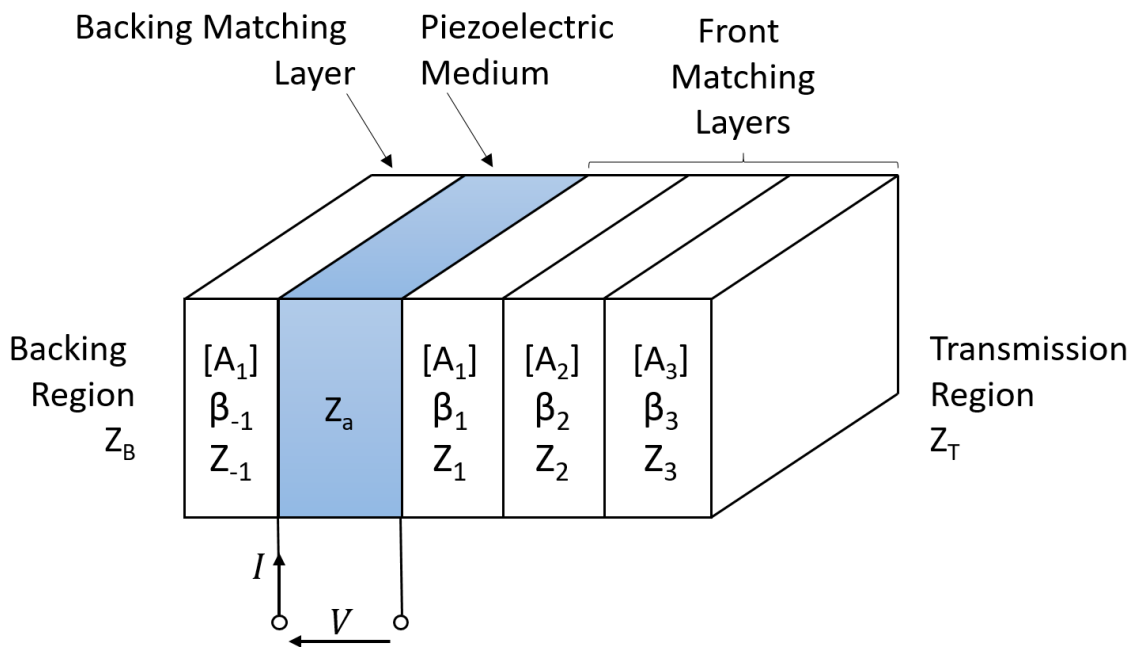

Figure 3.31: Diagram of the KLM Model

In Figure 3.31 the greyed element represents the piezoelectric component of the model. The derivation of KLM piezoelectric model is explained in detail in reference [34]. The work done in this thesis involved the non-piezoelectric acoustic layers following the piezo layer and so the derivation of the piezo element of the model will be left out. The piezoelectric layer takes the source current and voltage and treating the piezoelectric conversion as a linear process, uses the properties of the piezo to calculate a transfer matrix, the outputs of which are the force and velocity seen at the surface of the piezo (Figure 3.32).

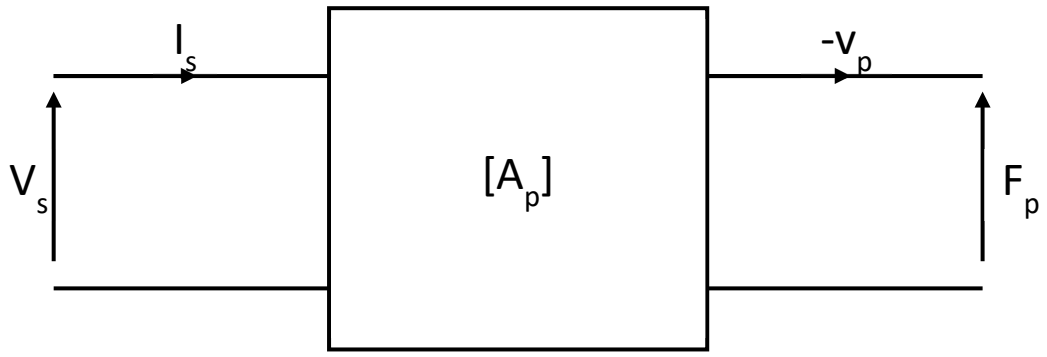

Figure 3.32: The Piezoelectric Element Converts the Current and Voltage into Velocity and Force

Each non-piezoelectric acoustic element represents a layer of material in line with the travel of the acoustic wave (represented diagrammatically in Figure 3.33). Each has its own transfer matrix that takes the previous velocity and force of the acoustic wave as an input and calculates the force and velocity of the acoustic wave after it has passed through the material as an output.

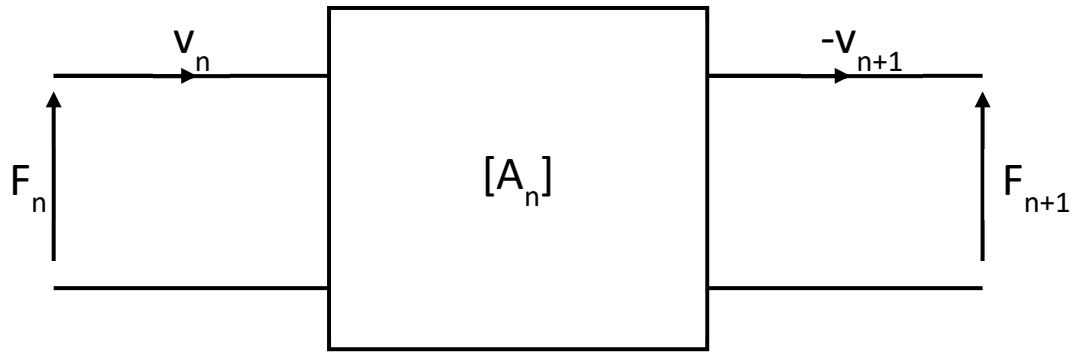

Figure 3.33: The Non-Piezoelectric Element

Each of the acoustic transfer matrices takes the form:

$$\begin{bmatrix} F_n \\ v_n \end{bmatrix} = \begin{bmatrix} \cosh(\gamma_n l_n) & Z_n \sinh(\gamma_n l_n) \\ \dfrac{\sinh(\gamma_n l_n)}{Z_n} & \cosh(\gamma_n l_n) \end{bmatrix} \begin{bmatrix} F_{n+1} \\ -v_{n+1} \end{bmatrix} = [A_n] \begin{bmatrix} F_{n+1} \\ -v_{n+1} \end{bmatrix}$$

Where the propagation coefficient $\gamma = \alpha + j\beta$, in which α is the attenuation coefficient and β is the wavenumber. The wavenumber $\beta = \omega/c$, where ω is the frequency in rad/s and c is the speed of sound in the material. The term l is the thickness of the material and Z is the acoustic impedance of the material.

The overall transfer matrix is found by multiplying all the transfer matrices in the correct order.

$$[A^{tr}] = [A_p]\prod_{n=1}^{N}[A_n]$$

This transfer matrix will give the force of the acoustic wave seen by the load given the source current and voltage.

$$\begin{bmatrix} V_s \\ I_s \end{bmatrix} = [A^{tr}]\begin{bmatrix} F_2 \\ 0 \end{bmatrix}$$

The velocity of the acoustic wave seen by the load can be calculated by dividing the force by the acoustic impedance of the load.

$$v_2 = {}^{F_2}/_{Z_L}$$

The process can be reversed to find the voltage and current on the receive side. The input and output power can then be calculated and thus the power transfer efficiency.

Building on a KLM model of ultrasonic UTET links[30] previously developed in our lab[30], the author added layers for porcine skin, loaded Sylgard silicone and the thin adhesive layer. For each material, the measured acoustic impedance, attenuation, thickness and speed of sound was used with the exception of the porcine skin's attenuation. The porcine skin's attenuation wasn't measured due to difficulty obtaining a sample with a thickness of half a wavelength. Instead, the attenuation of the porcine skin was used as a parameter when fitting the KLM model to measured data. Using the piezoelectric electromechanical coupling factor, k_t, the piezoelectric transducer's attenuation, α_p, and porcine skin attenuation, α_{skin}, as parameters, the KLM model was fit using a least-squares

fit to the average curve of each experiment involving the dry coupling as outlined in Section 3.8. These experiments included:

1. Matched sample, coupled to porcine skin using coupling gel
2. Matched sample, coupled to porcine skin using adhesive layer
3. Unmatched sample, coupled to porcine skin using coupling gel

The fitted parameters for the first of the experiments were used as the initial guess in the second experiment, and the fitted parameters from experiment two were used as the initial guess for experiment three, parameters from experiment three were fed into experiment one. The best fit for the transducer properties were taken to be the average of the best-fit parameters obtained by fitting to these three parameters

Results and Discussion

The fitted parameters used for the KLM model in each of the following experiments are:

$$k_t = 0.615, \alpha_p = 172\ \frac{Np}{m}, \alpha_{skin} = 106\frac{Np}{m},$$

In the following plots, the orange curve represents the KLM model, the blue curve the average of the experimental data and the grey curves are each individual experimental curve.

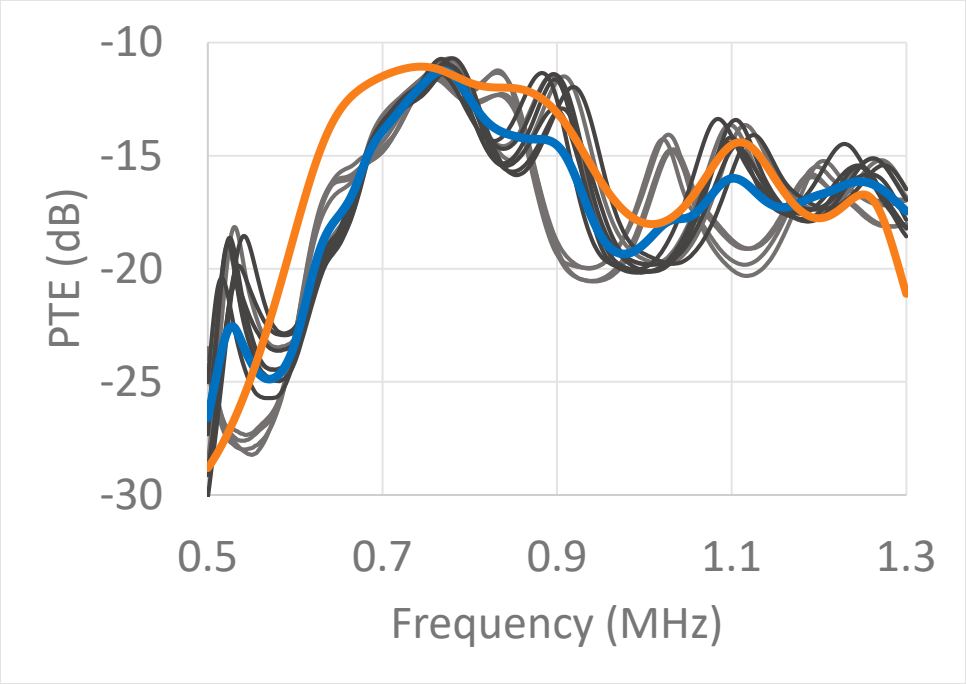

Figure 3.34: Matched Sample Coupled to Porcine Skin Using Coupling Gel

The KLM model (orange curve in Figure 3.34) is not a perfect quantitative match to the observed experimental data, but it does show good qualitative agreement, capturing the slope of the initial rise in efficiency if not the frequency at which the rise occurs. For the majority of the rest of the curve, the KLM model stays within the range of experimentally measured values. The KLM model also shows good qualitative agreement with the resonances in the experimental data, the maximum PTE being close in frequency and magnitude to the experimental maximum.

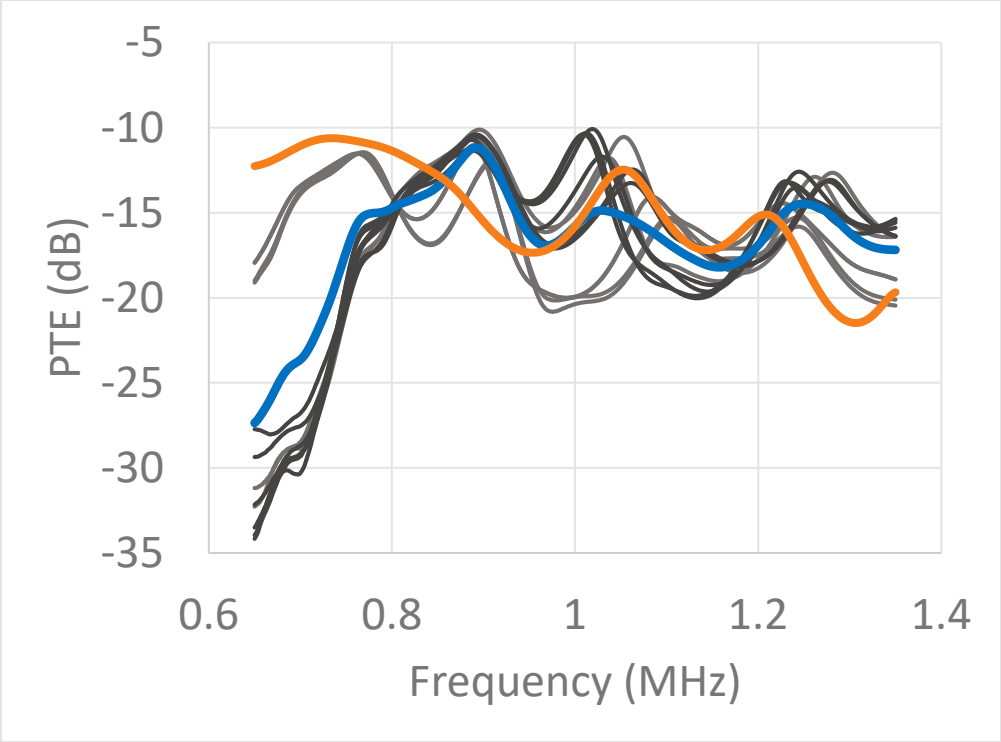

Figure 3.35: Matched Sample Coupled to Porcine Skin Using Adhesive Layer

For the experiment that used the silicone adhesive layer to couple to pork skin the KLM model once again overestimated the PTE at low frequencies (Figure 3.35). The data shows two typical patterns, one where the PTE is high and resonates at lower frequencies and one where the PTE is low for the low frequencies and resonates at a higher frequency. This is likely due to variation in the thickness of the adhesive and skin layers. Measurements through thicker samples will resonate at lower frequencies. If the sample were to shift so that the transducers were centred over a thicker part of the sample, another curve with a lower resonance would be observed. The modeled curve is similar to the measurements with lower frequency resonance.

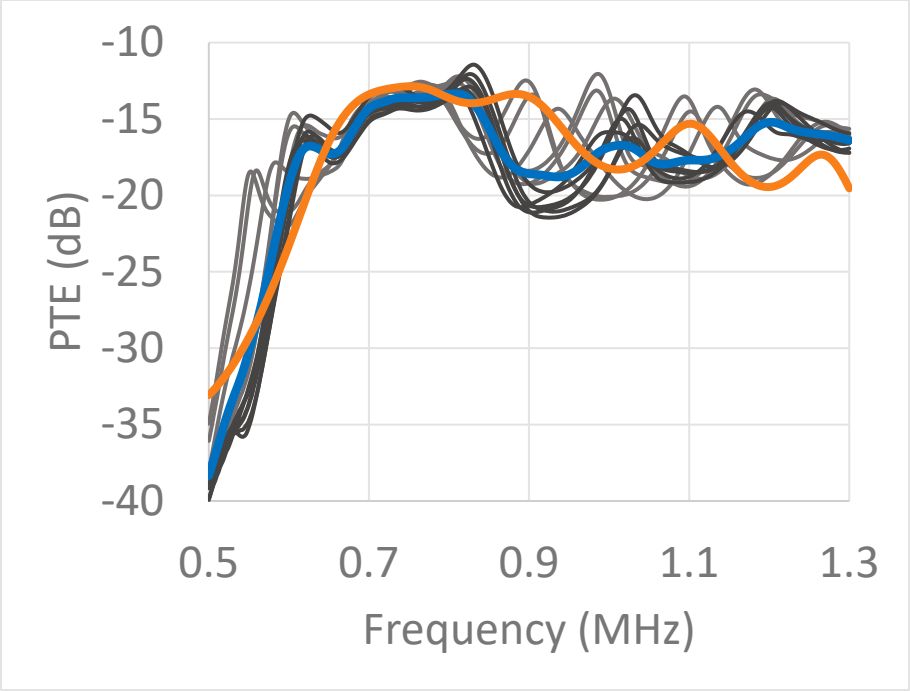

Figure 3.36: Unmatched Sample Coupled to Porcine Skin Using Coupling Gel

For the final experiment (Figure 3.36) the KLM model stays within the range of experimental values for nearly the entire range of data. The resonances occur at similar frequencies to the observed data and the model closely matches the magnitude of the local maxima and minima.

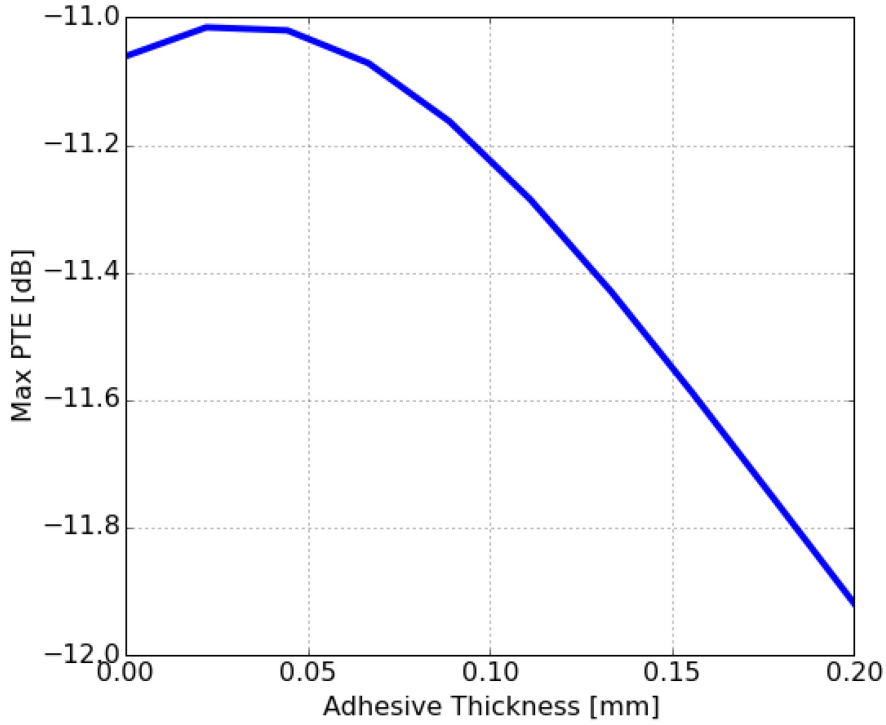

Figure 3.37: PTE Through Sample with Increasing Adhesive Layer Thickness

The KLM model shown in Figure 3.37 predicts that a thin layer of adhesive has a minuscule positive effect (~0.05dB) on the PTE for extremely thin layers (between 0 and 65µm). Although the adhesive layer is very thin, it affects the overall PTE by changing the total cavity length that the sound must travel through. Above 65µm in thickness, the PTE, compared to no adhesive layer, decreases by ~1dB at 0.2mm thick. At the measured adhesive thickness (Section 3.7) of 0.137±0.041mm, the KLM predicted a PTE decrease between ~0.15dB to 0.75dB. Experimentally, the difference between the maximum PTE without an adhesive layer and the minimum PTE with the adhesive layer is 0.8 dB (Section 3.8). It is possible, then, that the decrease in efficiency predicted by the KLM model can account for most of the observed reduction in efficiency from the adhesive layer.

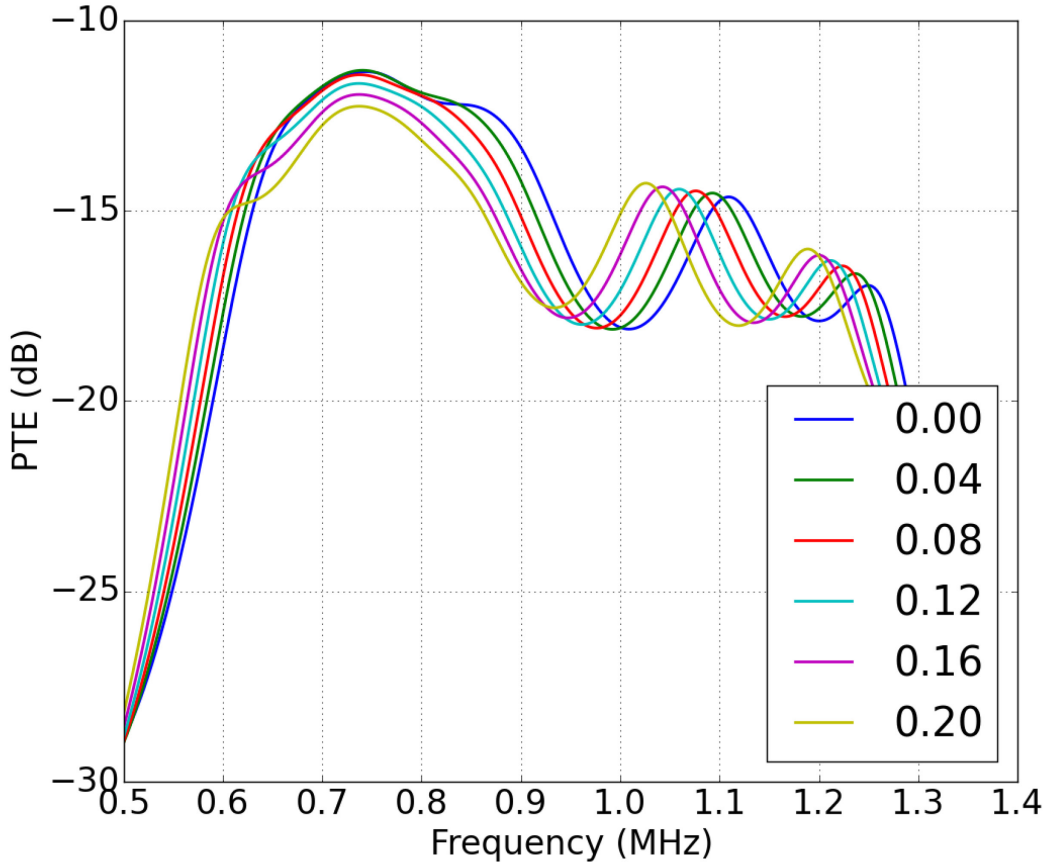

Figure 3.38: PTE Curves of Samples of Varying Adhesive Layer Thicknesses

Figure 3.38 shows the effect of adhesive layer thickness on the PTE over frequency. The transducer resonance is around 750 kHz. This creates a local efficiency maximum that stays static as the adhesive layer thickness is changed. It is apparent that the initial peak shifts to lower frequencies as the adhesive layer, and thus the cavity thickness, is increased (Figure 3.39).

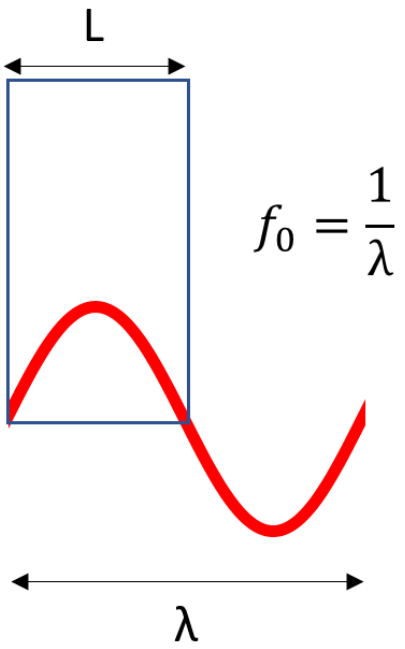

Figure 3.39: Fundamental Frequency Dependence on Cavity Thickness

As the first resonance lowers in frequency with increasing adhesive layer thickness, it leaves alignment with the transducer's resonance and loses the boost to efficiency caused by the system and transducer's resonance superimposing. This has implications for the end product; thicker skin will have a lower resonance, and each skin thickness will have its own resonant curve corresponding to the transducer resonance and the thickness resonance. This allows for fine tuning of the stack optimal thickness of the dry coupling, perhaps in the loaded silicone or the adhesive layer.

Conclusion

After fitting the KLM model to the PTE data, qualitative agreement between the data and model was observed. The model did a reasonably good job at capturing the efficiency magnitude and the frequency spacing between resonances.

The model also showed agreement with the PTE data from Section 3.8 for the effect of the adhesive layer. It was seen that there is an optimum adhesive layer thickness in which the system resonance overlaps with the transducer resonance. This would be unique to each individual patient as skin thickness and acoustic properties vary greatly between individuals. While the processing techniques developed in this study did not allow for tight

control over adhesive layer thickness, processes to achieve a desired thickness could be developed.

The adhesive layer's ability to fix the transducer to the patient's head was then examined.

3.10 Vibration Test

Introduction

A vibration test was designed to determine the effectiveness of the adhesive layer of the dry coupling. The integrity of the adhesive layer needs to remain intact, and not lose adherence to the substrate.

Methods

A Bruel and Kjaer Minishaker Type 4810 was used to shake the test samples while the accelerometer in a B&K 8001 impedance head was used to record the acceleration. The minishaker was driven at 20 Hz to 6.15g. A Teflon plate was fixed to the minishaker using a 10-32 threaded stud (see Figure 3.40). Teflon was used to provide a surface that is difficult to stick to, much like skin. Both Teflon and skin have very low surface energies (18 and 25 dynes/cm respectively) which makes them hard to adhere to [20]. The samples with the adhesive layer were pressed into the plate to form a strong bond, then the minishaker was left switched on for approximately four days. The amount of time it took for the samples to detach from the Teflon was observed using a camera and time-lapse software which captured a photo every minute.

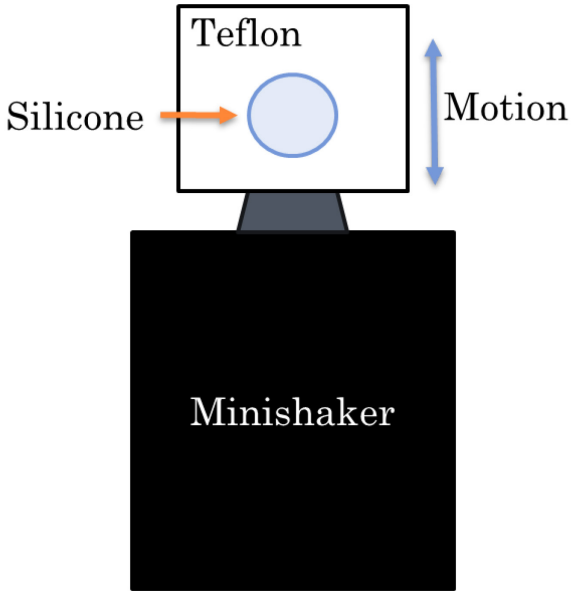

Figure 3.40: Vibration Test Diagram

Results and Discussion

The vibration test of the adhesive was performed in order to possibly find a loading condition in which the adhesive would delaminate to verify whether an external unit of the UTET system held in place by an adhesive dry coupling would withstand the rigours of real world activity. The results of the vibrations test showed that the samples, that were of a mass and shape similar to the final transducer unit, stayed on a vibrating Teflon plate for 96 consecutive hours. The samples experienced a maximum shear force of 82.6 mN, about 1.2 times the force the samples would experience if attached to a person's head while they performed a 30 cm jump.[35] The samples experienced this force 20 times per second for the entire 96-hour test.

Conclusion

This experiment showed that the adhesive could withstand extreme loading on a surface with low adhesion properties for a much longer period than a user would normally wear the device. Although there are real-world factors such as sweat, skin oils and dirt that may affect adhesion to skin but were not tested for in this experiment, the results show promise that the bond created by the adhesive layer may be adequate for real world use.

3.11 Real World Validation Test

Introduction

A qualitative experiment was performed to test the adhesive quality of the samples and to test how comfortable they were to have on a person's skin. Tests were designed to load the adhesive to a greater degree than a user would under normal circumstances. If the samples do not lose their adhesion during this test it provides an indication that the design will work in real world scenarios.

Methods

The samples are the final configuration used in this thesis, consisting of the silicone and adhesive layers where the silicone is of sufficient weight to simulate the weight of the UTET device. The following comments pertain to this experiment. A sample was worn by the author on the mastoid tip of the head. It was found by the author that while oily skin causes poor adhesion, the adhesion of the sample was restored after washing the skin and adhesive with mild soap, then drying with a paper towel. A sample was worn all day without any irritation or discomfort such that it was barely noticeable. The sample was worn lying down on a pillow for an extended period, with the head impressed and dragged against the pillow. The sample was worn while showering, during which the sample was subjected to soapy water and small impacts from the author's hand.

Results and Discussion

The results of this qualitative test show that not only is the sample comfortable to the point of being unnoticeable but it is also possible to regain the adhesion of the sample after it has been fouled by oil and dirt by washing it with soap and water. While adhered to the mastoid tip, the sample maintained its adhesion through challenging scenarios. The sample was able to stay adhered to the head while the user slept with it against a pillow. The sample did not detach from the head while showering during which the sample was subjected to impacts from the hand and immersed in fast flowing, soapy water while the hair was washed. After showering and drying off, the sample adhered even better than before showering, as the dirt particles and oil on the surface of the adhesive layer had been removed. The author wore the sample while doing exercise, including jumping jacks and running. Finally, the

author attempted to detach the sample through vigorously shaking the head. None of the aforementioned tests were able to cause the adhesion to fail, which shows a good qualitative measure that the strength of the adhesive is capable of daily usage by the user of the UTET device.

Despite the adhesive's ability to retain adhesion throughout the previous tests, it was still very comfortable to remove from the skin. This is a specific feature of the Soft Skin Adhesive silicone used, as it was designed for and typically used in the application of wound dressings where low force removal is an important property. The effect on the skin at the attachment point showed no discolouration and no wrinkling which is consistent with the SSA being used for sensitive skin applications.

Note that the adhesive only bonded where it contacted the skin. Because the mastoid tip is an uneven surface, only part of the dry coupling was able to form a bond with the skin. The adhesive is likely to perform even better on a patient with the implanted device under the skin, as the implant will create a flat surface for the dry coupling to adhere to. The larger surface area for the adhesive to adhere to will result in a stronger bond.

Conclusion

The dry coupling with adhesive was validated in real world scenarios which showed no appreciable loss of adhesiveness. The adhesive is adequate for use in real world conditions not only for its strength but it's comfort, removability and its ability to be washed and regain strength.

3.12 Chapter Conclusion

This chapter outlined the experimental work done to characterise the dry coupling material and test the robustness of the adhesive layer. First, the potential for silicone as a dry coupling material was demonstrated with only 21.1% efficiency lost compared to the ideal transmission conditions for the transducers. This was followed by an experiment that showed the advantage of using an adhesive material which resulted in the PTE staying high at very low levels of applied pressure.

The reflectivity of the Sylgard was characterised over a range of ZnO loading levels. The reflectivity was then measured off a porcine skin sample and mapped to the same

reflectivity of the Sylgard. The reflectivity determined the ZnO loading level (2022 ± 14 kg/m^3) that would match the Sylgard's acoustic impedance to that of the porcine skin sample.

The attenuation of the ZnO loaded Sylgard was characterised at -2.66 ± 0.15 dB/mm and the porcine skin acoustic impedance measured in the previous reflectivity experiment was independently confirmed using the attenuation model. The adhesive layer thickness was found using image processing to be 0.137±0.03 mm.

The PTE tests showed that matching the dry coupling's acoustic impedance to the porcine skin sample increased the PTE relative to the maximum achievable by 23.5% compared to a non-loaded silicone sample.

A KLM model of the system was validated against the PTE data which showed good qualitative agreement. The KLM predicted a PTE decrease between ~0.15 dB to 0.75 dB due to the addition of the adhesive layer which was close to the measured drop of 0.8 dB.

The vibrations test showed that the adhesive, when adhered to Teflon, could withstand 96 consecutive hours of vibration delivering a peak shear force of 82.6 mN at 20 Hz. This is 1.4 times the shear force the samples would experience while attached to the head of a person doing jumping jacks, an exercise in which the head experiences particularly high shear forces.

Finally, a real-world validation test of the adhesive showed that in many extreme loading cases, the adhesive was able to stay adhered to the head.

Chapter 4: Conclusion

This thesis described the design and preliminary verification of a key component in an ultrasound transcutaneous energy transmission system (UTET), the dry acoustic coupling material that allows ultrasound energy to be transmitted across the skin.

The author focused on silicones as the class of materials to be investigated for this application based on their favourable acoustic, adhesive and biocompatibility properties. A set of manufacturing processes were developed to produce a composite silicone dry coupling consisting of bulk Sylgard 184 coated with a thin layer of Dow Corning MG 7-9900 Soft Skin Adhesive that provided the required adhesion to skin, mechanical reliability and acoustic impedance. The manufacturing techniques the author developed resolved key issues with the generation of bubbles during curing of the silicone, allowed highly flat, parallel samples with tunable acoustic impedance to be made and resolved issues with the compatibility of the bulk and adhesive coating layers. The result of this work was a complete procedure for producing dry couplings for UTETs.

The dry couplings produced by this manufacturing process were verified in a set of experiments that characterized their acoustic power transmission efficiency, acoustic reflectivity, impedance and adhesion. It was found that the maximum PTE for an unloaded sample of Epoxies Etc. 20-1625 Optically Clear Silicone in water was 78.9% relative to the maximum PTE of the transducer pair in water. The dry coupling was then redesigned to use the stronger Sylgard 184 silicone with an adhesive top layer then loaded with ZnO powder to optimize the acoustic impedance of the Sylgard. When transmitting through porcine skin, optimization increased the PTE by 23.5% relative to the maximum achievable PTE. This means that designers could make a device with either a smaller battery or achieve 23.5% longer battery life with the same battery. This is a meaningful increase in efficiency, demonstrated by the fact that large manufacturers will add a new product with smaller differences in capacity. Energizer makes continuous low drain batteries like their 346 and 317 batteries with a difference of only 17.4% in battery capacity. The impedance optimisation was able to produce samples with acoustic impedances ranging from 0.96 ± 0.05 MRayls up to approximately 2 MRayls. Finally, the adhesive layer was tested by cyclically loading a sample in shear while adhered to a Teflon plate. The samples experienced a maximum

shear force of 82.6 mN at 20 Hz for 96 hours. This shear force is larger by a factor of 1.2 compared to the maximum shear force the head experiences performing a 30 cm jump.[35]

A preliminary validation of the device was undertaken by the author who wore it behind the ear for 48 hours while performing a variety of daily activities including showering, sleeping and exercise. Adhesion was maintained throughout this period and the device was found to be comfortable to wear and unobtrusive.

Based on these results, the dry coupling design presented in this thesis appears promising for use in a complete UTET system, possibly incorporating other technical developments made in our lab.[30]

While the dry coupling system developed here would be applicable to powering a range of implanted devices, the particular application area that was the focus of our design is the powering of cochlear implants and other implantable hearing aids currently powered by magnetic induction coils. For this application, the results of this study taken with previous findings from our lab[30] show that UTETs that incorporate a dry coupling can achieve efficiencies competitive with magnetic induction coil power links in a device that is approximately an order of magnitude smaller while achieving a high degree of comfort and durability.

The developments described in this thesis will enable the next phase of investigation in UTETs to focus on the validation of a complete UTET system that incorporates a dry coupling.

Bibliography

[1] S. Ozeri and D. Shmilovitz, "Ultrasonic transcutaneous energy transfer for powering implanted devices," *Ultrasonics*, vol. 50, no. 6, pp. 556–566, May 2010.

[2] S. Ozeri, D. Shmilovitz, S. Singer, and C.-C. Wang, "Ultrasonic transcutaneous energy transfer using a continuous wave 650 kHz Gaussian shaded transmitter," *Ultrasonics*, vol. 50, no. 7, pp. 666–674, Jun. 2010.

[3] H. Basaeri, "A review of acoustic power transfer for bio-medical implants - IOPscience." [Online]. Available: http://iopscience.iop.org/article/10.1088/0964-1726/25/12/123001/meta. [Accessed: 20-Aug-2017].

[4] H. Kawanabe, T. Katane, H. Saotome, O. Saito, and K. Kobayashi, "Power and Information Transmission to Implanted Medical Device Using Ultrasonic," *Jpn. J. Appl. Phys.*, vol. 40, no. Part 1, No. 5B, pp. 3865–3866, May 2001.

[5] S. Arra, J. Leskinen, J. Heikkila, and J. Vanhala, "Ultrasonic Power and Data Link for Wireless Implantable Applications," in *2nd International Symposium on Wireless Pervasive Computing, 2007. ISWPC '07*, 2007, p. .

[6] Y. Shigeta, Y. Hori, K. Fujimori, K. Tsuruta, and S. Nogi, "Development of highly efficient transducer for wireless power transmission system by ultrasonic," in *Microwave Workshop Series on Innovative Wireless Power Transmission: Technologies, Systems, and Applications (IMWS), 2011 IEEE MTT-S International*, 2011, pp. 171–174.

[7] J. Leadbetter, J. A. Brown, and R. B. Adamson, "The design of ultrasonic lead magnesium niobate-lead titanate (PMN-PT) composite transducers for power and signal delivery to implanted hearing aids," *Proc. Meet. Acoust.*, vol. 19, no. 1, p. 030029, Jun. 2013.

[8] A. Ben Amar, A. B. Kouki, and H. Cao, "Power Approaches for Implantable Medical Devices," *Sensors*, vol. 15, no. 11, pp. 28889–28914, Nov. 2015.

[9] I. Benedek and M. M. Feldstein, *Technology of Pressure-Sensitive Adhesives and Products*. CRC Press, 2008.

[10] R. Marks, S. P. Barton, and C. Edwards, Eds., *The Physical nature of the skin*. Lancaster, England ; Boston: MTP Press, 1988.

[11] T. E. G. Alvarez-Arenas, "Acoustic impedance matching of piezoelectric transducers to the air," *IEEE Trans. Ultrason. Ferroelectr. Freq. Control*, vol. 51, no. 5, pp. 624–633, May 2004.

[12] G. S. Kino, *Acoustic waves: devices, imaging, and analog signal processing*. Prentice Hall PTR, 1987.

[13] R. S. C. Cobbold, *Foundations of Biomedical Ultrasound*. Oxford University Press, 2006.

[14] “Maceration of the skin and wound bed. 1: Its nature and causes. (PDF Download Available),” *ResearchGate*. [Online]. Available: https://www.researchgate.net/publication/11195062_Maceration_of_the_skin_and_wound_bed_1_Its_nature_and_causes. [Accessed: 09-Jun-2017].

[15] “Layers of the Skin · Anatomy and Physiology.” [Online]. Available: http://philschatz.com/anatomy-book/contents/m46060.html. [Accessed: 09-Jun-2017].

[16] H. S. Tan and W. R. Pfister, “Pressure-sensitive adhesives for transdermal drug delivery systems,” *Pharm. Sci. Technol. Today*, vol. 2, no. 2, pp. 60–69, Feb. 1999.

[17] J. Nuutinen, I. Harvima, M.-R. Lahtinen, and T. Lahtinen, “Water loss through the lip, nail, eyelid skin, scalp skin and axillary skin measured with a closed-chamber evaporation principle,” *Br. J. Dermatol.*, vol. 148, no. 4, pp. 839–841, Apr. 2003.

[18] K. Agrawal and N. Chauhan, “Pressure ulcers: Back to the basics,” *Indian J. Plast. Surg. Off. Publ. Assoc. Plast. Surg. India*, vol. 45, no. 2, pp. 244–254, 2012.

[19] MED-EL, “Active vs. Passive.” [Online]. Available: http://www.medel.com/uk/show/index/id/1495/title/Active-vs--Passive/. [Accessed: 08-Mar-2017].

[20] K. Godbey, “Silicone Adhesives An Answer to Gentle Skin Adhesion,” Medical Device Summit, Aug. 2012.

[21] H. Fujii, C. Nakaya, H. Takeuchi, T. Kondo, and YasuoIshikawa, “Acoustic Properties of Lens Materials for Ultrasonic Probes,” *Jpn. J. Appl. Phys.*, vol. 34, no. Part 1, No. 1, pp. 312–315, Jan. 1995.

[22] I. of M. (US) C. on the S. of S. B. Implants, S. Bondurant, V. Ernster, and R. Herdman, *Silicone Chemistry*. National Academies Press (US), 1999.

[23] R. M. Marks, S. P. Barton, and C. Edwards, *The Physical Nature of the Skin*. Springer Science & Business Media, 2012.

[24] X. Thomas, “Silicones in Medical Applications,” in *Inorganic Polymers*, Nova Science Publishers, 2003.

[25] T. Jackets, “The Newton-Laplace Equation & Speed of Sound,” *Thermaxx Jackets*, 12-Dec-2014. .

[26] Y. Yamashita *et al.*, “Low-acoustic attenuation and high-mechanical strength silicone rubber lens doped with ZnO nanopowder for medical ultrasonic array probe,” in *IEEE Ultrasonics Symposium, 2008. IUS 2008*, 2008, pp. 883–886.

[27] “Zinc Oxide Nanopowder / Nanoparticles (ZnO, 99.9+%, 80-200 nm).” [Online]. Available: http://www.us-nano.com/inc/sdetail/349. [Accessed: 21-Jun-2017].

[28] Fastel Adhesives, “FastelTack SIL Product Description,” Data Sheet.

[29] “The design of ultrasonic lead magnesium niobate-lead titanate (PMN-PT) composite transducers for power and signal delivery to implanted hearing aids,” *Proc. Meet. Acoust.*, vol. 19, no. 1, p. 030029, May 2013.

[30] P. H. Vihvelin, “Design and Development of an Ultrasonic Power Transfer System for Active Implanted Medical Devices,” Dec. 2015.

[31] H. Vihvelin, J. Leadbetter, M. Bance, J. A. Brown, and R. B. A. Adamson, “Compensating for Tissue Changes in an Ultrasonic Power Link for Implanted Medical Devices,” *IEEE Trans. Biomed. Circuits Syst.*, pp. 1–1, 2015.

[32] ASTM, “Attenuation in water as a function of frequency.” [Online]. Available: https://www.astm.org/BOOKSTORE/DS68/pg41.pdf. [Accessed: 18-Oct-2016].

[33] “ImageJ.” [Online]. Available: https://imagej.nih.gov/ij/. [Accessed: 12-Jun-2017].

[34] *Foundations of Biomedical Ultrasound*. Oxford, New York: Oxford University Press, 2006.

[35] J. R. Funk, J. M. Cormier, C. E. Bain, H. Guzman, E. Bonugli, and S. J. Manoogian, “Head and Neck Loading in Everyday and Vigorous Activities,” *Ann. Biomed. Eng.*, vol. 39, no. 2, pp. 766–776, 2011.